Inaugural dissertation

for

obtaining the doctoral degree

of the

Combined Faculty of Mathematics, Engineering and Natural Sciences

of the

Ruprecht - Karls - University

Heidelberg

Presented by

M. Sc. Rachel Maria Röhrich

born in Schwäbisch Gmünd

Oral examination: December 16, 2022

The V-ATPase at the *trans*-Golgi network/early endosome during vegetative and reproductive development

Referees: Prof. Dr. Karin Schumacher

Prof. Dr. Alexis Maizel

Summary

V-ATPases are highly conserved proton pumps that function not only as proton pumps but are involved in many processes through interactions with different proteins. In plant cells, the *trans*-Golgi network/early endosome (TGN/EE) is a compartment of specific significance, as trafficking pathways converge there. Cargo from secretory, endocytic and recycling trafficking pathways travel through the TGN/EE. Acidification of the TGN/EE is accomplished by V-ATPase complexes with the VHA-a subunit isoform VHA-a1 in Arabidopsis. While V-ATPases which contain VHA-a1 localize to the TGN/EE, V-ATPases with VHA-a2 or VHA-a3 are targeted to the tonoplast, the limiting membrane of the vacuole. This thesis describes the mutant phenotype of the gene encoding the subunit VHA-a1. Strikingly, during vegetative development *vha-a1* is wildtype-like. It is shown that VHA-a2/VHA-a3-containing V-ATPases can compensate for the lack of VHA-a1 during vegetative growth. Given the subcellular specialization of VHA-a1 versus VHA-a2 and VHA-a3 this is astonishing and represents a striking example of functional redundancy of isoforms despite differential localization. I further show that VHA-a1 is essential for pollen development. VHA-a3-containing V-ATPases are not able to compensate for the lack of VHA-a1 in pollen development. Microspores in the *vha-a1* mutant are defective in pollen wall formation. As early as at the tetrad stage, when pollen wall development starts with the formation of the primexine, defects are visible in *vha-a1*. Rescue experiments with *VHA-a1* expressed under the control of different promoters revealed that tapetum-specific expression of *VHA-a1* does not rescue pollen development of *vha-a1*. For the process of primexine formation the results of this work suggest that primexine formation is largely governed by the gametophyte. In addition to the early defect, absence of VHA-a1 leads to a late defect, as seen from the lack of transmission of the mutant allele via the male gametophyte despite at the time of pollen release *vha-a1* and wildtype microspores in *vha-a1*/+ anthers are indistinguishable. Furthermore, the potential capability of pH sensing of the TGN/EE resident V-ATPase in Arabidopsis and the underlying molecular mechanism was analyzed by mutation of VHA-a1 histidine residues. While some VHA-a1 histidine substitution variants were able to rescue the defect in pollen development of *vha-a1*, others possibly cannot, suggesting that these histidine residues have an essential function. Moreover, this thesis shows that also the V-ATPase-associated VHA-AP1 is essential for the male gametophyte and that its knock-down results in reduced cell expansion.

Zusammenfassung

V-ATPasen sind hochkonservierte Protonenpumpen, die nicht nur als Protonenpumpen agieren, sondern durch Interaktionen mit unterschiedlichen Proteinen an vielen Prozessen beteiligt sind. In Pflanzenzellen ist das *trans*-Golgi Netzwerk/frühe Endosom (TGN/EE) ein Kompartiment von besonderer Bedeutung, da dort unterschiedliche Transportwege aufeinandertreffen. Fracht aus sekretorischen, Endozytose- und Recyclingtransportwegen durchquert das TGN/EE. Das TGN/EE wird von V-ATPase-Komplexen, welche die Untereinheit VHA-a1 besitzen, angesäuert. Während V-ATPasen, die VHA-a1 enthalten, am TGN/EE lokalisiert sind, werden V-ATPasen, die VHA-a2 oder VHA-a3 enthalten, zum Tonoplasten, der vakuolären Membran, transportiert. Diese Arbeit beschreibt den Mutanten-Phänotyp des Gens, das für die Untereinheit VHA-a1 kodiert. Bemerkenswerterweise ist *vha-a1* während der vegetativen Entwicklung wildtypähnlich. Es wird gezeigt, dass VHA-a2/VHA-a3-enthaltende V-ATPasen das Fehlen von VHA-a1 während des vegetativen Wachstums ausgleichen können. Angesichts der subzellulären Spezialisierung von VHA-a1 im Vergleich zu VHA-a2 und VHA-a3 ist dies erstaunlich und stellt ein eindrucksvolles Beispiel für die funktionelle Redundanz von Isoformen trotz unterschiedlicher Lokalisierung dar. Darüber hinaus zeige ich, dass VHA-a1 essentiell für die Pollenentwicklung ist. VHA-a3-enthaltende V-ATPasen sind nicht in der Lage, das Fehlen von VHA-a1 in der Pollenentwicklung auszugleichen. Mikrosporen der *vha-a1* Mutante sind defekt in der Bildung der Pollenwand. Rettungsexperimente, in denen *VHA-a1* unter der Kontrolle unterschiedlicher Promotoren exprimiert wurde, zeigten, dass Tapetum-spezifische Expression von *VHA-a1* die Pollenentwicklung von *vha-a1* nicht rettet. Für den Prozess der Bildung der Primexine deuten die Ergebnisse dieser Arbeit darauf hin, dass die Bildung der Primexine in großen Teilen vom Gametophyten ausgeht. Zusätzlich zu dem frühen Defekt führt das Fehlen von VHA-a1 zu einem späten Defekt, was die fehlende Übertragung von *vha-a1* durch den männlichen Gametophyten zeigt, obwohl zum Zeitpunkt der Pollenfreisetzung *vha-a1*- und Wildtypmikrosporen in *vha-a1*/+ Antheren ununterscheidbar sind. Außerdem wurden die mögliche Fähigkeit der pH Wahrnehmung der am TGN/EE lokalisierten V-ATPase, und der zugrundeliegende molekulare Mechanismus, durch Mutation von Histidinen in VHA-a1 analysiert. Während einige der VHA-a1 Histidinmutanten den Defekt in der Pollenentwicklung in *vha-a1* retten konnten, sind andere möglicherweise dazu nicht in der Lage, was auf eine essentielle

Funktion dieser Histidine hindeutet. Des Weiteren zeigt diese Arbeit, dass auch das mit der V-ATPase assoziierte VHA-AP1 essentiell für den männlichen Gametophyten ist, und dass seine Herunterregulierung zu reduzierter Zellexpansion führt.

Contribution to this work

The author states that this work was written independently and that the sources which have been used are indicated.

Other than the author and the supervisor, the following people contributed to this work:

Help with anther imaging and establishing imaging settings	Dr. Melanie Krebs
Electron microscopy of anthers after joint sample preparation	Dr. Stefan Hillmer, Steffi Gold
Joint creation of the indicated figures	Dr. Upendo Lupanga
Cloning of GreenGate constructs	Fabian Fink, Dr. Jana Askani
CLSM analysis of VHA-AP1-GSL-mNeongreen	Fabian Fink
Analysis of reciprocal crosses *vha-ap1* x wildtype	Florian Hinterberger
Support with plant work and media preparation	Beate Schöfer, Barbara Jesenofsky

Parts of Chapter 1 have been published in:

Lupanga U, Roehrich R, Askani J, Hilmer S, Kiefer C, Krebs M, Kanazawa T, Ueda T, Schumacher K. 2020. The Arabidopsis V-ATPase is localized to the TGN/EE via a seed plant-specific motif. *Elife* 1–40. doi:10.7554/eLife.60568

List of contents

List of figures

List of tables

List of abbreviations

Elements are abbreviated according to the International Union of Pure and Applied Chemistry (IUPAC) nomenclature

The single letter code is used for abbreviations of amino acids

%	percent
°C	degrees Celsius
µg	microgram
µl	microliter
µM	micromolar
µm	micrometer
3D	three-dimensional
A. tumefaciens	*Agrobacterium tumefaciens*
a1-TD	VHA-a1 targeting domain
ADP	adenosine diphosphate
amiR	artificial microRNA
Arabidopsis	*Arabidopsis thaliana*
ATG	autophagy related
ATP	adenosine triphosphate
ATP6AP1	ATPase H^+-transporting accessory protein 1
ATP6AP2	ATPase H^+-transporting accessory protein 2
ATP6S1	ATPase H^+-transporting subunit S1
bp	base pair(s)
CLSM	confocal laser scanning microscopy
ConcA	concanamycin A
COPII	coat protein complex II

CRISPR/Cas	clustered regularly interspaced short palindromic repeats/CRISPR-associated
cryoEM	Electron cryomicroscopy
C-terminal	COOH-terminal/carboxyl-terminal
DAPI	4′,6-diamidino-2-phenylindole
ddH_2O	double distilled water
Dex	dexamethasone
dex1	*defective in exine formation1*
DMSO	dimethyl sulfoxide
DNA	deoxyribonucleic acid
E	epidermis
E. coli	*Escherichia coli*
ECH	ECHIDNA
En	endothecium
ER	endoplasmic reticulum
ERES	ER exit sites
GC	generative cell
gDNA	genomic DNA
GFP	green fluorescent protein
GSL	glycine-serine-rich linker
GTPase	guanosine triphosphatase
GUS	β-Glucuronidase
h	hours
irx9l	*irregular xylem9-like*
K_a	acid dissociation constant
LC3	microtubule-associated protein 1A/1B-light chain 3
lot	*loss of TGN*

M	microspore
Marchantia	*Marchantia polymorpha*
Me	meiocyte
min	minutes
ml	milliliter
ML	middle layer
MM	microspore mother cell
mM	millimolar
Mp	*Marchantia polymorpha*
MS	Murashige and Skoog
ms1	*male sterility1*
mTurquoise	mTurq
nef1	*no exine formation1*
N-terminal	NH_2-terminal/amino-terminal
PAM	protospacer adjacent motif
PBS	phosphate buffered saline
PCP	planar cell polarity
PCR	polymerase chain reaction
pH	pondus hydrogenii (potential of hydrogen)
P_i	inorganic phosphate
pK_a	negative logarithm of K_a
RFP	red fluorescent protein
RNA	ribonucleic acid
rpg1	*ruptured pollen grain1*
rpm	revolutions per minute
SC	sperm cell
sec	seconds

SNARE	soluble N-ethylmaleimide-sensitive factor attachment receptor
SRβ	signal recognition particle receptor subunit β
SYP	SYNTAXIN OF PLANTS
T	tapetum
tde1	*transient defective exine1*
T-DNA	transfer DNA
TEM	transmission electron microscopy
TGN/EE	*trans*-Golgi network/early endosome
Ti plasmid	tumor inducing plasmid
UBQ10	*UBIQUITIN10*
upex	*uneven pattern of exine*
V-ATPase	V-type H^+-Adenosintriphosphatase
VC	vegetative cell
VHA	V-type H^+-ATPase
VHA-AP1	V-type H^+-ATPase accessory protein 1
VHA-AP2	V-type H^+-ATPase accessory protein 2
VHA-AP2L1	V-type H^+-ATPase accessory protein 2 like 1

Preamble

V-type H^+-Adenosintriphosphatases (V-ATPases) are rotary proton pumps that acidify endomembrane compartments and are crucial for eukaryotic cells. In this work, *Arabidopsis thaliana* was used to investigate the potential capability of the V-ATPase subunit VHA-a1 to act as a sensor of pH inside endosomal compartments. Furthermore, the phenotype of the *vha-a1* mutant was analyzed in this study and the V-ATPase-associated protein VHA-AP1 was examined. The first chapter of this thesis is dedicated to the description of the phenotype of the *vha-a1* mutant during vegetative development. Moreover, it deals with the analysis of VHA-a1 histidine residues in the context of pH sensing. The second chapter of this thesis is concerned with the analysis of V-ATPases during pollen development. The third chapter finally describes the localization of VHA-AP1 and the consequences of its knock-out and knock-down.

1 Chapter 1: The *vha-a1* mutant and VHA-a1 histidine substitutions

Aims of chapter 1

It was proposed that the V-ATPase might sense pH in the lumen of endomembrane compartments and transmit the information across the membrane to interaction partners in the cytosol. One goal was to investigate the potential pH sensing capability of the TGN/EE-resident V-ATPase in Arabidopsis. A second goal was to produce *vha-a1* null alleles, which can be used to analyze VHA-a1 versions with amino acid substitutions as well as VHA-a isoforms of different organisms in the absence of wildtype VHA-a1.

1.1 Introduction

1.1.1 Endomembrane trafficking and the *trans*-Golgi network/early endosome (TGN/EE) in plant cells

Endomembrane trafficking is crucial for all eukaryotic cells to perform housekeeping functions and for adaptation to specific conditions. It involves highly orchestrated fusion and fission of membranes and trafficking of vesicles with defined cargo to different destinations. In plant cells, the *trans*-Golgi network/early endosome (TGN/EE) is a hub of endomembrane trafficking in which secretory, endocytic and recycling pathways converge (Dettmer et al., 2006; Viotti et al., 2010). Cargos of different trafficking pathways meet in this compartment and are sorted for trafficking to different destinations, which makes this compartment special. By acting as a central sorting station, the TGN/EE is very important for many processes in plant growth and defense (LaMontagne and Heese, 2017; Rosquete et al., 2018).

Cargo from the endoplasmic reticulum (ER) is transported via the Golgi apparatus to the TGN/EE. Here, sorting into trafficking pathways that reach the plasma membrane (PM) or lead to the vacuole takes place. Endocytic cargo which was internalized from the plasma membrane also reaches the TGN/EE and can continue its journey from there to the vacuole for degradation or be recycled back to the plasma membrane (Dahhan and Bednarek, 2022).

V-ATPases are highly conserved, multisubunit proton pumps that acidify endomembrane compartments by pumping protons across membranes using energy from ATP hydrolysis. V-ATPases consist of two subcomplexes, V_1 and V_O. The V_1 subcomplex is cytosolic and responsible for ATP hydrolysis. The V_O subcomplex is membrane-integral and forms the proton translocation channel (Schumacher, 2014). It is assembled at the ER (Neubert et al., 2008). Generally, the V_O subunit VHA-a isoform determines the localization of the whole complex (Vasanthakumar and Rubinstein, 2020). In Arabidopsis, V-ATPases are localized at the TGN/EE and at the tonoplast, the limiting membrane of the vacuole. V-ATPases that contain VHA-a1 are targeted to the TGN/EE, while VHA-a2 or VHA-a3-containing V-ATPases localize to the tonoplast (Dettmer et al., 2006). Tonoplast resident V-ATPases can reach their destination via Golgi independent trafficking (Viotti et al., 2013).

The TGN/EE resident V-ATPase travels from the ER through the Golgi to the TGN/EE. It leaves the ER in COPII vesicles (Viotti at al., 2013; Lupanga et al., 2020), as shown in Figure 1. Assembly of COPII vesicles takes place at ER exit sites (ERES). Here, the cytosolic small GTPase Sar1 is activated by its GDP/GTP exchange factor SEC12 and recruitment of the COPII coat, which consists of the SEC23/24 and the SEC13/31 complexes, takes place (Brandizzi, 2018). Inducible expression of a dominant negative GTPase Sar1BH74L, which had been shown to block COPII-mediated ER export (daSilva et al., 2004; Takeuchi et al., 2000), led to the retention of VHA-a1 at the ER (Lupanga et al., 2020).

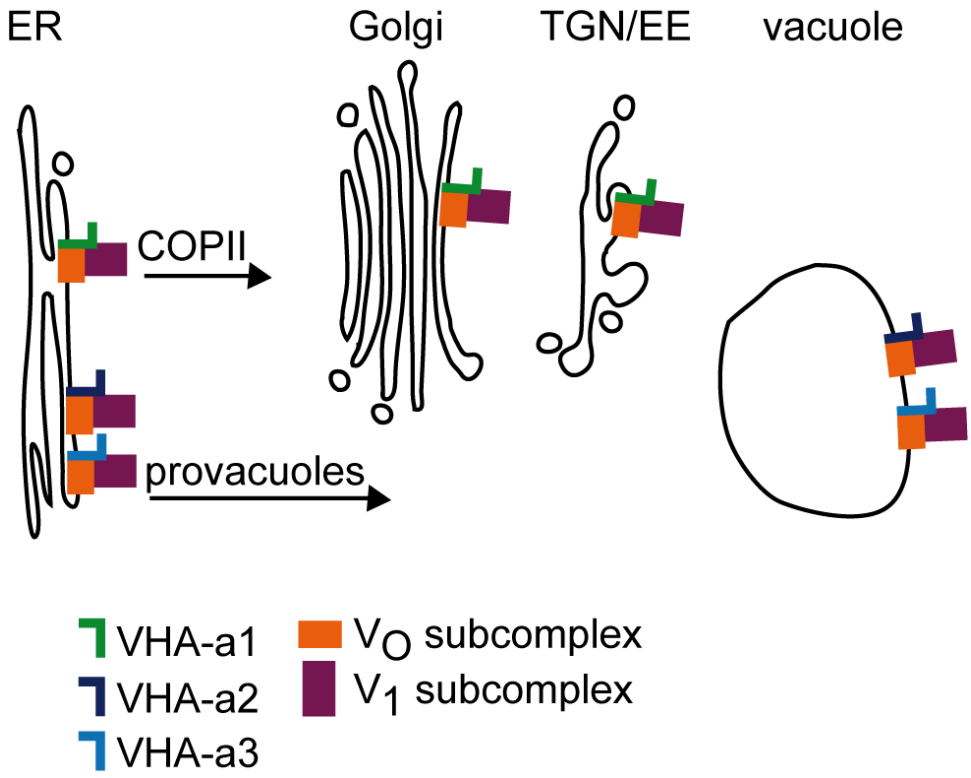

Figure 1. Trafficking of V-ATPase complexes in *Arabidopsis thaliana.* V-ATPase complexes are assembled at the ER (Neubert et al., 2008). Upon assembly VHA-a1-containing V-ATPases leave the ER in COPII-mediated ER export and travel via the Golgi to the TGN/EE (Dettmer et al., 2006; Viotti et al., 2013). The information for traveling to the TGN/EE is contained in the VHA-a1 targeting domain in the N-terminal half of VHA-a1 (Lupanga et al., 2020). V-ATPases that contain VHA-a2 or VHA-a3 are targeted to the tonoplast (Dettmer et al., 2006). They are able to reach the tonoplast in a Golgi-and TGN/EE-independent manner via provacuoles (Viotti et al., 2013).

VHA-a1 serves as a marker for the TGN/EE (Dettmer et al., 2006), as does SYNTAXIN OF PLANTS 61 (SYP61), a member of the syntaxin group of SNAREs (Sanderfoot et al., 2001), and many more TGN/EE resident proteins have been identified in recent years, for example ECHIDNA (ECH, Gendre et al., 2011; Uemura et al., 2014).

The central role of the TGN/EE in trafficking also means that its physiological conditions need to be tightly regulated. Acidic pH in the lumen of the TGN/EE is required for exocytosis, endocytosis and recycling and V-ATPases are required for this acidification (Dettmer et al., 2006; Luo et al., 2015). Together with proton-coupled antiporters, such as the Cl^-/NO^- proton antiporters ClCd and ClCf (Fecht-Bartenbach et al., 2007; Scholl et al., 2021) and the NHX-type cation proton exchangers NHX5 and NHX6 (Bassil et al., 2011; Dragwidge et al., 2019), and proteins for anion and cation efflux such as CCC1 (McKay et al., 2022), V-ATPases maintain pH homeostasis at the TGN/EE (Luo et al., 2015). The use of genetically encoded fluorescent pH sensors enables *in vivo* pH measurements. SYP61-pHusion was used to determine steady-state pH in the TGN/EE of epidermal root cells in Arabidopsis, which was found to be pH 5.6 compared to pH 7.2 in the cytosol (Luo et al., 2015). Contrary to the pH gradient in the secretory pathway in animal cells, in plant cells pH in the TGN/EE was lower than the pH of the late endosomal compartments (Martinière et al., 2013). Disturbed trafficking through the TGN/EE results in cell elongation defects as observed in the *ech* mutant (Gendre et al., 2011) and in RNA-mediated knock-down of *VHA-a1* (Brüx et al., 2008). Generally, inhibition of V-ATPase activity by genetic or pharmacological means, for example, through the use of the V-ATPase inhibitor Concanamycin A (ConcA, Huss et al., 2002), leads to elevation of TGN/EE pH and disturbed trafficking (Luo et al., 2015). Mild treatment with ConcA results in a change of TGN identity and loss of independence from the Golgi (Viotti et al., 2013). While inhibition of V-ATPase activity at the TGN/EE results in a strong reduction of cell expansion, lack of V-ATPase activity at the tonoplast does not cause severe cell expansion defects (Krebs et al., 2010).

1.1.2 The potential pH sensing capability of the endosomal V-ATPase

The V-ATPase is a multisubunit and multifunctional complex. Its most prominent and best understood function is pumping protons across membranes, but this is not its only function. V-ATPases were found to participate in many processes by interacting with different proteins (Abuammar et al., 2021; Eaton et al., 2021). A role of the V-ATPase in cell signaling via protein-protein interaction was found, for example, in the Wnt signaling pathway (Cruciat et al., 2010). Another example is the interaction of the V-ATPase with a protease of SARS coronaviruses which results in cleavage of a V-ATPase subunit and correlates with a decrease in intracellular pH. This suggests that SARS coronaviruses can modify V-ATPase activity to establish the pH gradient required for the replication of many viruses (Lin et al., 2005).

Also closely connected with its proton pumping function is the function of the V-ATPase in pH sensing. Investigations of the mechanochemistry of the V-ATPase pointed out that sensing luminal pH would be advantageous for the V-ATPase for efficient proton pumping (Grabe et al., 2000). Also, from the perspective of endosomes as acidic compartments, the presence of one or more pH-sensing proteins has been hypothesized and searched for (Marshansky, 2007). Indeed, in mammalian cells, it was later shown that in early endosomes the V-ATPase recruits cytohesin-2, a guanine nucleotide exchange factor, in a pH-dependent manner. At conditions of low pH in the endosomal lumen, interaction of cytohesin-2 and the V-ATPase subunit a was found to take place in the cytosol. This cytosolic interaction was reduced if luminal pH was elevated. Interaction of the V-ATPase subunit a with cytohesin-2 correlated with endocytosis efficiency, which was reduced at elevated pH (Hurtado-Lorenzo et al., 2006). The site in the V-ATPase subunit a N-terminus, which binds to the Sec7 domain of cytohesin-2 was determined. It was found that the interaction is evolutionarily conserved (Hosokawa et al., 2013). A study in neurons suggests that also in neurotransmitter release, the V-ATPase functions as a pH sensor (Poëa-Guyon et al., 2013). The molecular mechanism by which pH is sensed in the endosomal lumen and by which the information is transmitted to proteins in the cytosol is unknown. It was proposed that histidine residues of the C-terminal half of the V-ATPase subunit a could be involved in pH sensing by evoking a conformational change upon a change in protonation (Marshansky, 2007). Subunit a consists of a C-terminal half with eight transmembrane domains and an N-terminal half which is

accessible for interaction partners in the cytosol (Vasanthakumar and Rubinstein, 2020), as can be seen in Figure 2. Histidine residues can change their protonation state at physiological pH conditions. The imidazole ring of histidines has a pK_a of around 6. Factors like amino acids in the surroundings influence the protonation state, but generally, the imidazole ring is uncharged at neutral pH and doubly protonated and positively charged at acidic pH (Chen et al., 2022) (Supplementary Figure 4).

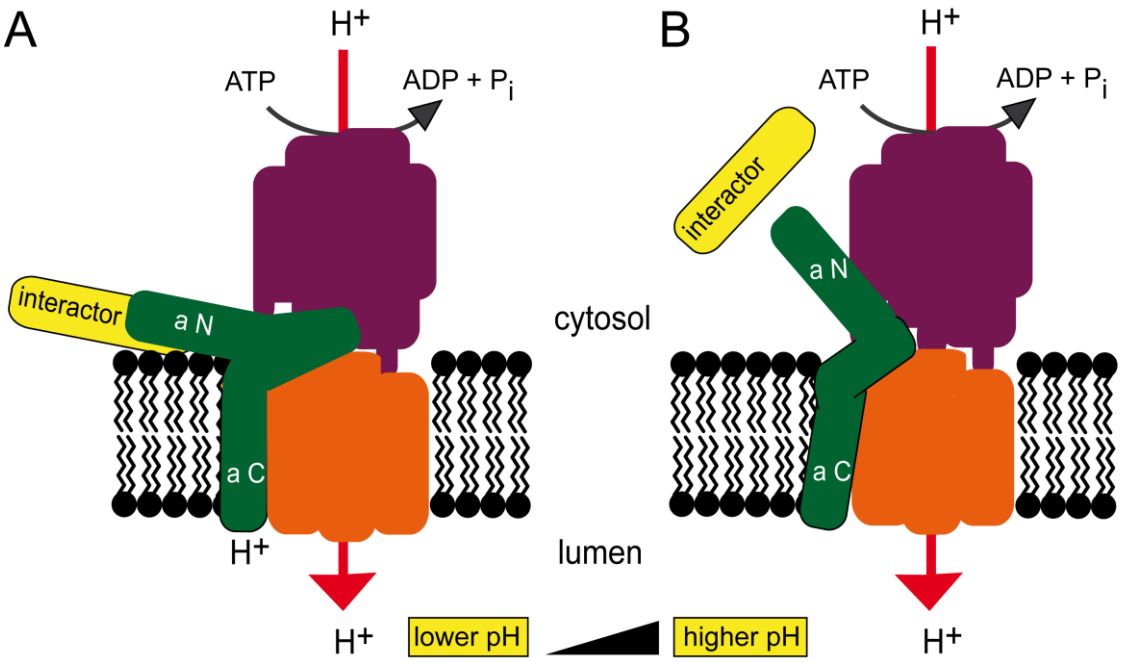

Figure 2. Hypothetical mechanism of pH-sensing by the V-ATPase. Protein interactions in the cytosol are dependent on intra-endosomal acidification, as shown in mammalian cells. **(A)** If pH in the lumen is low, interactions between the N-terminal half of subunit a (aN) of the V-ATPase and a cytosolic interaction partner (interactor) take place. **(B)** If pH in the lumen is increased, the interaction in the cytosol is reduced. The transduction of information about pH in the lumen across the membrane could happen via a conformational change of subunit a, which could be caused by differential protonation of histidine residues in the C-terminal half (aC) of subunit a (Hurtado-Lorenzo et al., 2006; Marshansky, 2007). The figure was adapted from Hurtado-Lorenzo et al., 2006.

Recently, the V-ATPase was shown to be a regulator of non-canonical autophagy. It was reported that (in LC3-associated phagocytosis) the V-ATPase interacts independently of its proton pumping function with ATG16L1, a component of the canonical as well as the non-canonical autophagy machinery, and recruits it to membranes in mammalian cells (Lei and Klionsky, 2022). The interaction of the V-ATPase and ATG16L1 was disrupted without affecting proton pumping of the V-ATPase in treatments with the *Salmonella* effector protein SopF which resulted in disruption of LC3 lipidation (Xu et al., 2019). This is another example of a process that seems to rely on the pH-sensing capability of the V-ATPase. Upon membrane damage and disruption of the proton gradient, the V-ATPase was suggested to be able to sense the pH increase in the lumen of acidic organelles. It was shown that disruption of the proton gradient, after treatment with the ionophore nigericin as well as after treatment with NH_4Cl, initiates the recruitment of ATG16L1 by the V-ATPase, leading to LC3 lipidation. SopF was demonstrated to abolish V-ATPase-ATG16L1-induced LC3 lipidation by binding to the GTP-bound ADP-ribosylation factor GTPase ARF1 and by ADP-ribosylating the V-ATPase V_O subunit c (Y. Xu et al., 2022).

Although the molecular mechanism of the putative pH sensing by the V-ATPase is unknown, it is well characterized for other proteins. Examples of proteins that undergo pH-dependent conformational changes due to differential protonation of histidine residues are the influenza B M2 protein (BM2, Zhang et al., 2019), the outer capsid protein VP2 of the bluetongue virus (Wu et al., 2019) and the human guanine nucleotide exchange factor RasGRP1 (Vercoulen et al., 2017). BM2 is a transmembrane protein that oligomerizes and forms a pH-activated proton channel consisting of a homotetramer. The switch of this proton channel from the closed to the open state was shown to be mediated by the protonation of the BM2 histidine 19 tetrad. The pH range in which the conformational change occurs is between pH 6 and pH 4.5. Protonation of a second histidine residue in BM2, histidine 27, likely supports the opening of the channel and facilitates proton conduction (Wang et al., 2009; Zhang et al., 2019).

In this thesis, the putative pH sensing capability of the V-ATPase was investigated in Arabidopsis by analysis of histidine residues of the VHA-a1 C-terminal half.

1.1.3 CRISPR/Cas9 and its use to generate gene knock-outs

Instead of being dependent on T-DNA insertion mutant lines, the application of the clustered regularly interspaced short palindromic repeats/CRISPR-associated (CRISPR/Cas) technology enables to generate mutant lines in a short amount of time. Even if T-DNA insertion lines for the gene of interest exist, there are advantages of CRISPR/Cas9-based lines compared to T-DNA insertion mutants. Highly relevant for the analysis of transgenes in the mutant background is the issue of gene silencing, which can occur in T-DNA insertion mutants. Silencing of transgenes can happen, for instance, when promoter sequences on the transgene of interest are also present on the T-DNA inserted in the gene of interest, as has been reported, e.g., in the case of the cauliflower mosaic virus 35S promoter (Daxinger et al., 2008; Mlotshwa et al., 2010).

The beginning of CRISPR research dates back to before the turn of the millennium when short regularly spaced repeats were found in *Haloferax mediterranei*, a halophilic archeal microbe, and other microbes (Lander, 2016). However, the starting point of a revolution for targeted genome editing was marked by the engineering of the naturally occurring complex between the trans-activating CRISPR RNA and the targeting CRISPR RNA as a single guide RNA (sgRNA) and showing its potential for targeted genome editing in eukaryotic cells (Cong et al., 2013; Jinek et al., 2012). Since then, massive research has been done on CRISPR system components and applications for fundamental and applied research questions. In 2020, Emmanuelle Charpentier and Jennifer Doudna were awarded the Nobel prize in Chemistry for their achievements in genome editing (https://www.nobelprize.org/prizes/chemistry/2020/press-release/).

In nature, CRISPR/Cas systems occur in bacteria and archaea, where they function in adaptive immunity (Horvath and Barrangou, 2010). CRISPR DNA repeats are present in about 90% of archeal genomes and in about 50% of bacterial genomes. CRISPR-Cas systems are currently categorized into two classes and six types. In class 1 systems a protein complex consisting of several Cas proteins forms for the cleavage of nucleic acids which are complementary to the CRISPR RNA. On the contrary, class 2 systems contain a single effector protein. In type II systems, this is an endonuclease of the Cas9 family. Immune memory is created in CRISPR-Cas systems in three stages: adaptation, precursor CRISPR RNA expression and processing, and interference. The adaptation stage involves the processing and integration of foreign nucleic acids, for instance, from

bacteriophages, into the CRISPR array. The CRISPR array is composed of repeats and spacers, whereby the spacers are derived from the nucleic acids of the intruder. Transcription of the CRISPR array and processing of the resulting precursor CRISPR RNA activates the memory. In case of renewed presence of nucleic acids corresponding to the spacer region, the CRISPR RNA recognizes the intruder via complementarity and acts as a guide. The effector then cleaves the intruding nucleic acids. The protospacer adjacent motif (PAM) is present in all characterized CRISPR-Cas systems with the exception of type III systems, and helps to distinguish between self and the intruder. For cleavage, the PAM is required, while the PAM is absent in the CRISPR array. In this way, auto-immune targeting of the CRISPR array is prevented (Hille et al., 2018; Koonin and Makarova, 2019).

Applications of CRISPR/Cas tools are vast. Generation of mutant alleles by induction of DNA double-strand breaks which can result in mutations due to repair via the error-prone non-homologous end joining (NHEJ) or due to precise sequence exchange by homology-directed repair (HDR) is one example (Ran et al., 2013). Many mutant alleles were generated from genes of many different organisms to analyze gene function in this way. Farther, applications range far beyond generating mutant alleles via induction of a DNA double-strand break at a site of interest. In prime editing, a catalytically impaired Cas9 endonuclease, such as Cas9 nickase, is fused to a reverse transcriptase and a prime editing guide RNA (pegRNA) which determines the target site and the edit. Cas9 nickase does not provoke a double-strand break but only cleaves one DNA strand. The pegRNA interacts with the liberated DNA strand at its primer-binding site, which allows the reverse transcriptase to copy the template part of the pegRNA at the desired position. With this technique, it is possible to introduce all twelve possible base-to-base conversions as well as insertions and deletions at a target site of interest (Anzalone et al., 2019). Another example of the application of CRISPR technology is Cas9-based transcriptional modulation, which can be used to activate or repress the expression of genes of interest (Kanafi and Tavallaei, 2022).

Targeted mutagenesis using CRISPR/Cas can be ubiquitous or cell type-specific in an organism of interest. Expression of *Cas9,* e.g., under the control of a stomatal lineage-specific promoter enabled to generate mutations specifically in stomata with the rest of the plant remaining unaffected (Decaestecker et al., 2019).

Already in 2015, Wang et al. used cell type-specific expression of *Cas9* in order to generate non-mosaic Arabidopsis plants with heritable mutations. They used egg cell-specific expression of *Cas9* and showed that this strategy is successful in generating heritable mutations with high efficiency. This was an improvement over mutants created using constitutive expression of *Cas9,* which were mostly mosaic in the T1 generation, probably due to mutagenesis only after the first embryonic cell division (Wang et al., 2015).

For the generation of knock-out mutants using CRISPR/Cas it is crucial to avoid off-target mutagenesis. CRISPR target sites not similar to other regions in the respective genome need to be selected. Typically, a CRISPR target site consists of 20 base pairs followed by a PAM sequence. For the Cas9 endonuclease of *Streptococcus pyogenes* the PAM is NGG (Ran et al., 2013). For its use in plants, the *Streptococcus pyogenes Cas9* coding sequence was codon optimized (Xing et al., 2014). Induction of the double-strand break happens three base pairs upstream of the PAM (Ran et al., 2013). gRNA design tools assist in selecting suitable target sites, and different gRNA design tools have different advantages and disadvantages concerning, e.g., on-target and off-target prediction (Cui et al., 2018). Off-target mutagenesis was observed for gRNAs with even three mismatching nucleotides to the off-target site in Arabidopsis (Zhang et al., 2018). Generally, mismatches distant from the PAM are tolerated better than mismatches close to the PAM (Hsu et al., 2013). In addition to off-target mutagenesis, in-frame ATGs, which could be used as alternative translational start codons downstream of a frameshift mutation can pose problems when aiming at generating null mutant alleles of a gene of interest. N-terminally truncated proteins can potentially be synthesized (Smits et al., 2019).

In this work, I used egg-cell specific promoter-controlled CRISPR/Cas9 (Wang et al., 2015) to generate *vha-a1* alleles.

1.2 Results

1.2.1 The *vha-a1* mutant is viable and defective in pollen development

In contrast to *vha-a2* and *vha-a3,* no homozygous *vha-a1* T-DNA insertion line has been identified. As V-ATPases are essential for embryogenesis and male gametophyte development (Dettmer et al., 2005; Strompen et al., 2005), *vha-a1* was considered to be not viable. For the analysis of VHA-a1 proteins with amino acid substitutions in a *vha-a1* mutant background CRISPR/Cas9 was used to generate *vha-a1* alleles. The aim was to obtain *vha-a1* null alleles. It was intended to produce alleles that are easy to genotype. To that end, in one approach, a CRISPR construct that contains two gRNAs was cloned to create a *vha-a1* allele with a deletion of the part between the two gRNA target sites. In all, three CRISPR/Cas9 constructs were cloned, one containing two guide RNAs (gRNAs), *CRISPR VHA-a1 I*, and two constructs containing a single gRNA each (*CRISPR VHA-a1 II + III)* for targeting *VHA-a1.* They all contain *Cas9* under the control of an egg cell-specific promoter which allows to generate non-mosaic mutants with inheritable mutant alleles (Wang et al., 2015). Wildtype plants and VHA-a1-GFP expressing plants were transformed with the CRISPR constructs.

T1 plants were analyzed by sequencing the PCR amplified region of the respective CRISPR target site, and independent *vha-a1* alleles were identified. As intended, an allele with deletion of the part between the target sites of gRNA1 and gRNA2 was identified and named *vha-a1-1*. *vha-a1-1* contains a 260 bp deletion which eliminates the *VHA-a1* start codon. Examples of alleles with single base pair insertions which were generated are *vha-a1-2, vha-a1-3* and *vha-a1-4*. They all contain single base pair insertions but in different exons of *VHA-a1*. The single base pair insertions cause frameshifts and early stop codons (Figure 3A).

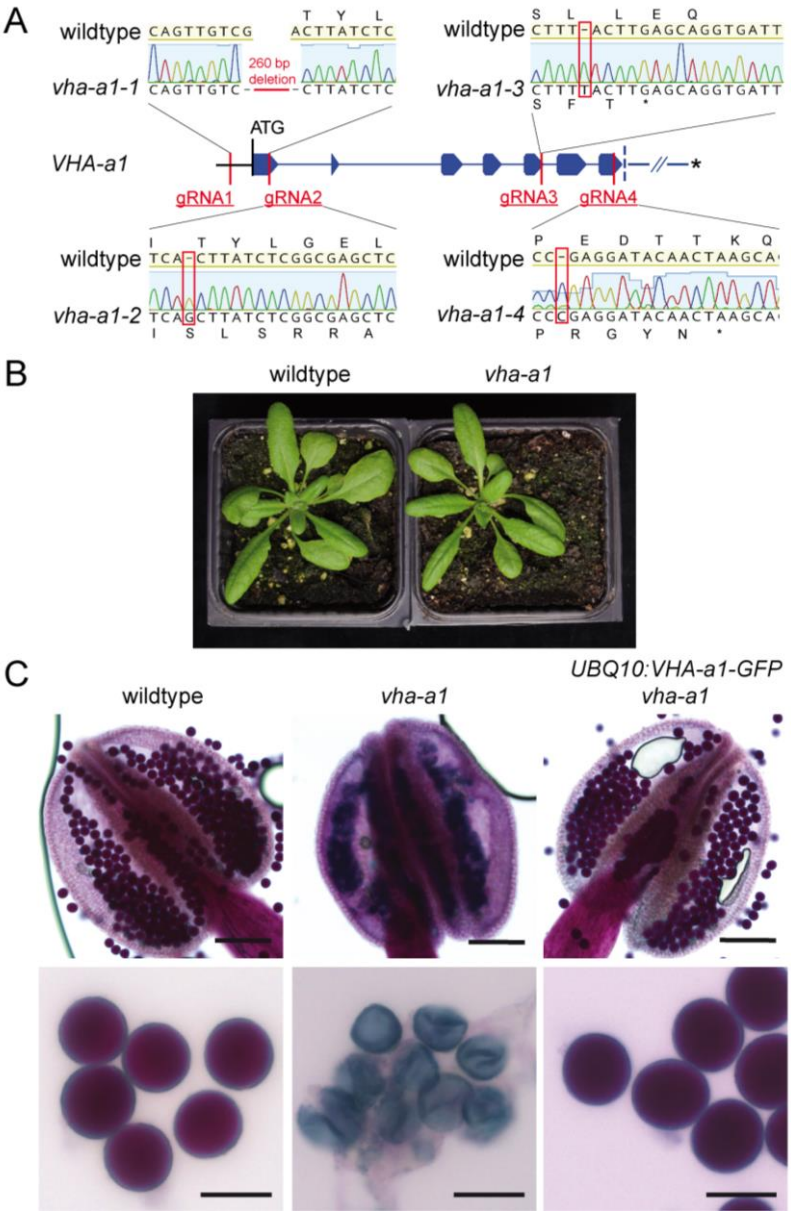

Figure 3. VHA-a1 is essential for pollen development but not for vegetative growth. CRISPR/Cas9 target sites in *VHA-a1* and *vha-a1* alleles that were generated. Shown are the first exons and introns of *VHA-a1*, the target sites of gRNAs directed against *VHA-a1* in independent CRISPR approaches and examples of mutant alleles that were obtained. *vha-a1-1* contains a 260 bp deletion which eliminates the start codon and *vha-a1-2*, *vha-a1-3* and *vha-a1-4* are examples of *vha-a1* alleles which contain a single base pair insertion which causes a frame shift and an early stop codon. **(B)** The *vha-a1* mutant is indistinguishable from wildtype during vegetative development. Plants were grown under long-day conditions (3.5 weeks, 22 °C and 16 h of light). **(C)** Pollen development is defective in *vha-a1,* and *UBQ10:VHA-a1-GFP* rescues pollen development of *vha-a1*. Alexander staining of anthers and microspores is shown. Scale bars, anthers: 100 µm, close-ups of pollen grains: 20 µm. This figure was created by myself and is published in Lupanga et al., 2020. It was modified for this thesis.

Surprisingly, not only in the progeny of transformed *VHA-a1-GFP* plants but also in the T1 of transformed wildtype plants, not just heterozygous *vha-a1/+* but also homozygous and bi-allelic *vha-a1* mutants were obtained. During vegetative development homozygous and bi-allelic *vha-a1* mutants were indistinguishable from wildtype (Figure 3B). However, they were sterile. Analysis of flowers showed that they were defective in pollen development. Alexander staining (Alexander, 1969) of anthers was used to analyze pollen. At the time of pollen release from anthers only debris of microspores was left in *vha-a1* (Figure 3C). Expression of *VHA-a1-GFP* under the control of the *VHA-a1* promoter (Dettmer et al., 2006) and under the control of the *UBIQUITIN10 (UBQ10;* Grefen et al., 2010 ; *UBQ10:VHA-a1-GFP*, this work, Lupanga et al., 2020) promoter rescued the defect in pollen development of *vha-a1*, demonstrating that the phenotype is indeed due to the lack of VHA-a1 (Figure 3C and Supplementary Figure 1).

The transgene *VHA-a1:VHA-a1-GFP* is also a target of all four gRNAs and *UBQ10:VHA-a1-GFP* is targeted by all but gRNA 1. Mutations in the endogenous locus were distinguished from mutations in the transgene by using primers specific for either gene or transgene (Figure 4A). Plants which carried the *vha-a1-2* mutation in the transgene were devoid of VHA-a1-GFP signal, showing that it is indeed a null allele (Figure 4B).

vha-a1 mutants were completely sterile but able to produce progeny if pollinated with wildtype pollen. Reciprocal crosses of *vha-a1-1/+* and wildtype showed that the *vha-a1-1* allele is not transmitted via the male gametophyte. Via the female gametophyte, the transmission of the *vha-a1-1* allele was normal (Figure 4C). Analysis of the progeny of *vha-a1-1* mutants with segregating *UBQ10:VHA-a1-GFP* showed that all homozygous *vha-a1-1* mutants possessed the rescuing *UBQ10:VHA-a1-GFP*. In contrast, heterozygous *vha-a1-1/+* mutants with and without *UBQ10:VHA-a1-GFP* were present.

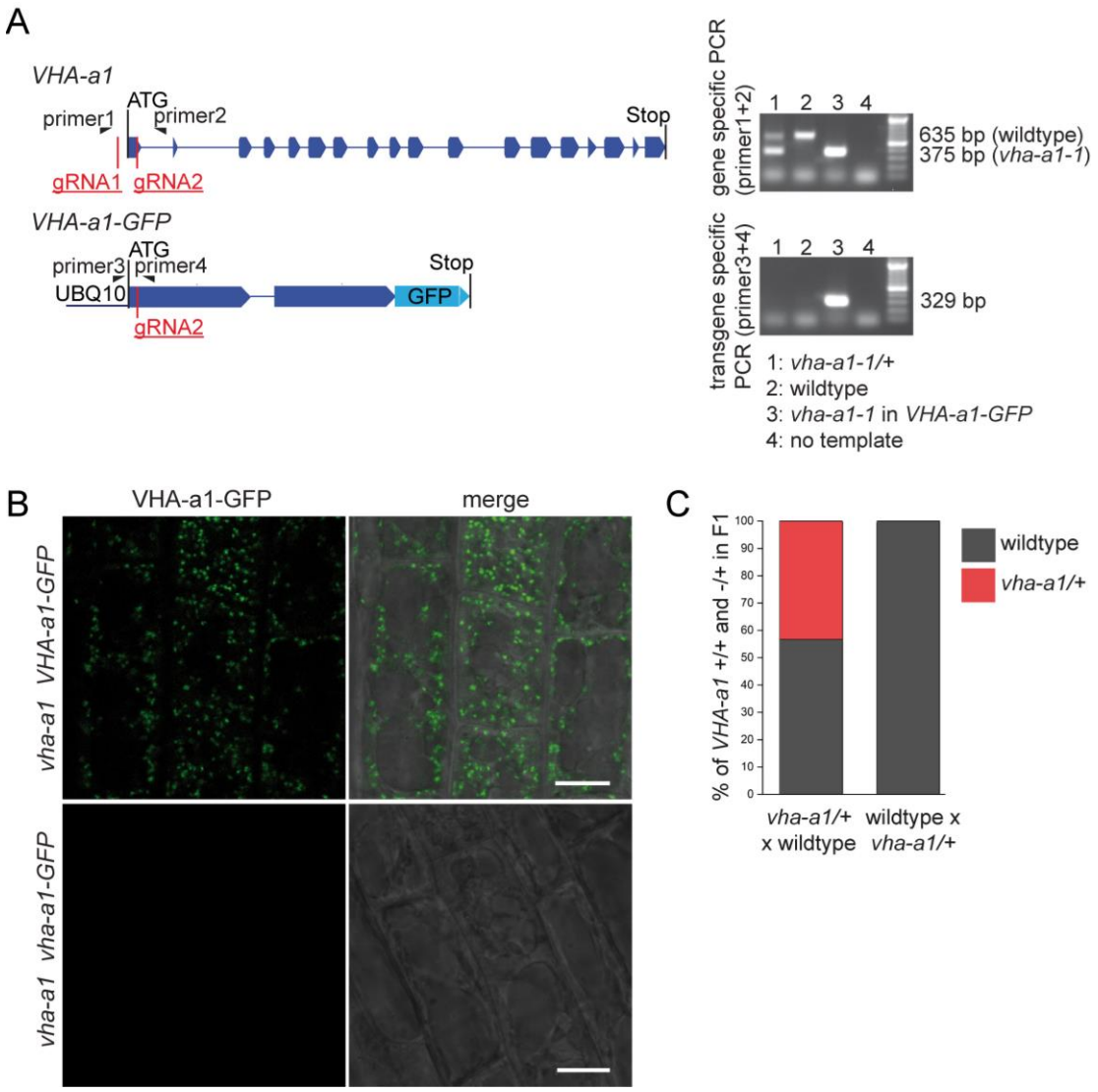

Figure 4. Mutations in *VHA-a1-GFP* result in the absence of GFP signal, and the *vha-a1* allele is not transmitted via the male gametophyte. (A) Gene and transgene specific primers allow distinguishing mutations in *VHA-a1* and *UBQ10:VHA-a1-GFP*. The *vha-a1-1* allele can be genotyped without sequencing. Agarose gel electrophoresis of PCR products leads to a band shift for the *vha-a1-1* allele compared to the wildtype allele due to the 260 bp deletion. **(B)** *UBQ10:VHA-a1-GFP* is a target of gRNA2. Mutations in the transgene *UBQ10:VHA-a1-GFP* corresponding to *vha-a1-2* (1 bp insertion at CRISPR site 2 leading to a frameshift and an early stop codon) led to the absence of GFP signal, indicating that VHA-a1-GFP was absent. Root cells of 8-day-old seedlings were analyzed by CLSM. Scale bars = 10 µm. **(C)** The *vha-a1* mutant allele is not transmitted via the male gametophyte. In reciprocal crosses, *vha-a1/+* x wildtype led to the transmission of the mutant *vha-a1* allele to the next generation, while wildtype x *vha-a1/+* did not. F1 plants analyzed for each of the crosses n = 30. Parts **(A)** and **(B)** of this figure were created by myself, are published in Lupanga et al., 2020, and were modified for this thesis.

When CRISPR-generated male sterile mutants that express *Cas9* in egg cells are pollinated, the incoming wildtype allele can be subjected to targeted mutagenesis after fertilization resulting in bi-allelic and homozygous mutants (Figure 5). After crossing *vha-a1* harboring the CRISPR T-DNA *(Cas9$^+$)* with wildtype and lines expressing transgenes that I wanted to analyze in the *vha-a1* mutant background, homo- or hemizygous lines were identified. A PCR with *Cas9*-specific primers was established to identify plants in which the CRISPR T-DNA is absent (*Cas9*$^-$). If the transgene rescued pollen development of *vha-a1*, homozygous *vha-a1 (Cas9*$^-$*)* mutants were selected in the F2 to maintain stable lines. For transgenes that did not rescue pollen development of *vha-a1,* this strategy enabled their analysis in a *vha-a1* mutant background instead of being limited to analysis in the heterozygous *vha-a1*/+.

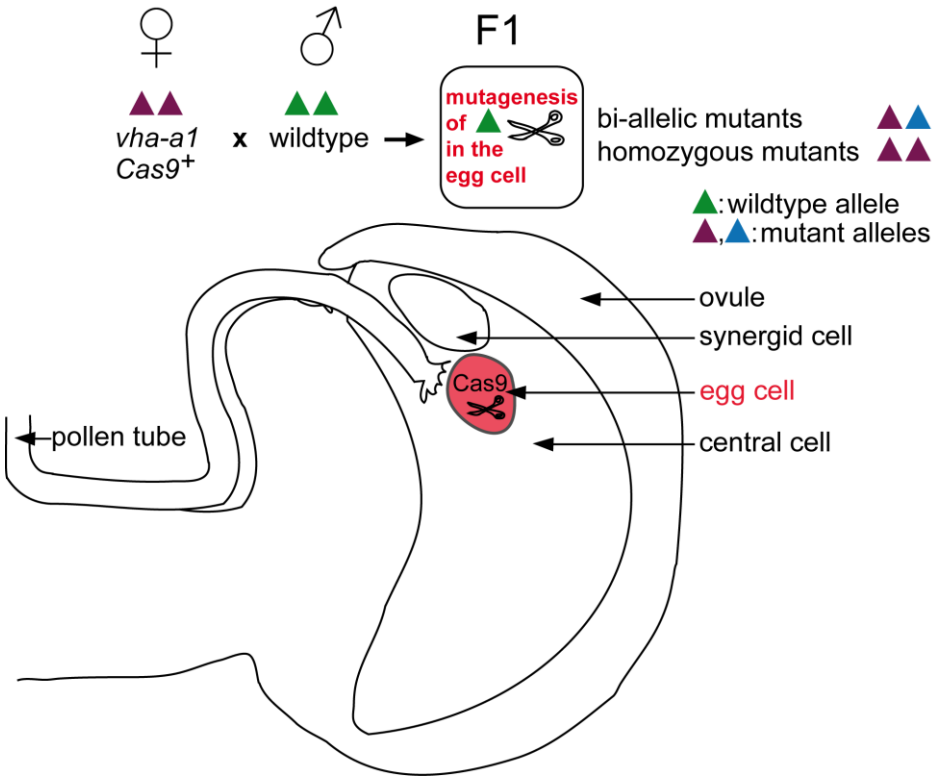

Figure 5. Working with male gametophyte lethal mutants using CRISPR/Cas9. Using a CRISPR system in which *Cas9* is expressed under the control of an egg cell-specific promoter (Wang et al., 2015) enables to work with mutants that are male gametophyte lethal. Male gametophyte lethal mutants (e.g. *vha-a1*) can be pollinated with pollen from a crossing partner (e.g. wildtype). *Cas9* is expressed in the egg cell in mutants that contain the CRISPR T-DNA (*Cas9*$^+$), and the paternal *VHA-a1* can be targeted by the CRISPR gRNA. Targeting the paternal allele can lead to homozygous mutants (if the maternal allele is recreated) or bi-allelic mutants (if a different allele is generated). Heterozygous mutants result if the paternal allele is not mutated.

1.2.2 Dedicated tonoplast VHA-a subunit isoforms compensate for the lack of VHA-a1 during vegetative growth

An explanation for the wildtype-like growth of *vha-a1* could be that the tonoplast dedicated VHA-a2-and/or VHA-a3-containing V-ATPase complexes can compensate for the lack of VHA-a1. To analyze this hypothesis, treatment of seedlings with Concanamycin A (ConcA), a specific inhibitor of V-ATPases (Huss et al., 2002), was used. Progeny of *vha-a1 VHA-a1-GFP (Cas9^{+})* mutants was used for this analysis. Etiolated seedlings in which the transgene was mutated had shorter hypocotyls and aberrant root cells compared to *vha-a1* mutants still expressing VHA-a1-GFP (Figure 6A and B). This suggests that a target of ConcA is present at the TGN/EE in *vha-a1* although in smaller amounts or with increased sensitivity to ConcA. To analyze if VHA-a2 or VHA-a3-containing V-ATPases are able to compensate for the lack of VHA-a1, *vha-a1 (Cas9^{+})* was crossed with *vha-a2 vha-a3* (Krebs et al., 2010).

In the F1 generation *vha-a1 vha-a2*/+ *vha-a3*/+ were identified by genotyping. *vha-a1 vha-a2*/+ *vha-a3*/+ mutants were strongly reduced in growth compared to *vha-a2*/+ *vha-a3*/+ mutants that are indistinguishable from wildtype (Figure 7A and C). This suggested that VHA-a2/VHA-a3-containing V-ATPase complexes compensate for the lack of VHA-a1. To determine if both VHA-a2 and VHA-a3 are indeed able to compensate for the lack of VHA-a1, *vha-a1 (Cas9^{+})* was crossed with the single mutants. Both *vha-a1 vha-a2*/+ and *vha-a1 vha-a3*/+ were reduced in growth (Supplementary Figure 2). *vha-a1 vha-a3*/+ showed a stronger reduction which matches with *VHA-a3* being expressed at higher levels than *VHA-a2*. To obtain mutants with even lower numbers of VHA-a wildtype alleles, *vha-a1 (Cas9^{+}) vha-a2*/+ *vha-a3*/+ was backcrossed with *vha-a2 vha-a3*. In accordance with the results of the crosses with the single mutants, *vha-a1*/+ *vha-a2*/+ *vha-a3* was smaller than *vha-a1*/+ *vha-a2 vha-a3*/+. The smallest plants were *vha-a1 vha-a2 vha-a3*/+ (Figure 7B). Neither *vha-a1 vha-a2*/+ *vha-a3* nor the homozygous triple mutant *vha-a1 vha-a2 vha-a3* was found, suggesting they are not viable. In line with this, transformation of the *vha-a2 vha-a3* double mutant with the construct *CRISPR VHA-a1 II* did not lead to a null triple mutant. In the T1 generation, only wildtype *VHA-a1* sequences were found with the exception of one mutated sequence. This, however, was not a null allele but a 88 bp deletion allele precisely eliminating intron 5 of *VHA-a1* and not affecting the coding sequence.

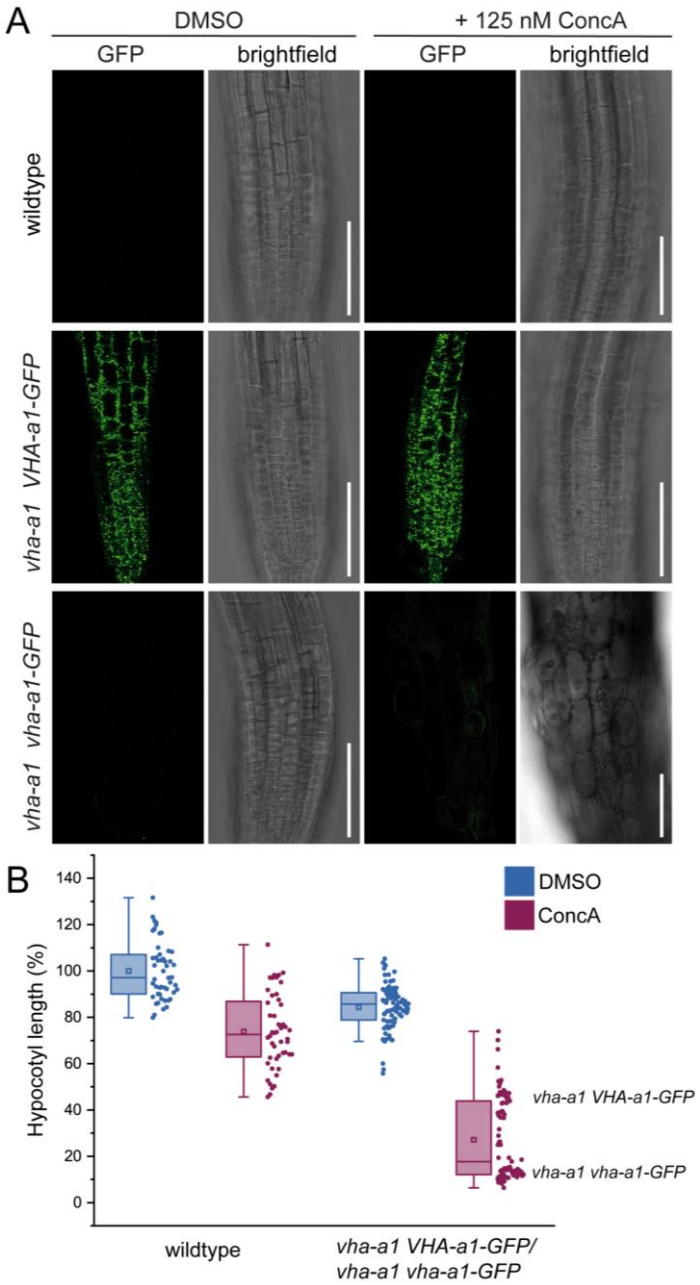

Figure 6. *vha-a1* is hypersensitive to Concanamycin A. (A) *vha-a1 vha-a1-GFP* root cells are hypersensitive to 125 nM Concanamycin A (ConcA), compared to wildtype and *vha-a1* mutants which are rescued by VHA-a1-GFP. Root tips of etiolated seedlings grown on vertically oriented plates (4 h light, 4 days in the dark, 22 °C). Scale bars = 75 µm. **(B)** Hypocotyl length of *vha-a1 vha-a1-GFP* mutants grown as etiolated seedlings further demonstrates the hypersensitivity to ConcA. Plants were grown on horizontally oriented plates (4 h light, 4 days in the dark, 22 °C). Box plot center lines, medians; center boxes, means with n ≥ 48 measurements from three biological replicates; box limits, 25th and 75th percentiles; whiskers extend to ±1.5 interquartile range. Parts **(A)** and **(B)** of this figure were created by Dr. Upendo Lupanga and myself and are published in Lupanga et al., 2020. Colors were modified for this thesis.

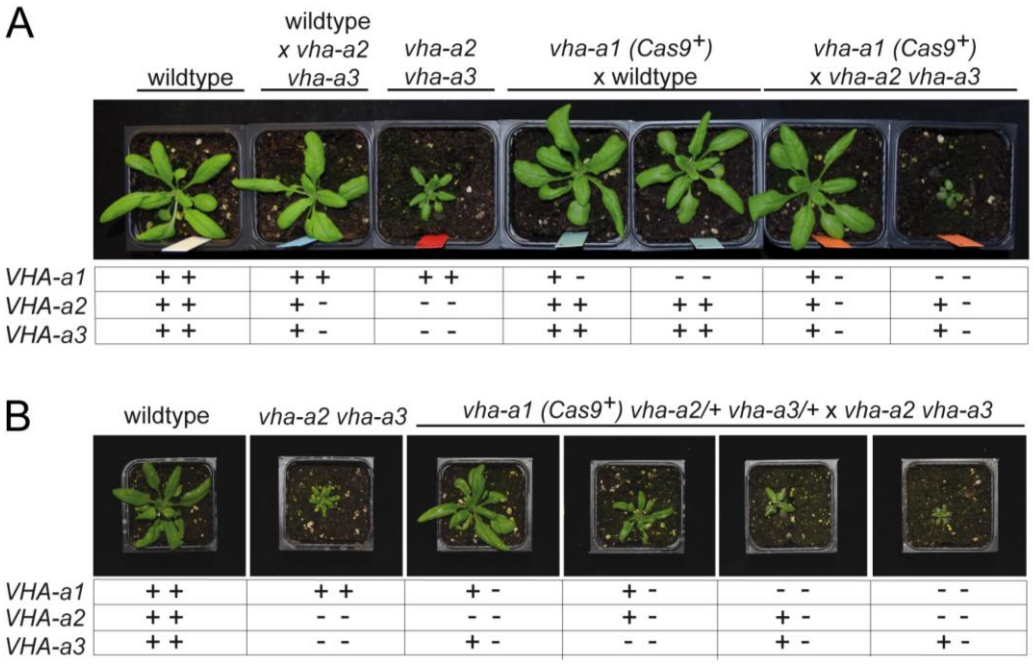
A
wildtype
wildtype x vha-a2 vha-a3
vha-a2 vha-a3
vha-a1 (Cas9+) x wildtype
vha-a1 (Cas9+) x vha-a2 vha-a3
VHA-a1 + + + + + + + - - - + - - -
VHA-a2 + + + - + + - - + + + - + -
VHA-a3 + + + - - - + + + + + - + -
B
wildtype
vha-a2 vha-a3
vha-a1 (Cas9+) vha-a2/+ vha-a3/+ x vha-a2 vha-a3
VHA-a1 + + + + + - + - - - - -
VHA-a2 + + - - - - + - + - - -
VHA-a3 + + - - + - - - + - + -
C
Rosette area (cm²)
24
20
16
8
4
0
n.s
n.s
n.s
n.s
wildtype
vha-a2/+ vha-a3/+
vha-a2 vha-a3
vha-a1/+
vha-a1
vha-a1/+ vha-a2/+ vha-a3/+
vha-a1 vha-a2/+ vha-a3/+

Figure 7. VHA-a2/VHA-a3-containing V-ATPases compensate for the lack of VHA-a1 during vegetative development. (A) *vha-a1 vha-a2/+ vha-a3/+* mutants are reduced in growth. *vha-a1(Cas9^{+})* was crossed with *vha-a2 vha-a3* and in the F1 *vha-a1 vha-a2/+ vha-a3/+* mutants which were small were obtained next to *vha-a1/+ vha-a2/+ vha-a3/+* which were wildtype-like. 3.5 week-old-plants are shown. **(B)** *vha-a1 (Cas9^{+}) vha-a2/+ vha-a3/+* was backcrossed with *vha-a2 vha-a3*. *vha-a1/+ vha-a2/+ vha-a3* is smaller than *vha-a1/+ vha-a2 vha-a3/+* and *vha-a1 vha-a2 vha-a3/+* was the smallest mutant found. 4 week-old-plants are shown. Plants were grown under long-day conditions (16 h of light and 22 °C). **(C)** Quantification of rosette areas of 3.5 week-old plants grown under long-day conditions (16 h of light and 22 °C). Box plot center lines, medians; center circles, means with n≥6 from two biological replicates; box limits, 25th and 75th percentiles; whiskers extend to ±1.5 interquartile range. n.s indicates no significant differences in the mean rosette areas compared to the wildtype mean rosette area (Two-sample t-Test, $p < 0.05$). Parts **(A)**, **(B)** and **(C)** of this figure were created by Dr. Upendo Lupanga and myself and are published in Lupanga et al., 2020. Colors were modified for this thesis.

When grown under long-day conditions, the *vha-a1 vha-a2/+ vha-a3/+* mutant showed purple color, especially at the lower leaf side of several leaves (Supplementary Figure 3). Its phenotype, thus, is substantially different from the phenotype of the *vha-a2 vha-a3* double mutant, which is also reduced in growth but has yellow leaf tips.

In summary, VHA-a2/VHA-a3-containing V-ATPases can compensate for the lack of VHA-a1 in the *vha-a1* mutant.

1.2.3 Detection of VHA-a3 in *vha-a1*

In order to investigate the localization of VHA-a3 in the *vha-a1* mutant, *vha-a1 (Cas9^{+})* was crossed with wildtype plants expressing *UBQ10:VHA-a3-mScarlet*. In the F1 generation, VHA-a3-RFP localization in root cells was analyzed using CLSM, and subsequently *vha-a1* mutants were identified. No difference in VHA-a3-mScarlet localization was found between wildtype, *vha-a1/+* and *vha-a1*. VHA-a3-mScarlet showed tonoplast localization and lacked TGN/EE signal (Figure 8).

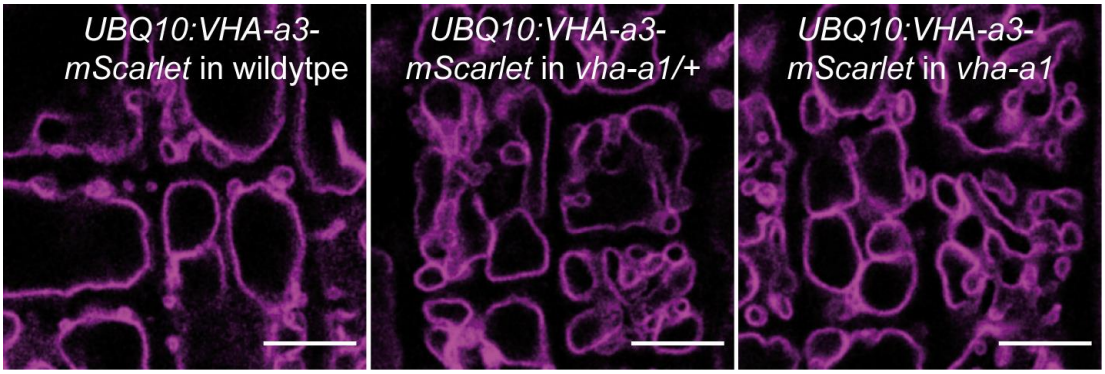

Figure 8. Detection of VHA-a3 in *vha-a1.* CLSM analysis of VHA-a3 tagged with mScarlet and expressed under the control of the *UBQ10* promoter. Tonoplast localization was found for VHA-a3-mScarlet in wildtype, *vha-a1/+* and *vha-a1.* VHA-a3 was not visible at the TGN/EE in *vha-a1.* Root tips of 8-day-old seedlings were analyzed by CLSM. Scale bars = 10 µm.

1.2.4 Site-directed mutagenesis of histidine residues in the VHA-a1 C-terminal half

Site-directed mutagenesis was performed to analyze if histidine residues in the C-terminal half of VHA-a1 are involved in the putative pH sensing by the V-ATPase. Based on their position in a 3D model of VHA-a1, histidine (H) residues were selected (Figure 9). Four of the eleven histidines in the VHA-a1 C-terminal half were excluded from the analysis. They were predicted to be positioned at the cytoplasmic side of the membrane and therefore not relevant for sensing pH in the TGN/EE lumen. Arginine (R) residues mimic a constantly protonated state (Mair et al., 2014). Each of the remaining histidines was mutated to arginine in VHA-a1 tagged with a glycine-serine-rich linker (GSL)-mVenus. First, I analyzed if the histidine substituted VHA-a1 versions localize to the TGN/EE. VHA-a1 H788R and VHA-a1 H793R were not detected in Arabidopsis (Figure 10A). When expressed transiently in *Nicotiana benthamiana* VHA-a1 H788R and VHA-a1 H793R showed signal at the ER (Figure 10B). This indicates that these mutations may render VHA-a1 non-functional and unable to leave the ER. Consequently, mutation of these histidine residues does not allow to investigate the pH sensing capability of the V-ATPase at the TGN/EE. TGN/EE localization was found for VHA-a1 H434R, VHA-a1 H494R, VHA-a1 H613R, VHA-a1 H713R and VHA-a1 H738R. They co-localized with VHA-a1-RFP Figure 10C). Next, a version of VHA-a1 was cloned in which three histidines were mutated at once, considering that histidine residues could

act redundantly in pH sensing. In VHA-a1 H3A three histidines are substituted with alanine (A, VHA-a1 H434A, H494A and H613A). Alanine residues mimic constantly neutrally charged histidine (Mair et al., 2014). The endocytic tracer FM4-64 (Bolte et al., 2004), which is first detectable at the TGN/EE upon entry into cells (Dettmer et al., 2006), co-localized with VHA-a1 H3A, showing that it localizes to the TGN/EE (Figure 11).

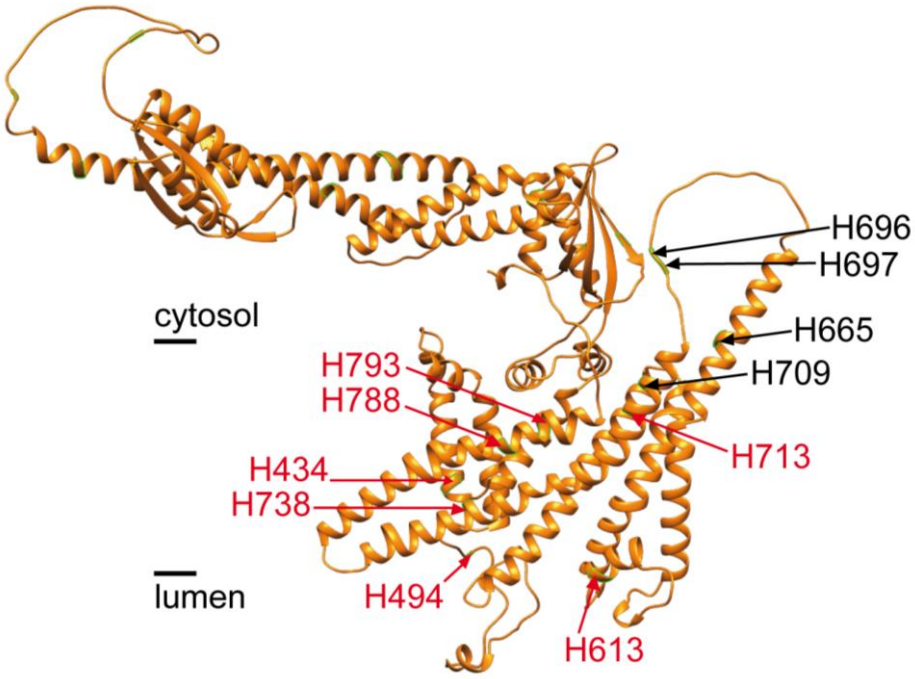

Figure 9. Histidine residues in the VHA-a1 C-terminal half of VHA-a1. 3D model of VHA-a1 showing the cytosolic N-terminal half and the membrane-integral C-terminal half. The eleven histidine residues of the C-terminal half are shown. The histidine residues labeled in red were analyzed. The 3D structure of VHA-a1 was generated using AlphaFold (Jumper et al., 2021; Varadi et al., 2022) and visualized with UCSF Chimera (Goddard et al., 2018; Pettersen et al., 2004).

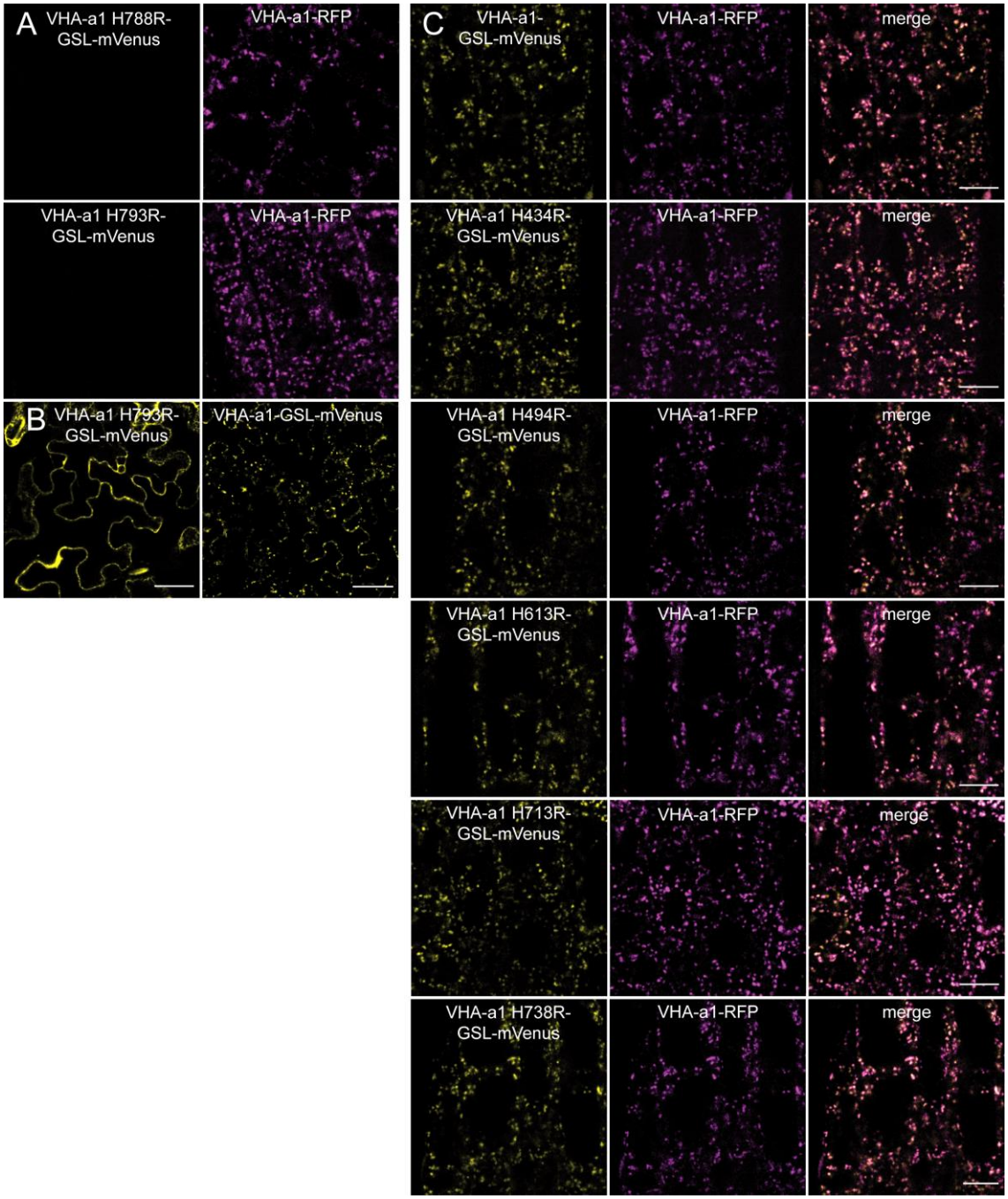

Figure 10. VHA-a1 H788R and VHA-a1 H793R do not reach the TGN/EE. (A) VHA-a1 versions in which histidine (H) 788 or 793 was substituted by arginine (R) were not detected in Arabidopsis root cells. The constructs were tagged with GSL-mVenus and driven by the *UBQ10* promoter. 8-day-old seedlings were analyzed by CLSM. Scale bars = 10 µm. **(B)** In *Nicotiana benthamiana,* VHA-a1 H793R was detected at the ER, while the wildtype protein was detected at the TGN/EE. Leaves were analyzed by CLSM 3 days after infiltration. Scale bars = 50 µm. **(C)** VHA-a1 versions in which histidine (H) 434, 494, 613, 713 or 738 was substituted by arginine (R) co-localized with VHA-a1-RFP at the TGN/EE. 8-day-old seedlings were analyzed. Scale bars = 10 µm.

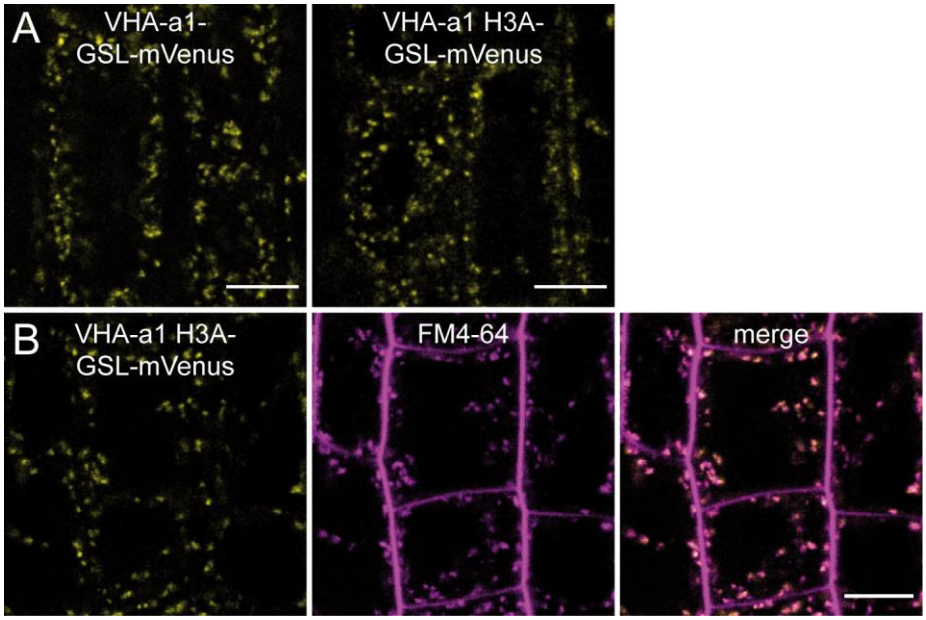

Figure 11. VHA-a1 H3A localizes to the TGN/EE. (A) VHA-a1 H3A in which the three VHA-a1 histidine (H) residues 434, 494 and 613 were mutated to alanine (A) shows the same localization as VHA-a1. VHA-a1 H3A tagged with GSL-mVenus was expressed under the control of the *UBQ10* promoter. **(B)** VHA-a1 H3A co-localizes with FM4-64 at the TGN/EE. Root cells of 6-day-old seedlings were analyzed by CLSM. Scale bars = 10 µm.

1.2.5 VHA-a1 H494R and VHA-a1 H713R rescue pollen development of *vha-a1*

To investigate if the VHA-a1 histidine mutants rescue the defect in pollen development of *vha-a1*, plants expressing the VHA-a1 histidine substitutions tagged with GSL-mVenus were crossed with *vha-a1-1 VHA-a1-GFP (Cas9$^-$)*. As opposed to crossing with *vha-a1-1 (Cas9$^+$)* mutants, this approach was used to circumvent the necessity to monitor mutations in the transgene. This would have been necessary when working with *Cas9*$^+$ mutants, as the *VHA-a1* histidine mutants are also targets of the CRISPR gRNAs. In the F2 generation, PCRs were performed to identify homozygous *vha-a1-1* mutants which do not contain VHA-a1-GFP. *vha-a1-1 carrying UBQ10:VHA-a1 H494R* and *vha-a1-1 UBQ10:VHA-a1 H713R* were obtained, indicating that both constructs rescue pollen development. For *UBQ10:H434R*, *UBQ10:VHA-a1 H613R, UBQ10:VHA-a1 H738R and UBQ10:VHA-a1 H3A,* only *vha-a1-1* mutants that still contained *VHA-a1-GFP* were obtained along with plants without *VHA-a1-GFP* which were

vha-a1-1/+ or wildtype. The same applied to *UBQ10:VHA-a1 H788R,* which does not localize to the TGN/EE and was used as control. The fact that these VHA-a1 versions potentially do not rescue pollen development of *vha-a1* points to the potential importance of the VHA-a1 histidine residues H434, H613 and H738 for a function of the V-ATPase.

In the F3 generation, again genotyping was performed, analyzing the progeny of plants that were identified as heterozygous mutants in F2. For *UBQ10:VHA-a1 H434R* and *UBQ10:VHA-a1 H613R* again only wildtype and *vha-a1-1/+* mutants were identified. For *UBQ10:VHA-a1 H738R* a *vha-a1-1* mutant was identified. *vha-a1-1* carrying *UBQ10:VHA-a1 H738R* was hypersensitive to ConcA (Figure 12A). Moreover, *vha-a1-1 UBQ10:VHA-a1 H738R* had many siliques which were shorter than wildtype siliques (Figure 12B) which indicates that *UBQ10:VHA-a1 H738R* rescues the defect in pollen development of *vha-a1* partially.

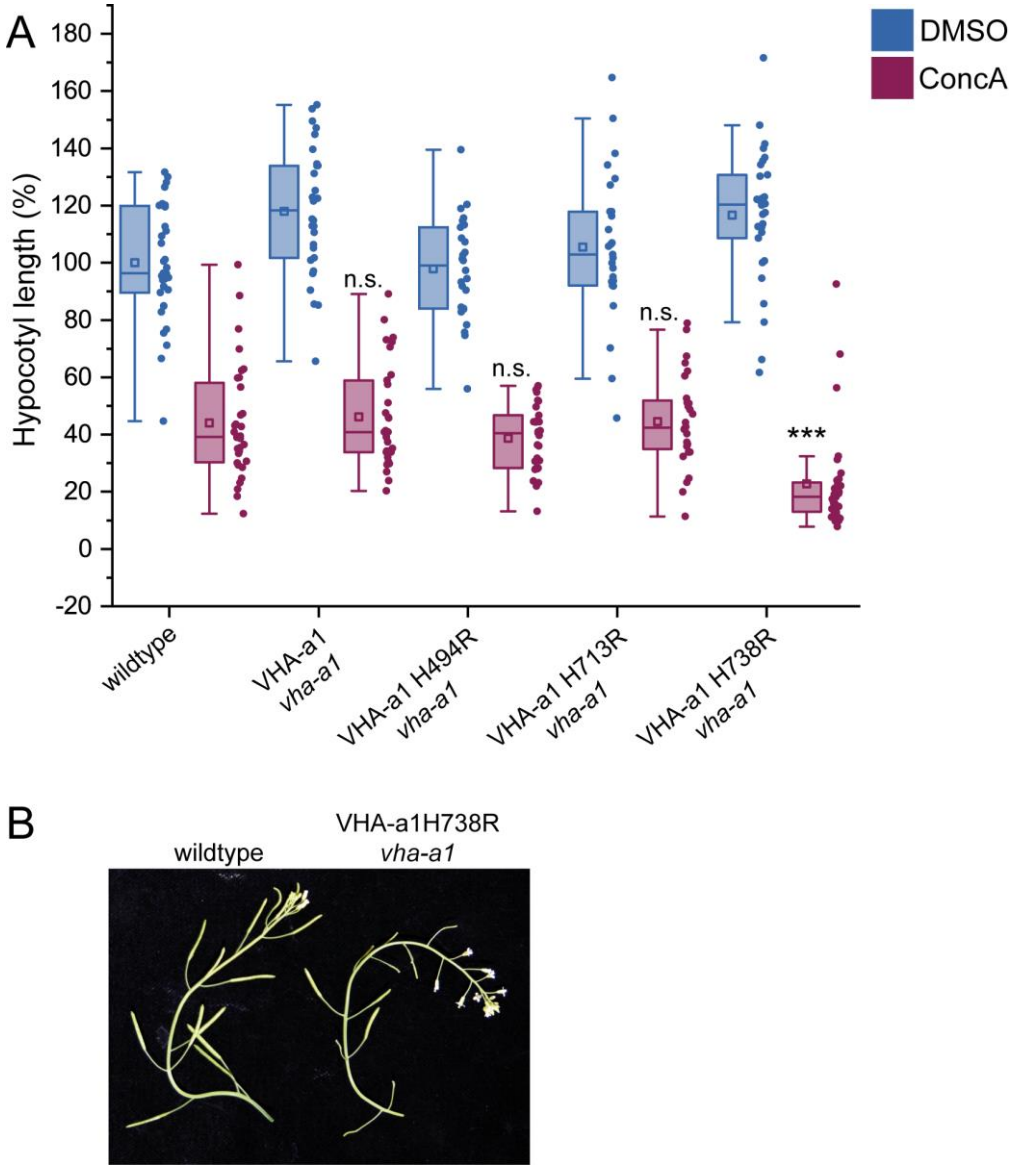

Figure 12 .VHA-a1 histidine mutants in *vha-a1.* (A) *vha-a1* expressing VHA-a1 H738R is hypersensitive to Concanamycin A (ConcA). *vha-a1* mutants expressing VHA-a1, VHA-a1 H494R, VHA-a1 H713R and VHA-a1 H738R tagged with GSL-mVenus under the control of the *UBQ10* promoter were analyzed on 125 nM ConcA. Hypocotyl lengths of etiolated seedlings grown on horizontally oriented plates are shown (4 h light, 4 days in the dark, 22 °C). Box plot center lines, medians; center boxes, means with n ≥ 26 measurements from two biological replicates; box limits, 25th and 75th percentiles; whiskers extend to ±1.5 interquartile range. Asterisks indicate differences in the mean values of ConcA treated wildtype and *vha-a1 VHA-a1 H738R* (one-way ANOVA followed by Tukey's test, ***, $p < 0.001$) n.s., not significant refers to differences in the mean values of ConcA treated wildtype and the remaining ConcA samples (one-way ANOVA followed by Tukey's test with significance levels $p < 0.05$). **(B)** Siliques of wildtype and *vha-a1 VHA-a1H738R*. Many short siliques are visible in *vha-a1 VHA-a1H738R.* Plants were grown under long-day conditions (16 h of light and 22 °C).

1.2.6 Localizing VHA-a1 histidine mutants to the tonoplast

In contrast to *vha-a1*, *vha-a2 vha-a3* has a phenotype during vegetative growth and can be deployed for compensation and functional analysis. Also, tonoplast localization of proteins is advantageous compared to TGN/EE localization due to the practicability of isolation of tonoplast vesicles. Thus, I aimed to localize the VHA-a1 histidine mutants to the tonoplast. Mutations in the VHA-a1 targeting domain (a1-TD) are necessary and sufficient for tonoplast localization of VHA-a1 (Dr. Upendo Lupanga, Lupanga et al., 2020). VHA-a1 L159T and VHA-a1 ΔEEI have been shown to complement the reduced growth phenotype of *vha-a2 vha-a3* (Dr. Upendo Lupanga, Lupanga et al., 2020). Both mutations were combined with H3A expressed under the control of the *UBQ10* promoter. VHA-a1 L159T H3A and VHA-a1 ΔEEI H3A both showed dual localization at the TGN/EE and at the tonoplast in wildtype and *vha-a2 vha-a3* (Figure 13A). Both constructs rescued the phenotype of *vha-a2 vha-a3* to a similar degree as the respective controls, suggesting that mutation of these histidine residues does not influence the functioning of VHA-a1 (Figure 13B).

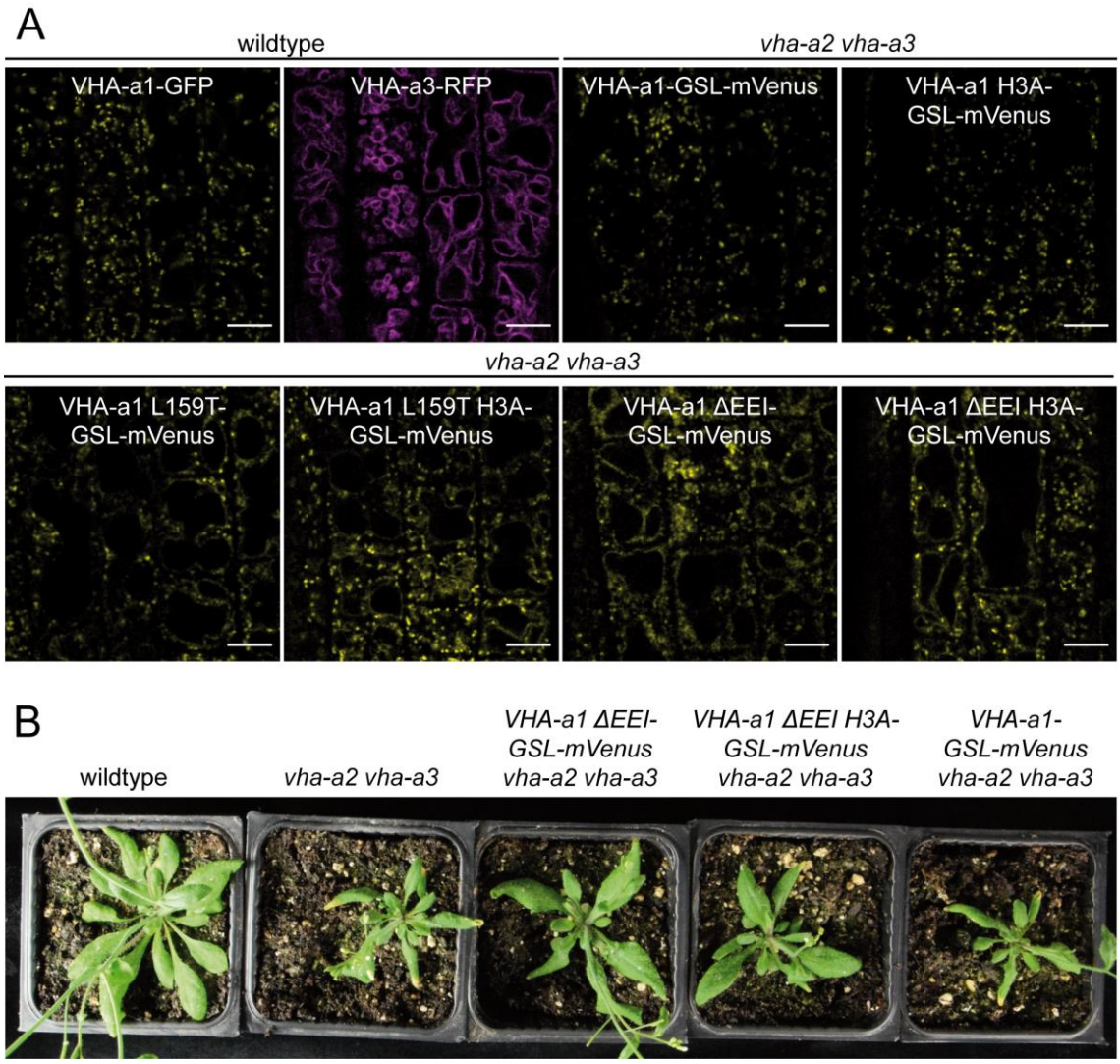

Figure 13. VHA-a1 histidine mutants at the tonoplast. (A) VHA-a1 L159T H3A and VHA-a1 ΔEEI H3A show dual localization at the TGN/EE and tonoplast, as VHA-a1 L159T and VHA-a1 ΔEEI. The constructs were tagged with GSL-mVenus and driven by the *UBQ10* promoter. Root tips of 8-day-old seedlings were analyzed using CLSM. Scale bars = 10 µm. **(B)** VHA-a1 ΔEEI H3A complements *vha-a2 vha-a3* to a similar degree as VHA-a1 ΔEEI. Plants were grown under constant light conditions. H3A, three histidine (H) residues mutated to alanine (A) VHA-a1 H434A, H494A, H613A.

1.3 Discussion

1.3.1 The *vha-a1* mutant is viable

In Arabidopsis, VHA-a1-containing V-ATPases localize to the TGN/EE and VHA-a2 or VHA-a3-containing V-ATPases travel to the tonoplast (Dettmer et al., 2006). The differential localization of V-ATPases raises the question if the specialization of different subunit a isoforms only concerns their localization or if V-ATPases at different localizations fulfill specialized functions. Characterization of the *vha-a1* mutant in this work illustrated the redundancy of subunit a isoforms. Egg-cell specific promoter-controlled CRISPR/Cas9 (Wang et al., 2015) enabled to generate homozygous *vha-a1* null mutants. Different *vha-a1* mutants generated in independent CRISPR approaches using different target sites in *VHA-a1* showed the same phenotype: Wildtype-like during vegetative growth and defective in pollen development. Due to the defect in pollen development there are no homozygous *vha-a1* T-DNA mutants. In contrast, the egg-cell specific expression of *Cas9* allowed to generate homozygous and bi-allelic *vha-a1* CRISPR mutants without male transmission of the mutant allele (Figure 5). It was not clear that the CRISPR approach would lead to *vha-a1* mutants that can be analyzed. Mutants of the gene encoding the V-ATPase VHA-E1 isoform were embryo-lethal (Strompen et al., 2005). However, due to the compensation of VHA-a2/VHA-a3-containing V-ATPases for the lack of VHA-a1, *vha-a1* mutants were obtained.

1.3.2 Functional redundancy of VHA-a isoforms despite differential localization

It was shown here that the *vha-a1* mutant is indistinguishable from wildtype during vegetative growth. In spite of being destined to acidify a different compartment, compensation by the tonoplast dedicated V-ATPase VHA-a isoforms is responsible for the wildtype-like growth of *vha-a1*. This was demonstrated as a further reduction of *VHA-a* wildtype alleles led to a gradually reduced size of mutants. *The vha-a1 vha-a2/+ vha-a3/+* mutant showed a dwarf phenotype and the smallest mutant obtained was *vha-a1 vha-a2 vha-a3/+* (The triple mutant *vha-a1 vha-a2 vha-a3* was not obtained, indicating that it is not viable).

With the specialization for a certain localization, functional diversification of the different isoforms would not have been unlikely. From an evolutionary perspective, VHA-a2 and VHA-a3 belong to the same clade, termed VHA-a3 clade, while VHA-a1 belongs to a separate clade, the VHA-a1 clade. The a1-TD which is necessary and sufficient for TGN/EE localization is conserved within the VHA-a1 clade. It is specific to seed plants. The a1-TD originates in the gymnosperms and is absent from chlorophytes, bryophytes, lycophytes and pteridophytes. The gene duplication event, which resulted in differential intracellular localization of V-ATPases, thus likely occurred in a common ancestor of all seed plants (Lupanga et al., 2020). The results of this study indicate that the gene duplication did not lead to the gain of novel functions for VHA-a1 besides the specialization in localization. VHA-a2/VHA-a3-containing V-ATPases can compensate for the lack of VHA-a1 during vegetative growth. Also the other way around, compensation was shown to be possible. VHA-a1 containing V-ATPases which are mislocalized to the tonoplast due to mutations in the a1-TD can complement the reduced growth phenotype of the *vha-a2 vha-a3* double mutant that lacks V-ATPase activity at the tonoplast (Krebs et al., 2010) to a large degree, although not to wildtype levels (Lupanga et al., 2020; Chapter 1.2.6). That growth compensation and acidification of the vacuole do not reach wildtype levels could be because of a lower coupling efficiency (Shoko Kawasaki-Nishi et al., 2001) or pH-dependent feedback regulation (Rienmüller et al., 2012).

In yeast, two subunit a isoforms are present, Stv1p, which grants Golgi/endosomal network localization, and Vhp1p, which is responsible for targeting V-ATPases to the vacuole (Finnigan et al., 2012). The targeting motif in Stv1p is not found in plant VHA-a isoforms, indicating that differential targeting by subunit a evolved independently multiple times (Lupanga et al., 2020). Upon reconstructions of the ancestral subunit a of yeast, it was proposed that V-ATPases containing the ancestral subunit acidified the Golgi as well as the yeast vacuole. It was further proposed that Golgi-acidification happened while on the way to the vacuole (Finnigan et al., 2011). In line with this, recently, Vhp1p-containing V-ATPases were shown to be the main players in the acidification of the Golgi while on their way to the vacuole, and not the Golgi-resident Stv1p-containing V-ATPases (Deschamps et al., 2020). On the contrary, in Arabidopsis, the TGN/EE-resident VHA-a1-containing V-ATPases are the main players in TGN/EE acidification. Knock-down of *VHA-a1* results in a strong reduction of cell expansion (Brüx

et al., 2008), which is due to reduced V-ATPase activity at the TGN/EE (Luo et al., 2015) and is not the case in the *vha-a2 vha-a3* double mutant (Krebs et al., 2010).

But also in plants a model is plausible in which one ancestral VHA-a acidified the TGN/EE on its way to the tonoplast. The bryophyte *Marchantia polymorpha* has only one subunit VHA-a isoform, which lacks a TGN/EE-retention signal, is present at both the TGN/EE and the tonoplast, and could acidify the TGN/EE on its way to the tonoplast. The situation in Marchantia could represent the ancient condition (Lupanga et al., 2020).

However, the subunit a of Marchantia (MpVHA-a) is not able the rescue pollen development of *vha-a1* (Supplementary Figure 9 ; Lupanga et al., 2020). Due to the lack of an aberrant phenotype of the *vha-a1* mutant during vegetative growth, it cannot be tested whether MpVHA-a can compensate for the lack of VHA-a1 at the TGN/EE during vegetative growth using the *vha-a1* mutant. The fact that MpVHA-a does not rescue the defect in pollen development of *vha-a1*, showed that during pollen development, MpVHA-a cannot compensate for the lack of VHA-a1. This suggested that VHA-a1 could have attained a new function during pollen development. However, the ability of VHA-a3-a1-TD to rescue pollen development of *vha-a1* (Chapter 2) demonstrated that besides localization at the TGN/EE acquired by VHA-a1 no new function was gained. Consequently, the tonoplast-destined isoforms can perform all functions of VHA-a1, at least at standard growth conditions.

On the contrary, adaptive specialization after duplication was shown for other isoforms with differential localization, e.g., the Troponin C isoforms TpnC41C and TpnC4 of Drosophila. Upon knock-out of one of the genes, the other is expressed but the two isoforms were not fully functionally redundant. While the TpnC4 isoform functionally substitutes for TpnC41C, the TpnC41C cannot replace TpnC4 (Chechenova et al., 2017).

The compensation of tonoplast-dedicated VHA-a isoforms in *vha-a1* suggests that they are present at the TGN/EE. In wildtype, VHA-a3 travels to the tonoplast via the provacuolar route, bypassing the Golgi and TGN/EE. In contrast, VHA-a1 leaves the ER via COPII vesicles (Viotti et al., 2013). It can be supposed that the presence of the a1-TD increases the affinity for VHA-a1 for SEC24, the cargo receptor of COPII vesicles, compared to VHA-a3 (Lupanga et al., 2020). This means that in the wildtype situation, there is competition between VHA-a1 and the tonoplast-dedicated VHA-a isoforms for

entry into COPII vesicles. In the *vha-a1* mutant, in the absence of VHA-a1 however, VHA-a2/VHA-a3 might enter COPII-dependent ER-exit (Figure 14).

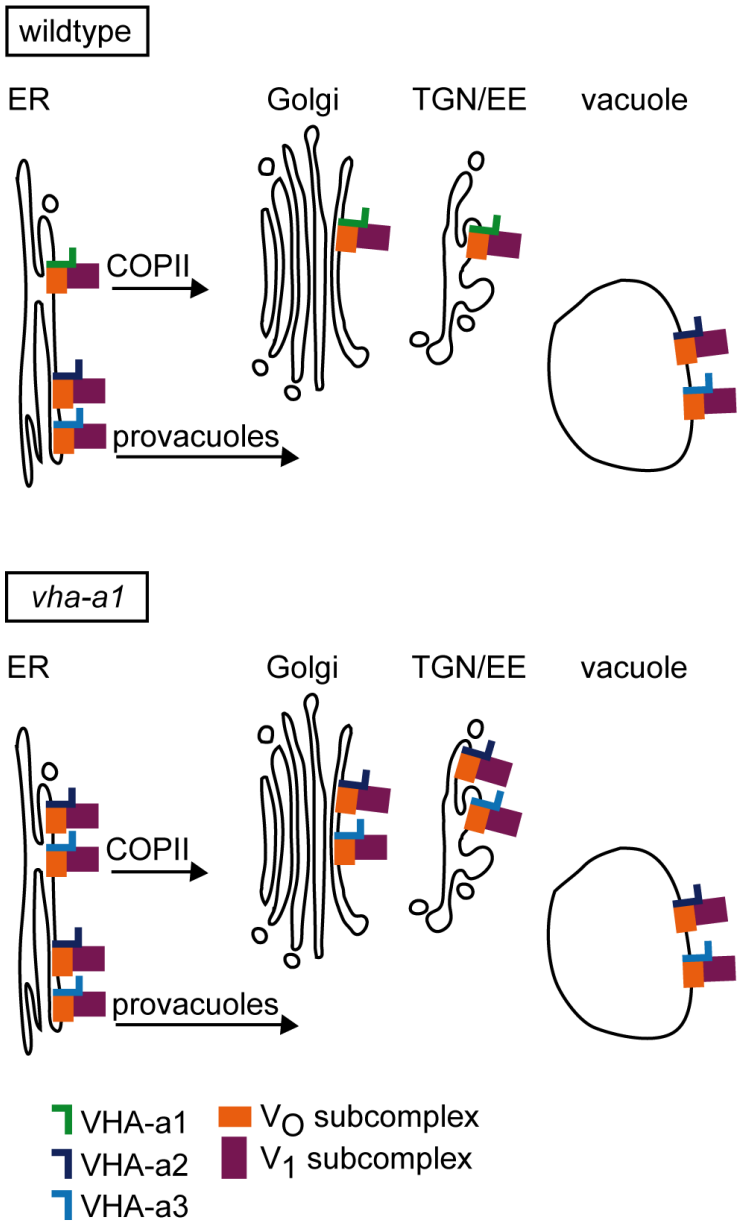

Figure 14. Current model of the trafficking of V-ATPase complexes in wildtype versus *vha-a1*. V-ATPase complexes are assembled at the ER. While in wildtype VHA-a1-containing V-ATPases leave the ER in COPII vesicles (upper part), in the *vha-a1* mutant in the absence of VHA-a1 VHA-a2/VHA-a3-containing V-ATPases enter the COPII-mediated trafficking pathway (lower part). VHA-a2/VHA-a3-containing V-ATPases leave the ER using the provacuolar trafficking pathway and reach the vacuole in a Golgi-and TGN/EE-independent manner (upper and lower parts). Based on Dettmer et al., 2006; Neubert et al., 2008; Viotti et al., 2013; Lupanga et al., 2020 and this work.

1.3.3 Discrepancy of the *VHA-a1* knock-out and knock-down

While VHA-a2/VHA-a3 containing V-ATPases compensate for the lack of VHA-a1 in the *vha-a1* mutant, RNA-mediated inducible knock-down of *VHA-a1* results in reduced cell expansion (Brüx et al., 2008). That VHA-a3 is not able to compensate for missing VHA-a1 in the knock-down situation could be due to competition for entry into COPII vesicles at the ER. In the *VHA-a1* knock-down, VHA-a1 amounts are reduced, but VHA-a1 is still present. This could maintain outcompetition of VHA-a3 by VHA-a1 for entry into COPII vesicles. In contrast, in the *vha-a1* mutant the lack of VHA-a1 could make VHA-a3 enter COPII vesicles and travel to the TGN/EE. VHA-a3-containing V-ATPases could be the more efficient proton pumps, and a few VHA-a3-containing V-ATPases could be enough for compensation. In yeast, a difference in coupling efficiency between V-ATPases containing different subunit a isoforms was found. Vph1p-containing V-ATPases were reported to have a 4-5-fold higher ratio of proton transport to ATP hydrolysis compared to V-ATPases containing Stv1p (Shoko Kawasaki-Nishi et al., 2001).

It is also possible that compensation that reaches the wildtype phenotype requires upregulation of VHA-a2 and VHA-a3 for sufficient protein amounts. mRNAs with mutations such as premature stop codons could act as a trigger for a transcriptional adaptation response. It is assumed that the nonsense-mediated decay pathway, for example, can trigger the upregulation of related genes under knock-out conditions (El-Brolosy and Stainier, 2017).

1.3.4 Detection of VHA-a3 in *vha-a1*

The hypersensitivity of *vha-a1* to the V-ATPase inhibitor ConcA, argues that a target of ConcA is present at the TGN/EE in *vha-a1*. Furthermore, the increasing reduction in rosette size along with the increasingly lower number of VHA-a wildtype alleles of mutant plants, in contrast to the non-aberrant phenotype of *vha-a1*, suggests that VHA-a2/VHA-a3-containing V-ATPases function at the TGN/EE when VHA-a1 is lacking. However, exclusively tonoplast localization was seen when analyzing VHA-a3 fused to fluorescent proteins in the *vha-a1* mutant. As outlined before, small amounts of VHA-a3 at the TGN/EE could be enough for compensation, assuming that VHA-a3 containing

V-ATPases have a high coupling efficiency. The fact that *vha-a1* is hypersensitive to ConcA would comply with small amounts of VHA-a3 at the TGN/EE. Therefore, further CLSM analyses using very bright and photostable fluorescent proteins fused to VHA-a3 could lead to the detection of VHA-a3 at the TGN/EE in *vha-a1*. It is also possible that VHA-a3 was not detected at the TGN/EE in *vha-a1*, because it acidifies the TGN/EE while traveling further to the tonoplast. In *vha-a1*, when there is no competition by VHA-a1 for entry into COPII vesicles, it is plausible that a portion of VHA-a3 leaves the ER using COPII vesicles. It might be that also in wildtype a portion of VHA-a3 travels via COPII-dependent trafficking. Nevertheless, the final destination of VHA-a3 might still be the tonoplast. VHA-a isoforms of the VHA-a3 clade do not possess the a1-TD. The a1-TD was shown to be an ER exit motif as well as a TGN/EE-retention motif (Lupanga et al., 2020). Without the a1-TD, functional VHA-a3 containing V-ATPases, which entered the COPII-dependent trafficking route, might go further to the tonoplast, while VHA-a3-a1-TD is retained at the TGN/EE.

VHA-a3 is able to travel to the TGN/EE. This was reported for VHA-a3 R729N, in which the arginine, which was shown to be essential for proton translocation in the yeast Vph1p (S Kawasaki-Nishi et al., 2001), is mutated to asparagine (Dissertation Neubert, 2012). While retained at the ER in wildtype and localized at the tonoplast in *vha-a2 vha-a3*, upon treatment of wildtype with the V-ATPase inhibitor ConcA VHA-a3 R729N was found at the TGN/EE (Dissertation Neubert, 2012).

It would be interesting to analyze the localization of VHA-a3 R729N in the *vha-a1* mutant. If VHA-a3 R729N localizes to the TGN/EE in *vha-a1* this could mean that non-functional V-ATPase complexes are retained at the TGN/EE while the functional VHA-a3 can travel further to the tonoplast.

These analyses are effortful currently because there are no stable *vha-a1* mutant lines. After crossing *vha-a1 (Cas9^{+})* with a wildtype plant expressing the construct of interest, different genotypes are obtained in the F1. The desired *vha-a1* null mutants are present as well as *vha-a1*/+ mutants and mutants with alleles that are not null alleles. Only after CLSM analysis of seedlings' roots genotyping can be performed to not harm the seedlings before. Working with stable lines would make analyses much easier. The generation of stable lines which are *vha-a1* null during vegetative development and in which a rescue construct (VHA-a1-XFP) is specifically expressed during pollen development is ongoing.

In addition, VHA-a3 was detected at the TGN/EE in the knock-down of the CORVET-specific subunit VPS8, in which VHA-a3 was dual localized at the TGN/EE and the tonoplast (Dissertation Askani, 2022). CORVET is a membrane tethering complex functioning in a specific trafficking pathway from the TGN/EE to the vacuole. This pathway depends on the RAB5-GTPase ARA7 (RAB5-dependent, RAB7-independent) (Takemoto et al., 2018). Expression of a dominant negative form of RAB5-GTPase also resulted in the localization of VHA-a3 at the TGN/EE and the tonoplast (Feng et al., 2017 ; Dissertation Askani, 2022).

1.3.5 What VHA-a1 can do, VHA-a3 can do too – including potentially sense pH

The fact that the *vha-a1* mutant is indistinguishable from wildtype during vegetative growth means there is no function of VHA-a1 that VHA-a2 and VHA-a3 cannot perform, at least under standard growth conditions. I started my investigation of the potential pH sensing capability of the V-ATPase with a specific focus on the TGN/EE-localized V-ATPase (VHA-a1 histidine residues) when I did not know yet about the functional redundancy of VHA-a isoforms. What became obvious after the revelation of the functional redundancy is that histidines that are involved in a potential pH sensing mechanism must be conserved between the VHA-a1 and the VHA-a3 clade. Therefore, it is also possible to use VHA-a3 in future experiments to examine conserved histidine residues of the C-terminal half. Analysis of mutated VHA-a3 proteins in a *vha-a2 vha-a3* background has the advantage that *vha-a2 vha-a3* is not male gametophytic lethal, in contrast to *vha-a1,* and complementation studies and functional analyses can be performed during vegetative growth using stable lines. Moreover, working with tonoplast proteins is easier than TGN/EE-localized proteins. Isolation of tonoplast vesicles is well-established compared to the purification of TGN/EE vesicles.

1.3.6 Hypersensitivity of *vha-a1* VHA-a1 H738R to ConcA

It was shown in this thesis that VHA-a1 rescues *vha-a1*, while *vha-a1* expressing VHA-a1 H738R is hypersensitive to the V-ATPase inhibitor ConcA. *vha-a1 VHA-a1 H738R* showed a stronger reduction in cell expansion than *vha-a1 VHA-a1* upon treatment with ConcA. This further underlines that V-ATPase activity at the TGN/EE is required for cell expansion. It is in line with the elevated TGN/EE pH observed in the *det3* mutant

concomitant with impaired secretion and recycling (Luo et al., 2015). In the *det3* mutant, V-ATPase activity at both the TGN/EE and the tonoplast is affected, as *det3* is a weak allele of the single gene encoding the subunit VHA-C (Schumacher et al., 1999). The *vha-a2 vha-a3* double mutant does not show a strong defect in cell expansion (Krebs et al., 2010), in contrast to the knock-down of *VHA-a1* (Brüx et al., 2008). The increased reduction in cell expansion of VHA-a1 H738R in *vha-a1* compared to VHA-a1 in *vha-a1* underscores that V-ATPase activity at the TGN/EE is crucial for cell expansion. In yeast Vhp1p, mutation of the corresponding histidine residue H743 was reported to decrease V-ATPase activity to 30 – 50% of wildtype activity (Toei et al., 2011). Although mutations of other residues decreased V-ATPase activity even more, e.g., mutation of Vph1p arginine 735 fully abolished proton translocation (S Kawasaki-Nishi et al., 2001), this is a strong decrease. Consequently, it is not astonishing that *VHA-a1 H738R* showed only partial rescue of the defect in pollen development in *vha-a1*. It is consistent with the assumption that there is competition for entry into the COPII-dependent trafficking pathway at the ER. VHA-a1 H738R, which possesses the a1-TD, might outcompete VHA-a3 for the entry into COPII vesicles in *vha-a1*.

1.3.7 The VHA-a1 histidine mutants that have not been shown to rescue the defect in pollen development in *vha-a1*

From the seven VHA-a1 histidine residues analyzed in this work, when singularly mutated to arginine, two did not reach TGN/EE localization, H788 and H793. VHA-a1 H788R and VHA-a1 H793R were not detected in Arabidopsis and were detected at the ER in transient expression in tobacco. Mutation of the corresponding Vph1p histidine residues decreased V-ATPase activity to less than 30% of wildtype activity in yeast (Toei et al., 2011). That the mutated VHA-a1 proteins were not detected in Arabidopsis and were found at the ER in tobacco could mean that these mutations resulted in incorrect protein folding, which led to the immediate degradation of the proteins (Howell, 2013). However, it is also possible that the VHA-a1 subunits harboring these mutations were incorporated into V-ATPase complexes which were then recognized as ineffective proton pumps and were degraded. VHA-a3 in which an arginine that was reported to be essential for proton translocation in the yeast Vph1p (S Kawasaki-Nishi et al., 2001) was mutated to asparagine, VHA-a3 R729N, was shown not to be able to leave the ER in wildtype (Dissertation Neubert, 2012). It was further shown that subunit VHA-C was

co-immunoprecipitated with VHA-a3 R729N, indicating that it was incorporated into V-ATPase complexes. VHA-a3 R729N was shown to be degraded by the 26S proteasome in wildtype. Remarkably, in a *vha-a2 vha-a3* mutant background VHA-a3 R729N was reported to be able to leave the ER and localize to the tonoplast. Treatment of VHA-a3 R729N expressing wildtype plants with the V-ATPase inhibitor ConcA, however, resulted in TGN/EE localization. Moreover, it was shown that the ER chaperone calnexin is required for the retention of VHA-a3 R729N at the ER. Further, VHA-a3E780Q, a VHA-a3 version with reduced V-ATPase activity of about 20% (deduced from the mutation in Vph1p), localized regularly to the tonoplast. A VHA-a3 version with the putative reduced V-ATPase activity to about 10% of wildtype activity, VHA-a3R790K, localized to the tonoplast and the TGN/EE (Dissertation Neubert, 2012). The difference between VHA-a1 and VHA-a3 versions with amino acid substitutions that putatively lead to a strong reduction in V-ATPase activity is concomitant with the different trafficking routes of VHA-a1 and VHA-a3 from the ER. VHA-a1 H788R and VHA-a1 H793R were not detected in Arabidopsis, while VHA-a3 R729N was found at the ER, which could mean that VHA-a1 and VHA-a3 undergo different quality control mechanisms and different degradation pathways. VHA-a1 H788R and VHA-a1 H793R could be quickly degraded, while possibly, there is a control mechanism for the entry into the provacuolar trafficking pathway that selects for V-ATPases with high V-ATPase activity.

VHA-a1 with a single amino acid substitution of one of the other five histidine residues (H434, H494, H613, H713 and H738) by arginine localized to the TGN/EE like the wildtype protein. Also, VHA-a1 H3A, in which histidines 434, 494 and 613 were mutated to alanines, localized to the TGN/EE. Of these VHA-a1 histidine mutants, VHA-a1 H494R and VHA-a1 H713 were able to rescue pollen development of *vha-a1,* and VHA-a1 H738R rescued partially (Chapter 1.3.6). Remarkably, no homozygous mutants without the rescuing VHA-a1-GFP were identified in an analysis of the progeny of the crosses *vha-a1 VHA-a1-GFP (Cas9$^-$)* x VHA-a1 H434R-GSL-mVernus and *vha-a1 VHA-a1-GFP (Cas9$^-$)* x VHA-a1 H613-GSL-mVernus in the F2 and F3 generation. It is possible that analysis of a larger number of plants would lead to identification of *vha-a1 VHA-a1 H434R* and *vha-a1 VHA-a1 H613R*. However, that the same result was obtained for these as for the control, VHA-a1 H788R, which is not detected in Arabidopsis and detected at the ER in tobacco, suggests that they are not able to rescue pollen development of *vha-a1*. This points to the potential importance of VHA-a1 H434 and

VHA-a1 H613 for a function of VHA-a1, potentially for pH sensing (Figure 15). Both of these histidine residues are conserved in the VHA-a1 and the VHA-a3 clade. According to the predicted pK_a values of 3.31 and 6.25 (PROPKA3.0; Olsson et al., 2011), respectively, VHA a1 H434 and VHA-a1 H613, would be able to be differentially protonated upon changing pH inside the TGN/EE (Supplementary Table 1).

To follow up the hypothesis that VHA-a1 H434 and VHA-a1 H613 might not rescue pollen development of *vha-a1*, crosses with *vha-a1 (Cas9$^+$)* can be performed. The presence of the CRISPR T-DNA requires genotyping of gene as well as transgene, as in this case, the transgene is also a target of the gRNA. To circumvent this, it is possible to mutate the CRISPR target site in the transgene to make the transgene resistant to the gRNA. Although laborious, this approach allows to generate homozygous and bi-allelic mutants which express constructs that do not rescue pollen development of *vha-a1*. In this way, *vha-a1 VHA-a1 H434R* and *vha-a1 VHA-a1 H613R* mutants could be obtained and analyzed.

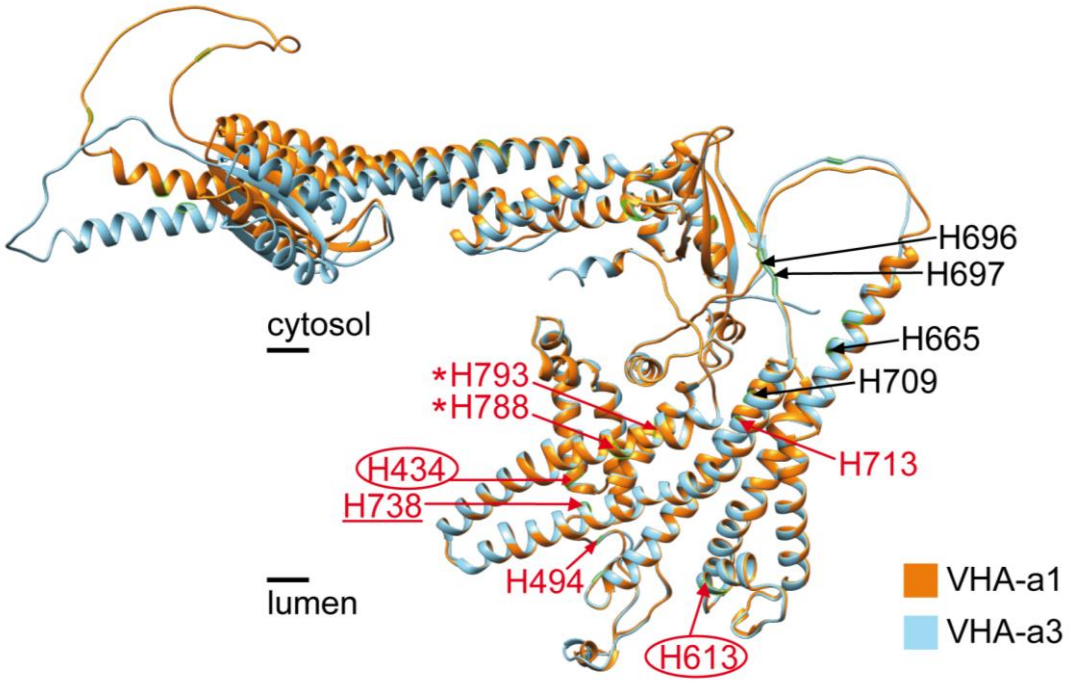

Figure 15. Effects of mutations of histidine residues in the VHA-a1 C-terminal half. 3D models of VHA-a1 and VHA-a3. The histidine residues of the VHA-a1 C-terminal half are labeled. Histidine residues labeled in red were analyzed in this work. For the histidines with encircled labels, when mutated to arginine, the resulting VHA-a1 protein was not found in a homozygous *vha-a1* mutant background so far, suggesting that these histidines could be important for the function of VHA-a1. For the histidines marked with asterisks, when mutated to arginine, the resulting VHA-a1 protein was not detected in Arabidopsis and was detected at the ER in tobacco. For the histidines with no addition to the red labeling, when mutated to arginine, the resulting VHA-a1 was able to rescue pollen development of the *vha-a1* mutant. Concerning the histidine with the underlined label, when mutated to arginine, the resulting VHA-a1 partially rescued pollen development of *vha-a1*. The 3D structures of VHA-a1 and VHA-a3 were generated using AlphaFold (Jumper et al., 2021; Varadi et al., 2022) and analyzed with UCSF Chimera (Goddard et al., 2018; Pettersen et al., 2004).

1.3.8 VHA-a1 histidine mutants at the tonoplast

VHA-a1 H434 and H613 are among the three histidines which have been mutated in VHA-a1 H3A (H434A, H494A and H613A). The VHA-a1 H3A mutations in the C-terminal half of VHA-a1 have been combined with mutations in the a1-TD in the N-terminal half to achieve tonoplast localization. With the protein being localized at the tonoplast,

compensation during vegetative growth could be analyzed using the *vha-a2 vha-a3* double mutant. That VHA-a1 L159T H3A and VHA-a1 ΔEEI H3A complemented the reduced growth of *vha-a2 vha-a3* to a similar degree as VHA-a1 L159T and VHA-a1 ΔEEI, indicates that the histidines are not important for the function of VHA-a1. However, before a conclusion can be drawn, quantification of the rosette sizes of these plants is necessary. These lines can be used for further analyses.

2 Chapter 2: V-ATPases in pollen development

Aims of chapter 2

The question was investigated why VHA-a2/VHA-a3-containing V-ATPases can compensate for the lack of VHA-a1 during vegetative growth but not during pollen development. The second objective was to reveal at which stage in pollen development VHA-a1 is essential.

2.1 Introduction

2.1.1 V-ATPases in pollen development

V-ATPases are essential for pollen development. This was first shown when characterizing a mutant of the gene encoding the catalytic V_1 VHA-A subunit. *VHA-A* is a single-copy gene. Analysis of a T-DNA insertion allele of *VHA-A* revealed complete male gametophytic lethality (Dettmer et al., 2005). Mutants exist in which the microspores cannot separate after the tetrad stage, yet the microspores which stay together are viable. This feature can be harnessed for tetrad analysis which enables to observe two mutant and two wildtype pollen grains together when heterozygous mutants are investigated (Preuss et al., 1994). Tetrad analysis of *vha-A/+* in a *quartet* mutant background showed two normal-looking and two aborted pollen grains. It was found that around the time of the second mitosis, many tetrads with only two viable microspores were present (Dettmer et al., 2005). Of the V-ATPase subunit VHA-E which is part of the peripheral stalk, three isoforms exist. VHA-E1 is essential for embryogenesis, VHA-E3 is mainly expressed in the endosperm and maternal tissues during seed development, and VHA-E2 is pollen-specific. At the early stages of pollen development, VHA-E1 was found in the microspore, while later in pollen development it was only detected in the two sperm cells. VHA-E2 was found in the vegetative cell, and VHA-E3 was found in the vegetative cell and in the sperm cells in mature pollen (Strompen et al., 2005). Concerning the subcellular localization of the VHA-E isoforms in microspores, VHA-E1 and VHA-E3 were found at the tonoplast in unicellular microspores, while VHA-E2-GFP was found in dots and was absent from the tonoplast. VHA-E2 belongs to an ancient clade consisting of both monocot and dicot sequences which is found in all higher plants, and the other members of this clade are also expressed specifically in pollen. However, analysis of *vha-E2* mutants showed that VHA-E2 is not essential for pollen development (Dettmer et al., 2010).

2.1.2 Pollen development and formation of the pollen wall

The reproductive structures of angiosperms, which constitute about 90% of all living land plants and to which Arabidopsis belongs, are flowers (Sauquet et al., 2017). In the Arabidopsis flower, four whorls of organs form, sepals, petals, stamens and the carpel.

Stamens are composed of anthers in which pollen develop and filaments which are stalks that carry the anthers. Stamen primordia contain three germ layers L1, L2 and L3 which give rise to the anther. L1 develops into the epidermis, L2 gives rise to the archesporial cells, which develop into the endothecium, middle layer, tapetum and microspores, and L3 forms the vascular and connective tissues. Of the four layers of the anther wall, epidermis, endothecium, middle layer and tapetum, the tapetum is the innermost layer next to the developing microspores. Anther development is remarkably conserved in angiosperms, in contrast to the diversification of stamen form and function and flower development which varies greatly between families of the angiosperm clade (Åstrand et al., 2021).

During the course of pollen development (Figure 16) communication between the different anther cells needs to be highly coordinated. Diploid microspore mother cells undergo meiosis giving rise to four haploid microspores that are arranged in tetrads. Microspores become free in the anther locule upon dissolution of the transient callose wall. Microspores become larger and undergo an asymmetrical division, pollen mitosis I, which leads to a generative cell in the vegetative cell. The generative cell undergoes pollen mitosis II, generating two sperm cells (Liu and Wang, 2021; Sanders et al., 1999). For double fertilization in the ovule, pollen tube growth through the pistil and support of the vegetative cell for the transport and development of the two sperm cells is required. One of the sperm cells will fuse with the egg cell to produce the embryo, and the other sperm cell will fuse with the central cell to produce the endosperm (Berger et al., 2008).

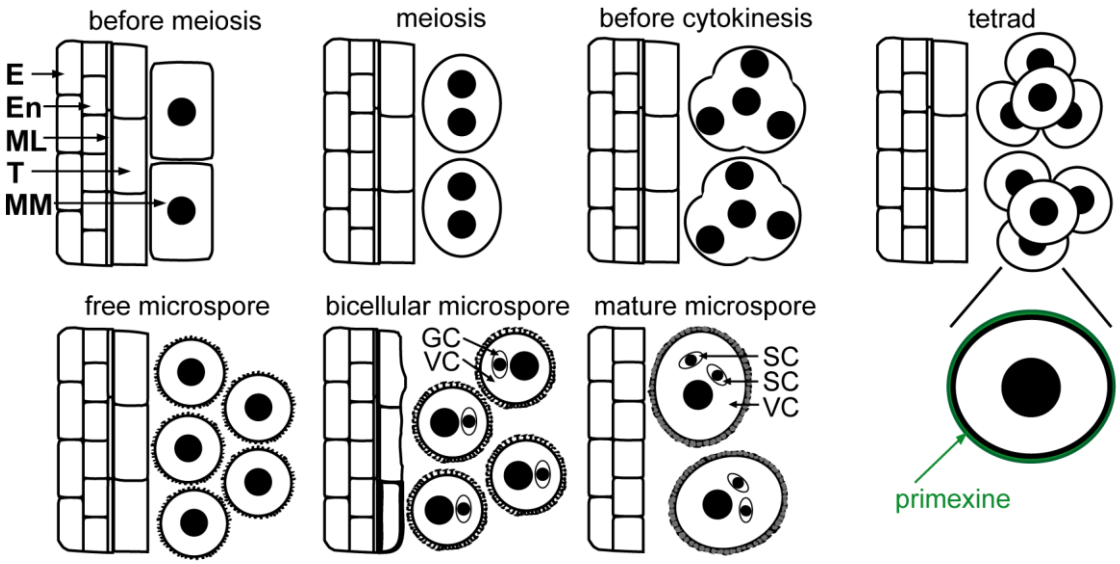

Figure 16. Pollen development in *Arabidopsis thaliana.* Diploid microspore mother cells undergo meiosis. After meiosis I and II, simultaneous cytokinesis takes place, resulting in haploid microspores arranged in tetrads. Development of the pollen wall starts at the tetrad stage with the formation of the primexine (shown in green). Microspores are free in the locule upon dissolution of the transient callose wall. Mitosis I happens to generate bi-cellular microspores with generative cells inside the vegetative cells. Mitosis II produces tricellular microspores in which the vegetative cell contains two sperm cells. The cells of the anther wall modulate their form and function during pollen development. E, epidermis; En, endothecium; ML, middle layer; T, tapetum; MM, microspore mother cell; GC, generative cell; VG, vegetative cell; SC, sperm cell.

Immense remodeling of microspores occurs during pollen development. The sporophytic anther tissues take part by releasing cues and providing materials and by drastically changing their own forms and functions. The endothecium drastically changes its appearance and expands greatly prior to pollen release (Sanders et al., 1999). The middle layer stops cell division at the stage of meiosis and degrades in the course of anther development (Xue et al., 2021). The tapetum is also a transient anther layer. It contains very specialized organelles and supplies the developing microspores with various molecules that they need. Tapetal cells undergo highly structural changes and finally undergo programmed cell death (Quilichini et al., 2014). Tapetal cells have high secretory activity. In this way, they play a role in the dissolution of the transient callose wall by secretion of callases into the anther locule. Another important function of the tapetum is the secretion of pollen wall material. The pollen wall consists of exine, intine and tryphine. Intine formation is assumed to be mainly controlled by the microspore (Shi

et al., 2015). Tapetal cells synthesize sporopollenin, which is the major component of the exine, and they also synthesize material for the tryphine (Blackmore et al., 2007). Sporopollenin is a complex polymer consisting of fatty acid derivatives, phenylpropanoids and phenolics. It is also referred to as the “diamond of the plant world” as it is extremely tough and resistant when confronted with pressure, heat, non-oxidative chemicals and biological stresses. As such, sporopollenin is pivotal for desiccation-tolerant gametophytes. It is not only found in pollen but also in the outer shell of land plant spores. Genes encoding key enzymes in the biosynthesis of sporopollenin are conserved among land plants, suggesting that it helped plants to proliferate successfully on dry land. For the colonialization of land by plants, the ability to produce sporopollenin is assumed to be pre-adaptive, as the ability to produce sporopollenin was also found in algae (Ariizumi and Toriyama, 2007; Grienenberger and Quilichini, 2021; Hackenberg and Twell, 2019).

Pollen wall formation starts with the formation of the primexine at the tetrad stage. The primexine is a thin extracellular layer that forms outside of the microspore plasma membrane (Wang et al., 2021). The primexine functions as a scaffold for developing exine elements, it is essential for sporopollenin deposition. Defective primexine formation constitutes one category of defects that leads to aberrant exine pattern formation, besides defective sporopollenin synthesis and defective callose wall formation. Examples of mutants that are defective in primexine formation are the male sterile mutants *dex1*, *nef1*, *rpg1*, *tde1* and *ms1*. Heterozygous plants of these primexine mutants produce normal primexines. Hence, it has been proposed that primexine formation could be under the control of the diploid sporophytic anther tissues, but little is known (Ariizumi and Toriyama, 2011, 2007). Primexine formation could be under sporophytic or gametophytic control or both.

Mature pollen walls consist of the intine, the innermost layer, the exine, which can be subdivided into the nexine and the sexine (baculum and tectum), and the tryphine, which was deposited in the exine cavities and on the exine surface (Ariizumi and Toriyama, 2011).

In this work, I analyzed why VHA-a2/VHA-a3 do not compensate for the lack of VHA-a1 in pollen development by examining the presence and localization of V-ATPase complexes in anthers and studying the defect in pollen development of *vha-a1*.

2.2 Results

2.2.1 VHA-a1 and VHA-a3 are present throughout pollen development

To understand why VHA-a2/VHA-a3-containing V-ATPases compensate for the lack of VHA-a1 during vegetative growth but not during pollen development, we investigated the presence and functions of VHA-a1 and VHA-a3 in pollen development. At first, I examined when and where in pollen development VHA-a1 and VHA-a3 are present. Plants expressing VHA-a1-GFP and VHA-a3-RFP under the control of their own promoters (Dettmer et al., 2006; Brüx et al., 2008) were used for this analysis. Besides, plants additionally expressing the signal recognition particle receptor (SR) subunit SRβ tagged with mTurquoise under the control of the *UBQ10* promoter (*UBQ10:SRβ-mTurquoise*, Dr. Jana Askani) were used. SRβ is a membrane integral protein that localizes to the rough endoplasmic reticulum (Miller et al., 1995) and was useful for visualizing the position and number of nuclei in microspores due to its localization at the nuclear envelope. CLSM analysis of anthers was performed, which had been fixed and cleared using ClearSee (Kurihara et al., 2015).

Both VHA-a1-GFP and VHA-a3-RFP were detected in microspores at all stages of pollen development and did not co-localize (Figure 17, Supplementary Figure 5, Supplementary Figure 6 and Supplementary Figure 7). VHA-a1-GFP and VHA-a3-RFP were not only present in the microspores but also in all cell types of the anther wall. Particularly noticeable was the strong VHA-a1-GFP signal in cells of the tapetum (Figure 18, Supplementary Figure 10 and Supplementary Figure 11). As VHA-a3 was present during all stages of pollen development, it can be ruled out that the reason why VHA-a3 does not rescue pollen development of *vha-a1,* is that VHA-a3 is not expressed at a particular stage during pollen development.

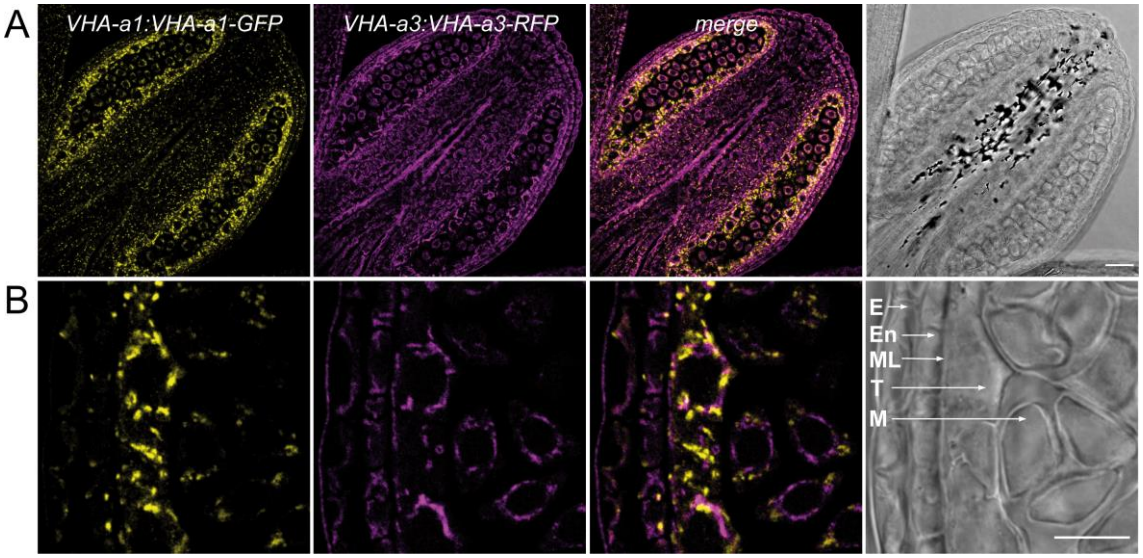

Figure 17. VHA-a1-GFP and VHA-a3-RFP in anthers at the tetrad stage. (A) Anthers at the tetrad stage from plants expressing *VHA-a1-GFP* and *VHA-a3-RFP* under the control of their own promoters. CLSM analysis was performed using cleared anthers. Scale bar = 25 µm. **(B)** Close-up on anther wall and developing microspores. E, epidermis; En, endothecium; ML, middle layer; T, tapetum; M, microspore; scale bar = 10µm.

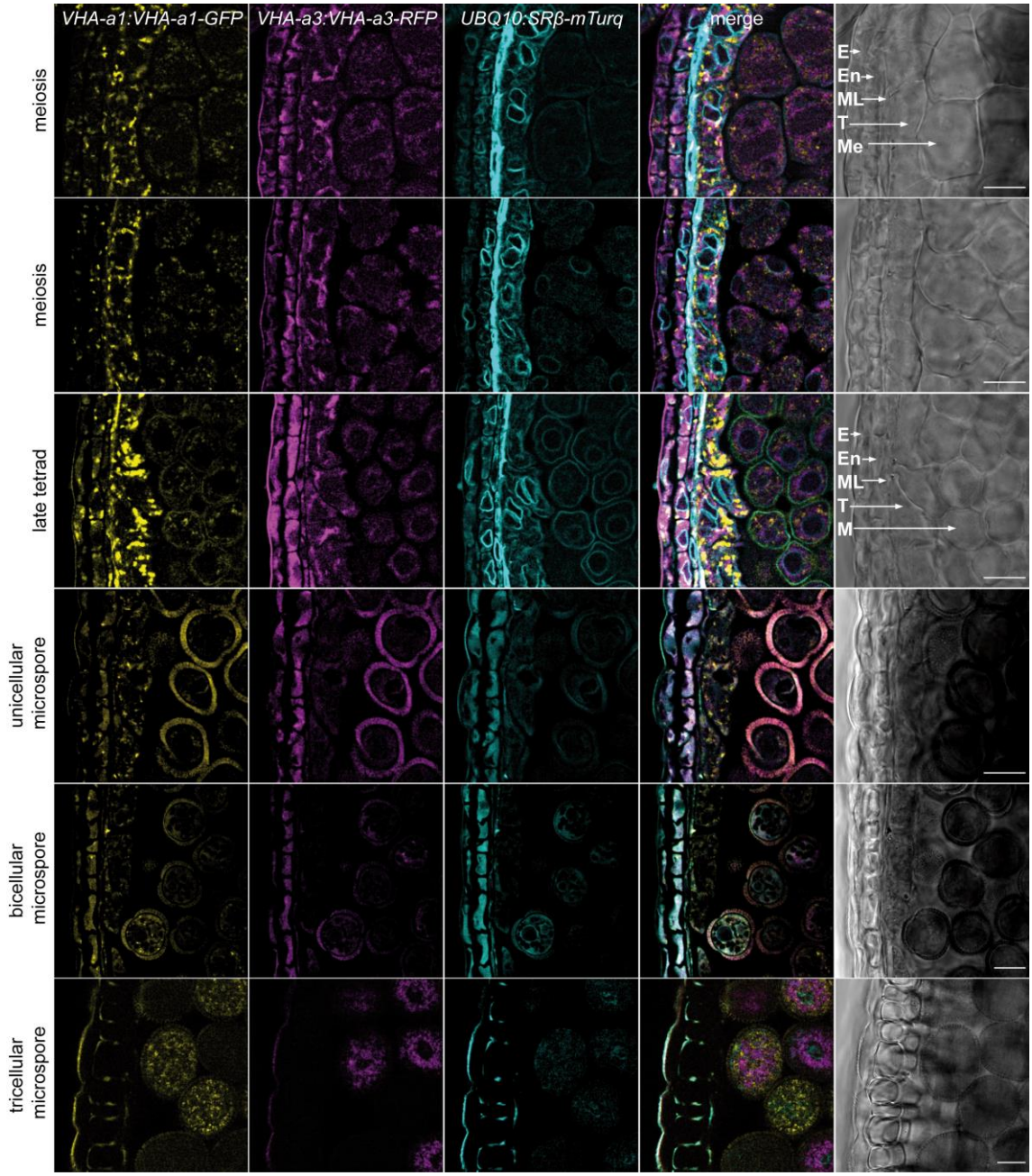

Figure 18. VHA-a1-GFP and VHA-a3-RFP in pollen development. Anthers were harvested from F1 plants with segregating *VHA-a1:VHA-a1-GFP*, *VHA-a3:VHA-a3-RFP* and *UBQ10:SRβ-mTurquoise.* CLSM analysis was performed using cleared anthers of developmental stages from meiosis to the tricellular microspore stage. E, epidermis; En, endothecium; ML, middle layer; T, tapetum; Me, meiocyte; M, microspore; scale bars = 10 µm.

2.2.2 TGN/EE localized V-ATPases are essential for pollen development

Having excluded the possibility that VHA-a3 is absent at a critical stage in pollen development, I next asked why VHA-a3 despite being present cannot compensate for the lack of VHA-a1 in pollen development. Firstly, it could be that VHA-a3 amounts are not sufficient. Thus, in the following analysis, the *UBQ10* promoter was used to drive *VHA-a3* expression. *UBQ10*-driven expression of *VHA-a1* was known to rescue pollen development of *vha-a1* (Figure 3C). *vha-a1 (Cas9^{+})* was crossed with wildtype plants expressing *UBQ10:VHA-a3-GFP.* In the F1 generation CLSM analysis was performed to ensure that VHA-a3-GFP was present (Figure 19B). Subsequently, plants were genotyped and *vha-a1* mutants were identified. *vha-a1* mutants expressing *UBQ10:VHA-a3-GFP* were sterile (Figure 19A and Supplementary Figure 8). The fact that VHA-a3 does not rescue pollen development even when expressed under *UBQ10* argued that VHA-a1 might have acquired a novel function during evolution required for pollen development, which VHA-a3 does not have. Thus, I analyzed if a version of VHA-a3 that contains the VHA-a1 targeting domain necessary and sufficient to target VHA-a3 to the TGN/EE (Dr. Upendo Lupanga, Lupanga et al., 2020) rescues pollen development of *vha-a1*. *vha-a1 (Cas9^{+})* was crossed with wildtype plants expressing *UBQ10:VHA-a3-a1-TD-GFP* and the F1 progeny was analyzed. *vha-a1 UBQ10:VHA-a3-a1-TD-GFP* mutants were fertile (Figure 19A). Thus, *UBQ10:VHA-a3-a1-TD-GFP* rescues pollen development of *vha-a1*. As VHA-a3-a1-TD rescues pollen development of *vha-a1*, we concluded that beyond TGN/EE-localization VHA-a1 has not acquired additional novel functions and that TGN/EE-localization of V-ATPases is essential for pollen development.

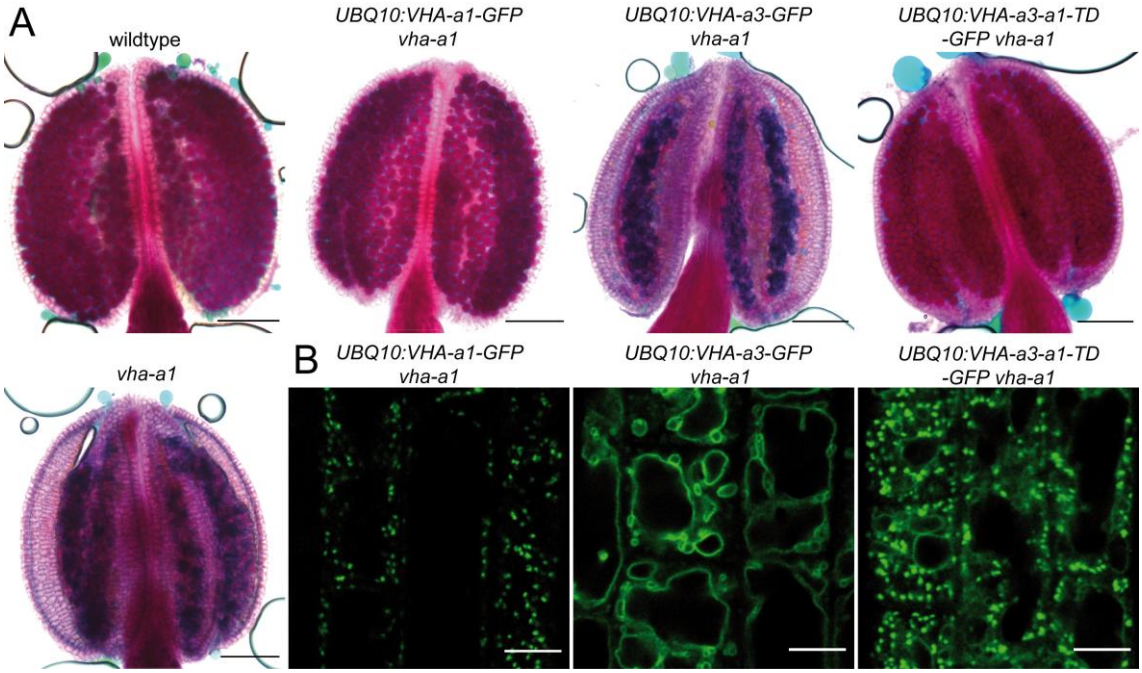

Figure 19. TGN/EE-localized V-ATPases are essential for pollen development. (A) Alexander staining shows viable microspores in wildtype anthers and aborted microspores in *vha-a1* anthers. VHA-a1-GFP and VHA-a3-a1-TD-GFP rescue male gametophyte development of *vha-a1* while VHA-a3-GFP does not. The *UBQ10* promoter was used in all cases. Scale bars = 100 µm. **(B)** Subcellular localization of VHA-a1-GFP, VHA-a3-GFP and VHA-a3-a1-TD in *vha-a1* at the TGN/EE, the tonoplast and both TGN/EE and tonoplast, respectively. CLSM analysis of root cells of 8-day-old seedlings. Scale bars =10 µm.

2.2.3 Pollen development is not affected in the heterozygous mutant

In contrast to the homozygous *vha-a1* mutant, which is sterile, the heterozygous mutant lacks aborted microspores at the time of pollen release, as shown by Alexander staining. Instead of possessing the expected ratio of 1:1 aborted versus wildtype-like microspores, only wildtype-like microspores were present in *vha-a1*/+ anthers (Figure 20A). However, reciprocal crosses had shown that the mutant *vha-a1* allele was not transmitted via the male gametophyte. To investigate whether exine morphology is aberrant in *vha-a1* pollen in the *vha-a1*/+ mutant, CLSM analysis was performed using the autofluorescent properties of the exine. No difference between the exine of pollen from wildtype and pollen from *vha-a1*/+ was observed (Figure 20B). This suggests that in the *vha-a1*/+ mutant a defect occurs after pollen release, which prevents the transmission of the mutant *vha-a1* allele.

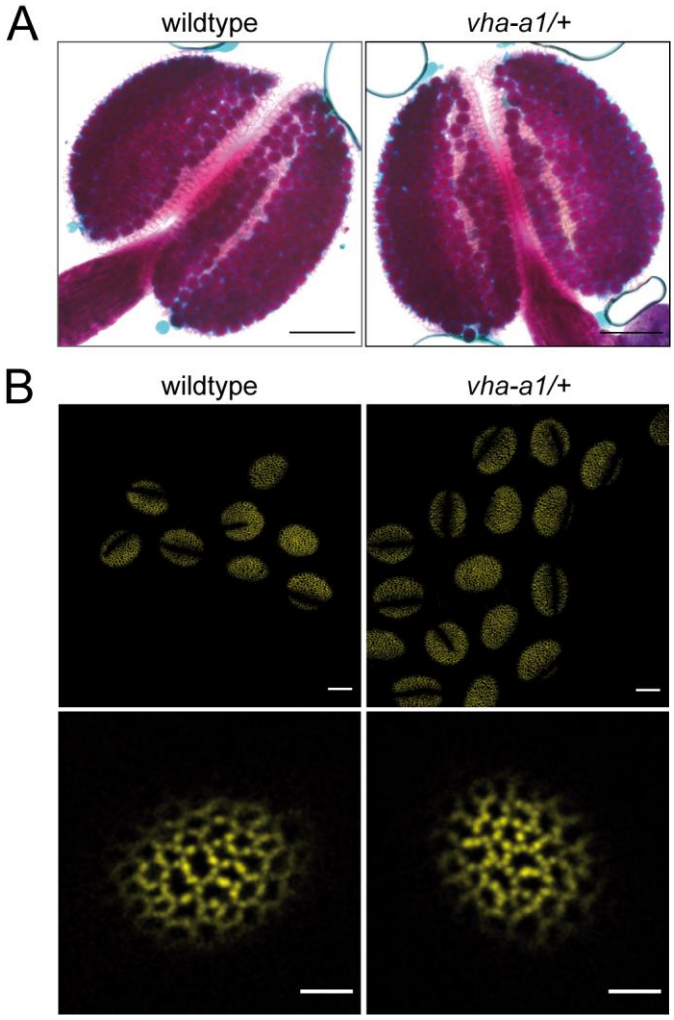

Figure 20. The heterozygous *vha-a1/+ is* wildtype-like at the time of pollen release. **(A)** Alexander staining of pollen before release shows the lack of aborted microspores in *vha-a1/+* anthers. *vha-a1/+* anthers are indistinguishable from wildtype. Scale bars = 100 µm. **(B)** Exine morphology of *vha-a1/+* pollen is normal. CLSM analysis of *vha-a1/+* and wildtype pollen using the autofluorescent properties of the exine showed no difference between *vha-a1/+* and wildtype. Pollen analyzed for each genotype n > 40.

2.2.4 Expression of *VHA-a1* under the control of the *MSP1* promoter rescues the late defect of *vha-a1/+*

I aimed to generate stable *vha-a1* mutant lines that express *VHA-a1* specifically during pollen development but are otherwise devoid of VHA-a1, for further analyses of *vha-a1* during vegetative development. To this end, the promoters MSP1 and MSP3 were selected to drive *VHA-a1* expression (Honys et al., 2006). Both promoters were reported

to be specifically expressed in developing microspores and the tapetum (Honys et al., 2006 and illustrated in Figure 21A). Heterozygous mutants were transformed with *MSP1:VHA-a1* and *MSP3:VHA-a1*. In the T1 generation, genotyping was performed to identify *vha-a1/+ MSP1:VHA-a1* and *vha-a1/+ MSP3:VHA-a1.* As expected, genotyping showed that both wildtype and *vha-a1/+* mutants containing the transgene were present. In the T2 generation, I analyzed if *MSP1:VHA-a1* and *MSP3:VHA-a1* rescue pollen development of *vha-a1*. For *MSP3:VHA-a1* no *vha-a1* mutants were found, suggesting that it does not rescue. For *MSP1:VHA-a1* the presence of homozygous *vha-a1* mutants along with *vha-a1/+* and wildtype was revealed. However, *vha-a1 MSP1:VHA-a1* plants were sterile (Figure 21D). Thus, although the expression of *VHA-a1* under the *MSP1* promoter allows for male transmission of the *vha-a1* allele by rescuing the late defect, the early defect of *vha-a1* in pollen development is not rescued.

2.2.5 Tapetum-specific expression of *VHA-a1* does not rescue pollen development of *vha-a1*

The lack of an aberrant phenotype of heterozygous mutants points to a sporophytic defect. Of the diploid sporophytic cell types of the anther, the tapetum was the best candidate in terms of cell types in which VHA-a1 could be essential. Tapetal cells have high secretory activity and VHA-a1-GFP is highly abundant in tapetal cells when expressed under its own promoter (Figure 18). Therefore, I investigated whether VHA-a1 is essential in the tapetum.

I tested if tapetum-specific expression of *VHA-a1* was able to rescue pollen development of *vha-a1*. The *A9* promoter was chosen that is known to drive tapetum-specific gene expression (Feng and Dickinson, 2010; Paul et al., 1992 and shown in Figure 21A). Instead of transforming *vha-a1/+* mutants with *A9:VHA-a1*, *vha-a1/+* mutants which express *MSP1:VHA-a1* were transformed with *A9:VHA-a1. MSP1:VHA-a1* enables the transmission of the mutant *vha-a1* allele via the male gametophyte. On the one hand, this allowed for analysis of *A9:VHA-a1* in a *vha-a1* mutant background. On the other hand, this combination would allow to rescue both the late and the early defect if *A9:VHA-a1* was able to rescue the early defect.

vha-a1/+ MSP1:VHA-a1 were transformed with *A9:VHA-a1-mScarlet (A9:VHA-a1-mScarlet,* Fabian Fink). Analysis if expression of *VHA-a1* under the *A9* promoter rescues the early defect in pollen development of *vha-a1* was performed in the T1 generation. As

expected, genotyping identified *vha-a1 MSP1:VHA-a1 A9:VHA-a1-mScarlet* mutants (Figure 21B). The fact that they were sterile indicates that expression of *VHA-a1* under the *A9* promoter does not rescue (Figure 21D). To ensure that VHA-a1-mScarlet is expressed in these plants, anthers of *vha-a1 MSP1:VHA-a1 A9:VHA-a1-mScarlet* were analyzed by CLSM. VHA-a1-mScarlet was detected specifically in the tapetum (Figure 21C). Altogether, this suggests that tapetum-specifc expression of *VHA-a1* does not rescue the early defect in pollen development of *vha-a1* and thus it is unlikely that VHA-a1-containing V-ATPases in the tapetum are essential for pollen development.

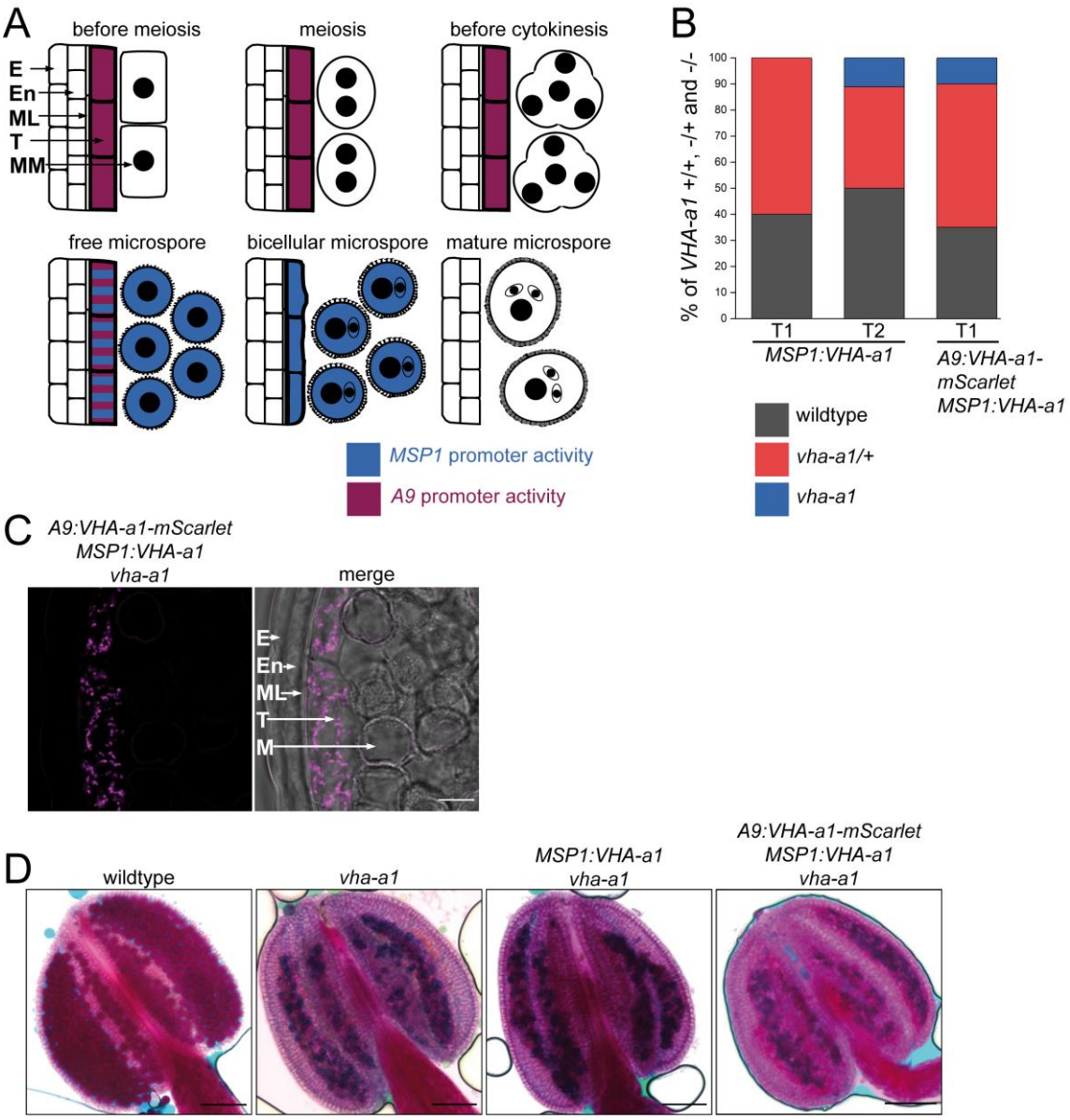

Figure 21. Tapetum-specific expression of *VHA-a1* does not rescue pollen development of *vha-a1.* (A) *MSP1* and *A9* promoter activity according to Honys et al., 2006 and Paul et al., 1992, respectively. E, epidermis; En, endothecium; ML, middle layer; T, tapetum; MM, microspore mother cell. **(B)** Expression of *MSP1:VHA-a1* rescues the late defect of *vha-a1*/+. Quantification of wildtype, *vha-a1*/+ and *vha-a1* mutants after transformation of heterozygous *vha-a1*/+ with *MSP1:VHA-a1* and *A9:VHA-a1-mScarlet*. T1 *MSP1:VHA-a1* n = 10, T2 n = 36, T1 *A9:VHA-a1-mScarlet* n = 20. **(C)** Expression of *A9:VHA-a1-mScarlet* shows tapetum-specific signal. It did not rescue pollen development of *vha-a1.* E, epidermis; En, endothecium; ML, middle layer; T, tapetum; M, microspore, scale bar = 10 µm. **(D)** Alexander staining of anthers shows defective pollen development in *vha-a1, MSP1:VHA-a1 vha-a1 and A9:VHA-a1 vha-a1*. Scale bars = 100 µm.

2.2.6 *vha-a1* is defective in pollen wall formation

As the lack of VHA-a1 in the sporophytic anther tissue seemed not to be the reason for the defect in pollen development of *vha-a1*, another explanation for the lack of an aberrant phenotype of the heterozygous mutant was that microspore mother cell-derived gene product is present long enough in *vha-a1*/+ to prevent the defect. In this scenario, the defect in *vha-a1* likely occurs early in pollen development. To reveal at which stage in pollen development the defect occurs in *vha-a1*, anthers were stained with the fluorescent dye DAPI to visualize DNA and analyzed using CLSM. DAPI staining enabled to identify the different stages of meiosis and helped to find anthers before and after mitosis I and II (Supplementary Figure 12). Until the tetrad stage wildtype and *vha-a1* anthers were indistinguishable (Figure 22 A-D). A major defect became visible at the late tetrad stage in *vha-a1*. At the tetrad stage, pollen wall formation starts with the formation of the primexine outside the microspore plasma membrane (Ariizumi and Toriyama, 2011). While microspores in wildtype showed a uniform exterior of developing pollen wall, many microspores in *vha-a1* lacked this surrounding or were unevenly surrounded by developing pollen wall material (Figure 22G and H, Supplementary Figure 13). Degenerated microspores were visible in *vha-a1* from the late tetrad stage on (Figure 22H). A few multinucleated cells were observed in *vha-a1* at the tetrad stage (Supplementary Figure 14). At the unicellular microspore stage wildtype microspores showed a prominent exine, which *vha-a1* microspores were lacking (Figure 22I and J). At this developmental stage most *vha-a1* microspores were degenerate. Consistent with the results from the Alexander staining, when microspores were mature and tricellular in wildtype, only debris was present in *vha-a1* (Figure 22K and L). Observation of tapetal cells showed no difference between the tapetum in wildtype and *vha-a1* (Figure 22A-J).

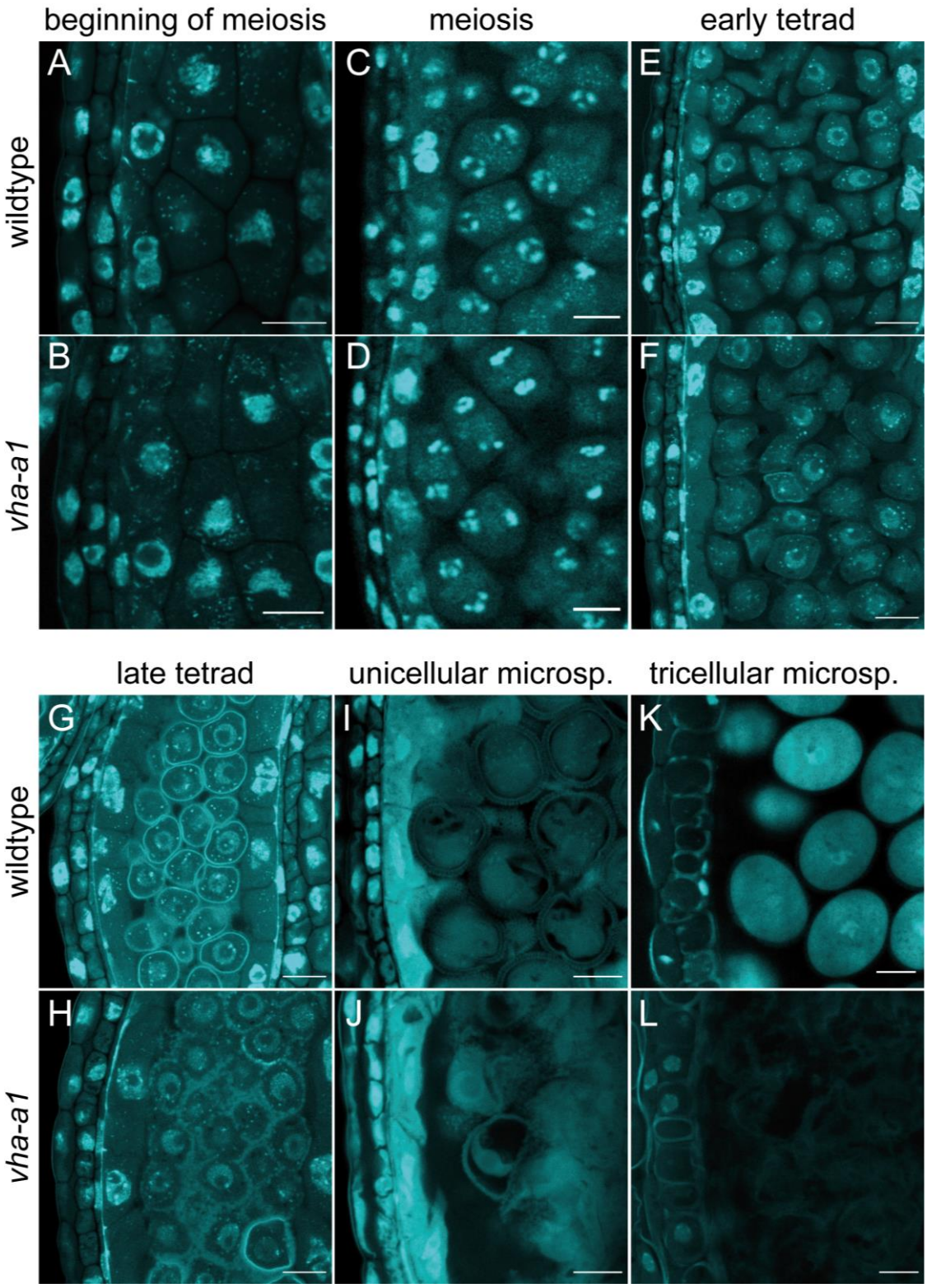
beginning of meiosis
meiosis
early tetrad
wildtype
vha-a1
A
B
C
D
E
F
late tetrad
unicellular microsp.
tricellular microsp.
wildtype
vha-a1
G
H
I
J
K
L

Figure 22. *vha-a1* is defective at the tetrad stage. During meiosis *vha-a1* is indistinguishable from wildtype **(A-D).** From the tetrad stage on, *vha-a1* is different from wildtype **(E-L)**. Pollen wall formation starts with the formation of the primexine at the tetrad stage. In wildtype microspores are uniformly surrounded by developing pollen wall **(G)**. In *vha-a1* many microspores are unevenly surrounded by developing pollen wall **(H)**. At the unicellular microspore stage microspores in wildtype possess a prominent exine **(I)**, which microspores in *vha-a1* are lacking **(J)**. At the tricellular microspore stage only debris of microspores is left in *vha-a1* **(L)**. CLSM analysis was performed using cleared anthers which were stained with DAPI. Scale bars =10 µm.

Secretory activity of tapetal cells was analyzed by examination of the transient callose wall which is dissolved by callase (β-1,3-glucanase) that is secreted from tapetal cells into the locule (Ariizumi and Toriyama, 2007). In order to visualize the transient callose wall in *vha-a1* anthers, fluorescent staining of callose using aniline blue was performed. In addition to staining with aniline blue anthers were stained with DAPI and CLSM analysis was performed. There was no difference in callose wall appearance and timing of callose dissolution between *vha-a1* and wildtype (Figure 23). This indicates once more that VHA-a1 is not essential in tapetal cells.

In order to investigate *vha-a1* anthers on an ultrastructural level, transmission electron microscopy (TEM) was performed. Concerning tapetal cells, again, no difference was found between wildtype and *vha-a1* (Figure 24A and B). The lack of a normal exine in *vha-a1* was shown, which corroborates the results from the CLSM analysis (Figure 24C, E, D and F). Moreover, accumulations of sporopollenin between the tapetum and the middle layer in *vha-a1* were revealed (Figure 24B). In summary, this shows that *vha-a1* is defective in pollen wall formation.

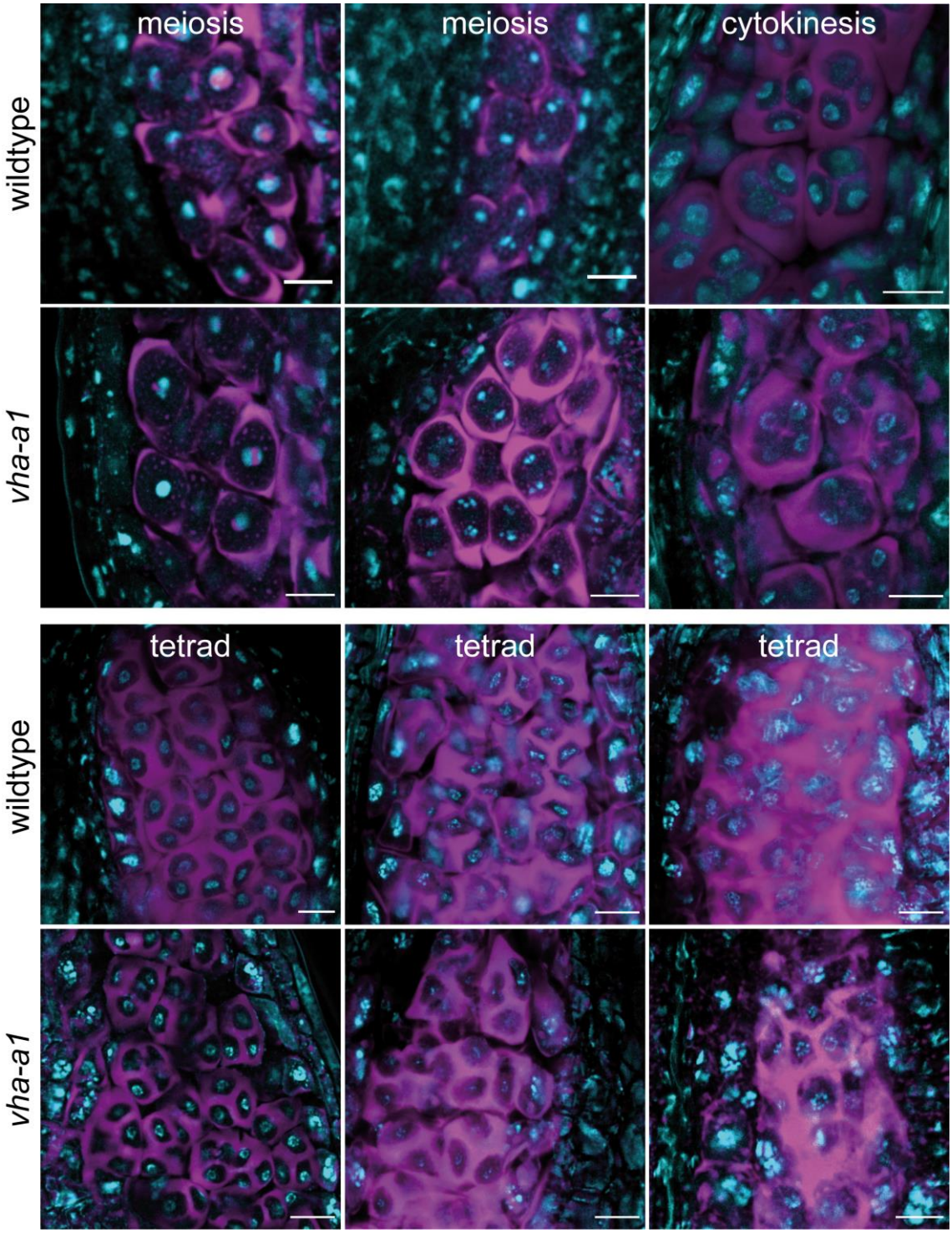

Figure 23. *vha-a1* has no general defect in secretion from the tapetum. Wildtype and *vha-a1* anthers stained with DAPI and the callose staining aniline blue were analyzed using CLSM. No difference in callose wall appearance and callose dissolution was observed between wildtype and *vha-a1*. The aniline blue staining showed the transient callose at the callose wall as well as at the cell plate in meiosis. Scale bars = 10 µm.

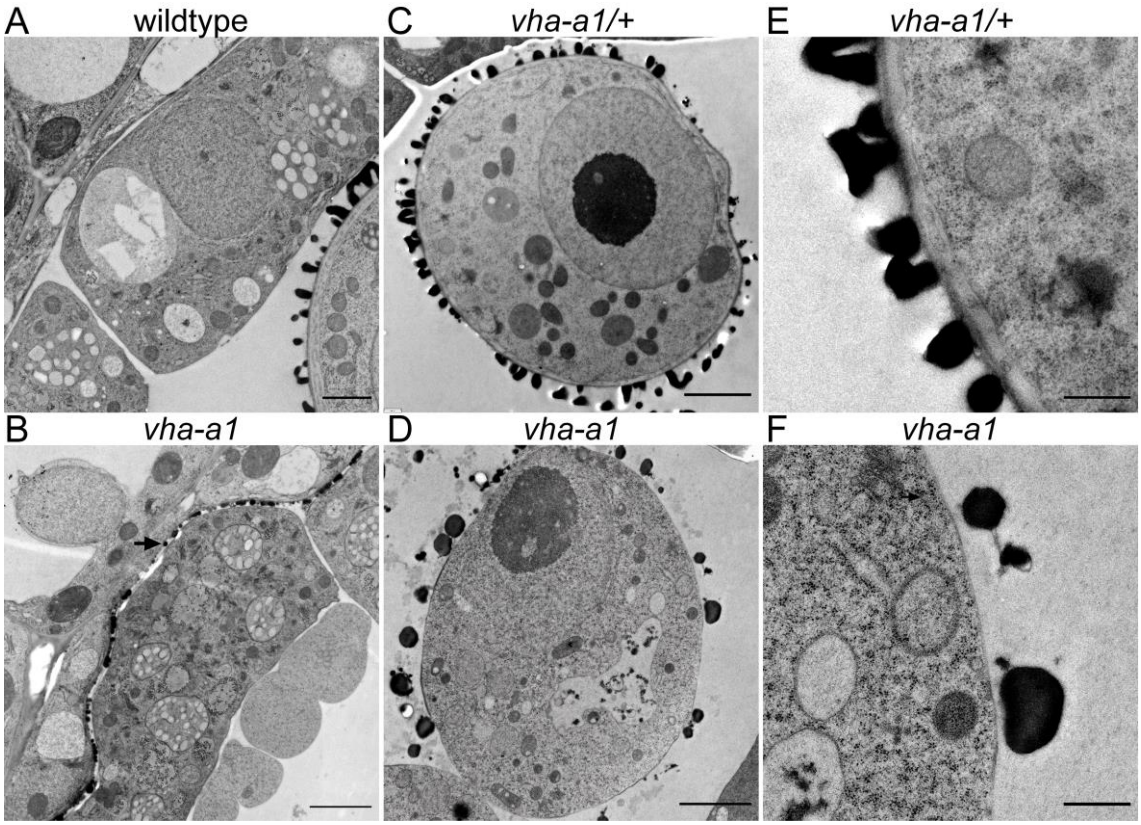

Figure 24. *vha-a1* is defective in pollen wall formation. (A, B) TEM of the tapetum in wildtype **(A)** and *vha-a1* **(B).** Tapetal cells of *vha-a1* are normal. Accumulation of electron-dense material, presumably sporopollenin, is seen between the tapetum and the middle layer in *vha-a1* (black arrow, **B**). Scale bars = 2 µm. **(C, D)** TEM of unicellular microspores in *vha-a1/+* **(C)** and *vha-a1* **(D)**. Scale bars = 2 µm. **(E, F)** Close-ups of the microspores in **(C, D)**. A normally developing pollen wall of the microspore in *vha-a1/+* **(E)** and the lack of a normal pollen wall of the microspore in *vha-a1* is shown **(F)**. Scale bars = 0.5 µm. The electron micrographs were acquired by Dr. Stefan Hillmer.

2.2.7 At the tetrad stage VHA-a1-GFP is detected in all microspores in segregating lines

The occurrence of the defect early in pollen development in *vha-a1* matched the hypothesis that VHA-a1 is essential in the developing microspores and that *vha-a1/+* lacks an aberrant phenotype because microspore mother cell-derived VHA-a1 is present long enough to prevent the defect. Following this hypothesis, I analyzed plants with segregating *VHA-a1:VHA-a1-GFP*. F1 plants of the cross *UBQ10:SRβ-mTurquoise* crossed with *VHA-a3:VHA-a3-RFP VHA-a1:VHA-a1-GFP* showed that after meiotic

cytokinesis VHA-a1-GFP was still present in all microspores. At the tetrad stage, at which the defect occurs in *vha-a1* but not in the heterozygous mutant, all microspores still contained VHA-a1-GFP (Figure 25A). Only later VHA-a1-GFP signal was absent in a subset of microspores (Figure 25B). Consequently, in the heterozygous mutant, VHA-a1 protein that was synthesized before meiotic cytokinesis could prevent the early defect in the mutant microspores. Altogether, this shows that it is plausible that VHA-a1 is essential in the male gametophyte.

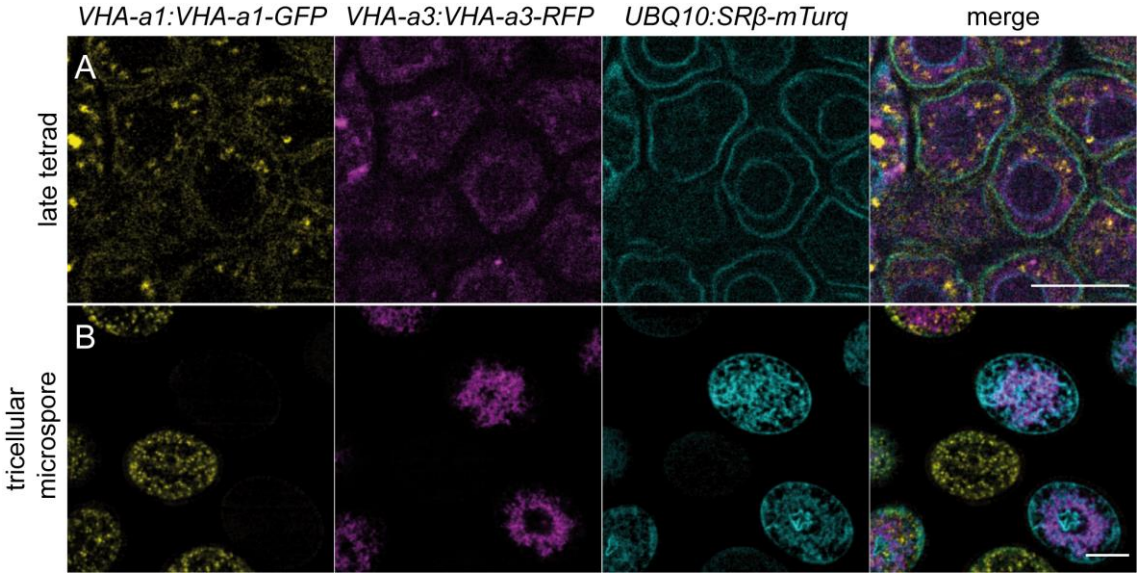

Figure 25. In segregating plants, all microspores contain VHA-a1-GFP at the late tetrad stage. (A) Plants segregating for *VHA-a1:VHA-a1-GFP*, *VHA-a3:VHA-a3-RFP* and *UBQ10: SRβ-mTurquoise* were analyzed. At the late tetrad stage still all microspores showed VHA-a1-GFP signal. **(B)** At the tricellular microspore stage only microspores that possessed *VHA-a1:VHA-a1-GFP* showed VHA-a1-GFP signal. Cleared anthers were analyzed using CLSM. Scale bars = 10 µm.

Summarized, *vha-a1* is defective in pollen wall formation. *vha-a1*/+ does not have this early defect but has a late defect which prevents the transmission of the mutant allele (Figure 26).

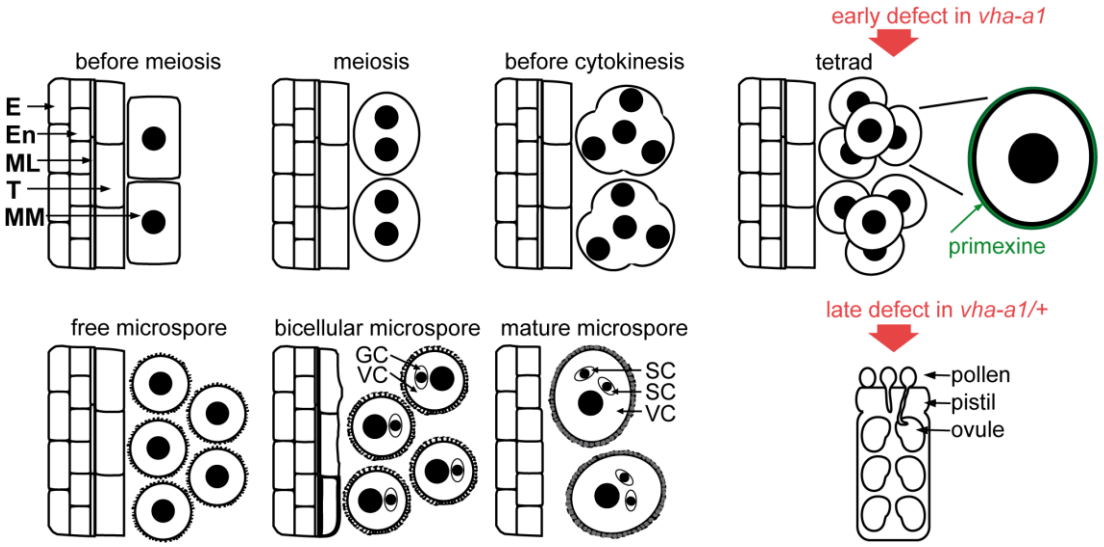

Figure 26. The early defect in *vha-a1* and the late defect in *vha-a1/+*. The early defect of *vha-a1* occurs at the tetrad stage when pollen wall formation starts with the formation of the primexine. The late defect of *vha-a1*/+ happens after the release of pollen from anthers. E, epidermis; En, endothecium; ML, middle layer; T, tapetum; MM, microspore mother cell; GC, generative cell; VC, vegetative cell; SC, sperm cell.

2.3 Discussion

2.3.1 Evolution of the a1-TD coincided with the evolution of non-motile sperm

The results of this work suggest that TGN/EE localization of V-ATPases is essential in microspores. While VHA-a3 is not able to compensate for the lack of VHA-a1 in pollen development, VHA-a3-a1-TD can. The a1-TD is necessary and sufficient to localize VHA-a3 to the TGN/EE and is a seed plant specific motif (Lupanga et al., 2020). The sexual reproduction of seed plants is independent of water and motile gametes due to the innovation of guided delivery of sperm through pollen tubes and desiccation-tolerant gametophytes (Hackenberg and Twell, 2019). The a1-TD originates with the gymnosperms (Lupanga et al., 2020). Remarkably, thus, the evolution of the a1-TD coincided with the evolution of non-motile sperm of seed plants.

However, an essential role of VHA-a1 in microspores, which fits the evolutionary history of the a1-TD, is only one possibility to explain the observed defect of *vha-a1* in pollen development. The other possibility is that VHA-a1 fulfills an essential role in the anther tissue.

2.3.2 High amounts of VHA-a1 in the tapetum

The tapetum is a cell layer with high secretory activity, which provides the developing microspores with molecules, such as enzymes, RNAs and pollen wall materials. It is the innermost layer of the anther wall (Ariizumi and Toriyama, 2011; Lei and Liu, 2020). Secretion by tapetal cells requires COPII-dependent trafficking. The COPII GTPase SAR1 was shown to be essential in the tapetum. Mutants of the gene encoding the SAR1B isoform are male sterile. Tapetum-specific expression of *SAR1B* was shown to partially rescue the defects in anthers in *sar1b* and to partially restore male fertility (Liang et al., 2020). Similarly, the mutant of the gene encoding the COPII coat component SEC31B shows reduced male fertility. Tapetum-specific expression of *SEC31B* rescued the *sec31b* mutant phenotype. Furthermore, a protein traveling via COPII vesicles showed a strong signal at the plasma membrane in tapetal cells in wildtype, while in *sec31b* only a weak signal of this protein was reported (Zhao et al., 2016).

Consequently, an explanation for why VHA-a3 cannot compensate for the lack of VHA-a1 in pollen development seemed likely to be due to its inability to substitute for VHA-a1 in tapetal cells. In support of this hypothesis, VHA-a1-GFP was found in high amounts in the tapetum when expressed under the control of its own promoter. However, tapetum-specific expression of *VHA-a1* did not rescue male gametophyte development of *vha-a1*. VHA-a1-mScarlet was present in tapetal cells without rescuing pollen development of *vha-a1*. There is no reason to assume that VHA-a1-mScarlet is a non-functional VHA-a1 version. It showed the same localization in tapetal cells as VHA-a1-GFP, which was shown to rescue pollen development of *vha-a1* when expressed under the control of its own promoter or the *UBQ10* promoter. Also, the timing of the tapetum-specific *VHA-a1* expression is no explanation for the inability to rescue. *VHA-a1-mScarlet* was expressed under the control of the *A9* promoter, which was also used by Zhao et al., 2016 and Liang et al. 2020 to rescue pollen development of the COPII subunit mutants. Moreover, VHA-a1-mScarlet was observed throughout the lifetime of the tapetum in the tapetum.

Hence, likely V-ATPases are required in high amounts in the tapetum, as suggested by the high amounts of VHA-a1-GFP when expressed under its own promoter, but likely also in the tapetum VHA-a3 is able to compensate for the lack of VHA-a1. VHA-a3-RFP expressed under its own promoter was also present at all developmental stages in tapetal cells. The *vha-a1* mutant possesses normally looking tapetal cells, as was shown in CLSM and TEM analyses. This is in contrast to the *sec31b* mutant in which aberrant morphologies of tapetum organelles was reported (Zhao et al., 2016). Moreover, in the *vha-a1* mutant tapetal cells undergo programmed cell death normally and there is no general defect in secretion from the tapetum. The timing of the dissolution of the callose wall, which requires secretion of callase from the tapetum, is the same in *vha-a1* and wildtype.

2.3.3 V-ATPases in microspores

Analysis of the *vha-A/+* mutant showed that V-ATPases are essential in pollen development (Dettmer et al., 2005). Moreover, it is clear from the examination of *vha-A/+* that V-ATPases are critical in microspores. Ultrastructural analysis of *vha-A* microspores from heterozygous mutants showed aberrant Golgi morphologies (Dettmer et al., 2005). This suggests that endomembrane trafficking in microspores is disturbed when

V-ATPase activity is lacking. Another example of the importance of endomembrane trafficking in microspores was provided by the analysis of the mutant of the gene encoding the SNARE protein SEC22. SEC22 functions in vesicle trafficking between the ER and the Golgi. Ultrastructural analysis of *sec22* microspores also revealed aberrant Golgi morphologies (El-Kasmi et al., 2011). In this work, I showed that the defect in pollen development of *vha-a1* occurs at the tetrad stage. While in wildtype, microspores establish the primexine outside of their plasma membrane at this stage, which represents the beginning of pollen wall development, in the *vha-a1* mutant microspores with abnormal surroundings were observed. Starting at the tetrad stage *vha-a1* showed degenerated microspores. At the unicellular microspore stage most microspores in *vha-a1* were degenerated, while wildtype microspores showed a prominent exine, which was not seen in *vha-a1*. Altogether, this suggests that the secretory activity of microspores could be required for primexine formation.

2.3.4 Primexine formation – controlled by the gametophyte or sporophyte?

Mutants of COPII components, which have reduced male fertility, as *sec31b* and *sec23ad,* or are male sterile, as *sar1b*, and the *vha-a1* mutant have in common that they are defective in pollen wall formation. In all of these mutants, sporopollenin accumulations between the tapetum and the middle layer and at the surface of microspores were shown by TEM analyses (Aboulela et al., 2018; Liang et al., 2020; Tanaka et al., 2013; Zhao et al., 2016). The fact that sporopollenin accumulates outside of the tapetum means that the exit of sporopollenin from tapetal cells and arrival in the locule was accomplished. However, secretion of other components that are biosynthesized in the tapetal cells and could be essential for primexine formation could be impaired. An important difference between *vha-a1* and COPII component mutants such as *sar1b* and *sec31b* is that the latter could be rescued by tapetum-specific expression (Liang et al., 2020; Zhao et al., 2016), while *vha-a1* could not. This suggests that COPII-dependent trafficking is crucial in the tapetum as well as in the microspores. While in *vha-a1* VHA-a3 might be able to compensate for the lack of VHA-a1 in the sporophytic tapetum, it might not be able to compensate in the gametophytes.

Primexine formation could be under the control of the gametophyte or the sporophyte or both. Though assumed earlier that primexine formation is a microspore-controlled

process (Piffanelli et al., 1998), it was also proposed that primexine formation could be under the control of the sporophyte. This hypothesis was based on the heterozygous mutants' phenotypes of mutants defective in primexine formation. *dex1, nef1, ms1, tde1 and rpg1* show defects in primexine formation, while the heterozygous mutants produce exclusively pollen with normal primexine and lack pollen with the mutant phenotype (Ariizumi and Toriyama, 2011). In the diploid cells of the sporophyte, the mutant and the wildtype allele are present in the heterozygous mutants. If the defect is due to an essential function of the sporophyte, the presence of the wildtype allele in the heterozygous mutants could prevent the defect.

Based on the same observation that the heterozygous mutants *upex1/+* and *irx9l/+* produced exclusively wildtype-like pollen, it was suggested that the glycosyltransferases UPEX1 and IRX9L function in the sporophyte (Li et al., 2017).

Although it is also true for *vha-a1/+*, that exclusively wildtype-like pollen are produced and aborted microspores are lacking, our results from the tapetum-specific expression of *VHA-a1* argue against an essential role of VHA-a1 in the tapetum. Based on the results of this work, it is more likely that primexine formation is under the control of the gametophyte. No tapetum defect was detected in *vha-a1*, and still primexine formation is defective. This is in accordance with the results from analysis of the *rpg1* mutant reported very recently by Zhang et al., 2022. RPG1 is a sugar transporter (Chen et al., 2010) and the *rpg1* mutant is defective in primexine formation. The primexine is strongly reduced in *rpg1* and the exine pattern disturbed (Guan et al., 2008; Sun et al., 2013). Zhang et al., 2022 found RPG1-GFP, expressed under the control of its own promoter, in microsporocytes and microspores but not in the tapetum. Additionally, RPG1 was shown to shuttle between the TGN/EE and the plasma membrane in microspores. Recycling of RPG1 from the TGN/EE to the plasma membrane was shown to be AP1-dependent and its impairment interferes with primexine formation (M. Xu et al., 2022).

2.3.5 Why is *vha-a1/+* not defective in primexine formation?

In the *vha-a1/+* mutant, also the diploid microspore mother cells are a source of VHA-a1. The absence of the defect in primexine formation in *vha-a1/+* can be explained by microspore mother cell-derived VHA-a1 protein or transcript, which remains long enough to prevent the defect in primexine formation. In plants in which VHA-a1-GFP was

segregating, VHA-a1-GFP was still detected in all microspores at the tetrad stage at which the defect in *vha-a1* is visible. This indicates that also the lifetime of endogenous VHA-a1 could be long enough to be partitioned in heterozygous plants to all microspores in meiotic cytokinesis.

Furthermore, also *VHA-a1* transcript could be present after meiotic cytokinesis in all microspores. Germline specification and cycle progression are required to be integrated into pollen development. In animals, gametes directly develop from the haploid products of meiosis. On the contrary, in plants, the haploid products of meiosis undergo mitotic divisions to form reproductive structures. In contrast to early land plants, in which multiple mitotic divisions take place, in angiosperms, the male gametophyte is so reduced that germ cell specification needs to take place within only two mitotic divisions (Twell, 2010). In Arabidopsis, the transition to postmeiotic gametophyte differentiation involves inhibition of translation at the end of meiosis through recruitment of the translation initiation factor eIF4F into P-bodies. It is unclear if transcripts are degraded or persist (Cairo et al., 2022). In maize, it was shown that transcripts persist long, and biallelic expression continues for 11 days after meiosis, followed by a rapid switch to monoallelic expression at mitosis I (Nelms and Walbot, 2022). Consequently, in addition to the possibility of VHA-a1 protein remaining long enough to prevent the defect in primexine formation in *vha-a1*/+, potentially also translation of *VHA-a1* transcripts could still take place after meiotic cytokinesis.

2.3.6 The late defect in *vha-a1*/+

Although the heterozygous mutant is not defective in primexine formation and lacks aborted microspores, there is no transmission of the mutant *vha-a1* allele via the male gametophyte. This suggests that microspores that contain the *vha-a1* allele are impaired in a late male gametophytic function which results in deficits compared to microspores with the wildtype allele before or during fertilization. At the time of pollen release from anthers, no difference was found between wildtype- and *vha-a1*-containing microspores in the *vha-a1*/+ mutant. Alexander staining showed no difference between *vha-a1*/+ and wildtype anthers and the exine morphology of pollen grains from *vha-a1*/+ anthers was normal. Either, despite having a normal exine pattern and wildtype appearance *vha-a1* pollen are already different from wildtype pollen at the time of pollen release, or VHA-a1 is essential for a process after pollen release.

The late defect in *vha-a1/+* could occur at pollen germination, pollen tube growth or fertilization.

For the fast tip growth of pollen tubes high coordination of processes and tight regulation of conditions are required. Pollen tube growth requires massive vesicle trafficking to deliver cell wall material to the tube tip (Çetinbaş-Genç et al., 2022). Moreover, in pollen tube guidance male-female communication is crucial, in which molecules that are secreted from pollen tubes play a role and pollen tube plasma membrane-localized receptor-like protein kinases are required to perceive the female signals (Hafidh and Honys, 2021). A mutant that is defective in TGN/EE formation, the *lot* mutant, is defective in pollen tube growth. TGN/EE disruption in the *lot* mutant was reported to result in impaired post-Golgi trafficking and swelling of pollen tubes in the style but not *in vitro*, which suggests that the regulation of pollen tube-style interaction was disturbed (Jia et al., 2018).

There is no visual differentiation between wildtype and *vha-a1*-containing microspores in the heterozygous mutant. Future analyses could therefore additionally be performed using homozygous *vha-a1* mutants in which the rescuing *VHA-a1-GFP* is segregating. This way, via the GFP fluorescence, microspores with and without the rescuing VHA-a1-GFP could be told apart.

A further indication regarding the occurrence of the late defect of *vha-a1/+* and a potential tool for its analysis are *MSP1:VHA-a1-XFP* expressing plants. Expression of *VHA-a1* driven by the *MSP1* promoter (Honys et al., 2006) enabled the transmission of the *vha-a1* allele via the male gametophyte. It specifically rescued the late defect of *vha-a1/+*, but not the early defect of *vha-a1*.

2.3.7 *vha-A/+* anthers contain aborted microspores, while *vha-a1/+* lacks aborted microspores

In contrast to VHA-a1, VHA-A is a single gene encoded subunit. Lack of VHA-A means an overall lack of V-ATPase activity. Hence, CRISPR/Cas9 under the control of an egg-cell specific promoter targeting *VHA-A* is not expected to result in homozygous null mutants. VHA-E1 is essential for embryogenesis (Strompen et al., 2005), thus, plants that lack V-ATPase activity should not be found. Accordingly, no triple mutant *vha-a1 vha-a2 vha-a3* was obtained in this work (Chapter 1.2.2). However, theoretically, if pollen

development could be analyzed in a homozygous *vha-A* mutant, it should share the early defect (primexine defect) with *vha-a1*.

Concerning the heterozygous mutants, *vha-A*/+ anthers have wildtype-looking and aborted microspores in a ratio of 1:1 (Dettmer et al., 2005), while *vha-a1*/+ lacks aborted microspores. Aberrant microspores were observed in *vha-A*/+ mutants after the first mitosis. Ultrastructural analysis of *vha-A* microspores showed microspores with a well-developed intine and exine, but misshaped Golgi stacks (Dettmer et al., 2005). A reason for the lack of the defect at this stage in pollen development in *vha-a1*/+, could be different protein lifetimes. In *vha-a1* microspores in the *vha-a1*/+ mutant, VHA-a1 could still be present around the first mitosis while VHA-A could be shorter lived. Alternatively, it is possible, although less likely, that the difference is caused by the presence of VHA-a2 and VHA-a3. V-ATPases could be required at the tonoplast at this stage in pollen development. However, the phenotype of the *vha-a2 vha-a3* double mutant, which has no defect in pollen development, argues against it. Else, although also less likely, VHA-A could fulfill an additional function beyond proton pumping that is specific to VHA-A and essential for pollen development.

2.3.8 Why is VHA-a3 not able to rescue pollen development of *vha-a1*?

The question remains why VHA-a3 can replace VHA-a1 during vegetative growth but not during pollen development. I have shown in this work that the defect in pollen development is not due to the absence of VHA-a3. VHA-a3-RFP expressed under the control of its own promoter was present throughout pollen development in developing microspores and cells of the anther wall. In addition, complementation analysis using expression driven by the *UBQ10* promoter revealed that VHA-a3 is not able to rescue pollen development of *vha-a1*, while VHA-a3-a1-TD can. As VHA-a3-a1-TD differs from VHA-a3 only in the 33 amino acids-containing region of the a1-TD, no other features of VHA-a1 that VHA-a3 does not have, are needed besides TGN/EE localization. Consequently, while in *vha-a1* VHA-a3 could be able to travel to the TGN/EE during vegetative growth, during pollen development, it could not be able to reach the TGN/EE. This could be due to COPII isoform specificity of VHA-a3. The SEC24 subunit recognizes cargo proteins for incorporation into COPII vesicles (Miller et al., 2003). Arabidopsis possesses three SEC24 isoforms, SEC24A, SEC24B and SEC24C. It could be that

VHA-a3 is able to enter COPII vesicles only in the presence of a specific SEC24 isoform. It was reported that the three SEC24 isoforms are expressed at different times in the plant lifecycle. Promoter:GUS analysis showed no difference in expression between the three isoforms in seedlings, but in reproductive development, differences were shown. Concerning SEC24A, GUS activity was detected in ovules, pollen grains and embryos. Regarding SEC24B, GUS activity was found in sepals, petals, stamens with pollen grains, pistils as well as flower buds. For SEC24C, GUS activity was shown in sepals, stamens with pollen grains, pistils, flower buds and in parts of the silique (Tanaka et al., 2013). Moreover, microarray expression analyses showed that the three isoforms are expressed at different stages in pollen development (Conger et al., 2011). Information about expression in the early stages of pollen development before the unicellular microspore stage is lacking. However, it might be that VHA-a3 enters COPII vesicles that contain a specific SEC24 isoform during vegetative growth and that this SEC24 isoform is not present early in pollen development.

3 Chapter 3: The V-ATPase-associated VHA-AP1

Aims of chapter 3

VHA-AP1, which is associated with the V-ATPase, has not been functionally characterized before. It is a potential essential component of Arabidopsis V-ATPase complexes. The objective was to investigate the function of VHA-AP1.

3.1 Introduction

3.1.1 The V-ATPase-associated proteins VHA-AP1 and VHA-AP2

Research on the structure of V-ATPase complexes of different organisms has shed light on the subunit composition and the functions of V-ATPase subunits. Electron cryomicroscopy (cryoEM) analyses were done with V-ATPase complexes of yeast (Benlekbir et al., 2012; Mazhab-Jafari et al., 2016; Oot et al., 2016; Roh et al., 2018; Vasanthakumar et al., 2022, 2019; Zhao et al., 2015), of the insect *Manduca sexta* (Muench et al., 2009), bovine (Gregorini et al., 2007; R. Wang et al., 2020), rat (Abbas et al., 2020) and human (L. Wang et al., 2020). Very recently, cryoEM analysis of the lemon V-ATPase added the structure of the first plant V-ATPase to the collection (Tan et al., 2022).

The 3D structures shaped the understanding of V-ATPase composition, the rotary mechanism of proton pumping coupled to ATP hydrolysis, assembly and regulation of the enzyme. Insights were gained, for instance, into conformational changes during autoinhibition of the V_1 subcomplex and during reversible dissociation of the V_1 and V_O sub-complexes (Oot et al., 2016; Vasanthakumar et al., 2022)

Furthermore, differences between V-ATPase complexes of different organisms were revealed. A great difference between the yeast and the mammalian V_O subcomplex is the absence of the protein ATP6AP2 in the yeast V-ATPase (Abbas et al., 2020). Moreover, the human ATP6AP1, which is also part of the V_O subcomplex, differs from the yeast V_Oa1p, as it possesses a large luminal domain. Apart from the domain in the lumen, the transmembrane domain of human ATP6AP1 and yeast V_Oa1p are conserved in structure and sequence (Roh et al., 2018; L. Wang et al., 2020). ATP6AP1 and ATP6AP2 are both situated in the c-ring of V_O (L. Wang et al., 2020). They both possess one transmembrane domain and belong to the type I transmembrane proteins. ATP6AP1 is also called Ac45 and ATP6S1, while ATP6AP2 is also known as (pro)renin receptor (PRR). In the lemon V-ATPase VHA-AP1 does not have the large luminal domain which was observed for ATP6AP1 in the human V-ATPase, but was also absent in yeast V_Oa1p. In addition, the lemon V-ATPase lacks subunit f compared to yeast and mammalian V-ATPases and its subunit H has a different conformation, which might

prevent ATP synthesis in order to allow for the very low pH of the juice sac cell vacuole of lemon. VHA-AP2 is present in lemon (Tan et al., 2022).

Consequently, the structural analyses of V-ATPases also added VHA-AP1 and VHA-AP2 to the picture which were missing in early descriptions of the V-ATPase complex composition (Nishi and Forgac, 2002; Sze et al., 2002) and are often called accessory subunits. This is how ATP6AP1 was introduced when it was first co-purified in biochemical purification of the V-ATPase from bovine cells (Supek et al., 1994). Biochemical purifications of the bovine V-ATPase also identified ATP6AP2 (Ludwig et al., 1998). ATP6AP1 and ATP6AP2 interact via their N-terminal parts (Rujano et al., 2017).

V_Oa1p functions in the assembly of the V_O subcomplex in the ER in yeast (Ryan et al., 2008). Drosophila ATP6AP2 was shown to be able to functionally replace V_Oa1p in yeast. In combination with Drosophila ATP6AP1, Drosophila ATP6AP2 compensated even more efficiently for the lack of Voa1p in yeast (Guida et al., 2018). This indicates that ATP6AP1 and ATP6AP2 function in V-ATPase assembly at the ER, as also suggested by Jansen et al., 2016; Kinouchi et al., 2010; Rujano et al., 2017 . However, ATP6AP1 and ATP6AP2 are not only present at the ER. ATP6AP2 was found, for example, at the plasma membrane involved in the planar cell polarity (PCP) signaling pathway in Drosophila (Buechling et al., 2010; Hermle et al., 2013). Also, ATP6AP1 was found at different subcellular localizations (Jansen et al., 1998). CryoEM of human V-ATPase showed that ATP6AP1 is required for the assembly of V_O as a scaffold for ATP6AP2, c-ring subunits and subunit d. As was shown for the yeast V_Oa1p (Roh et al., 2018), after assembly, human ATP6AP1 remains integrated in V-ATPase complexes (L. Wang et al., 2020). Thus, it has the potential to fulfill more functions, for example, to act in signaling, as has been shown for ATP6AP2, which functions in PCP and Wnt signaling (Buechling et al., 2010; Cruciat et al., 2010; Hermle et al., 2013).

Moreover, both ATP6AP1 and ATP6AP2 are cleaved (Cousin et al., 2009; Holthuis et al., 1999), and it is not yet known what consequences the cleavages have for the functions of the proteins. In plants, nothing had been elucidated about the functions of VHA-AP1 and VHA-AP2.

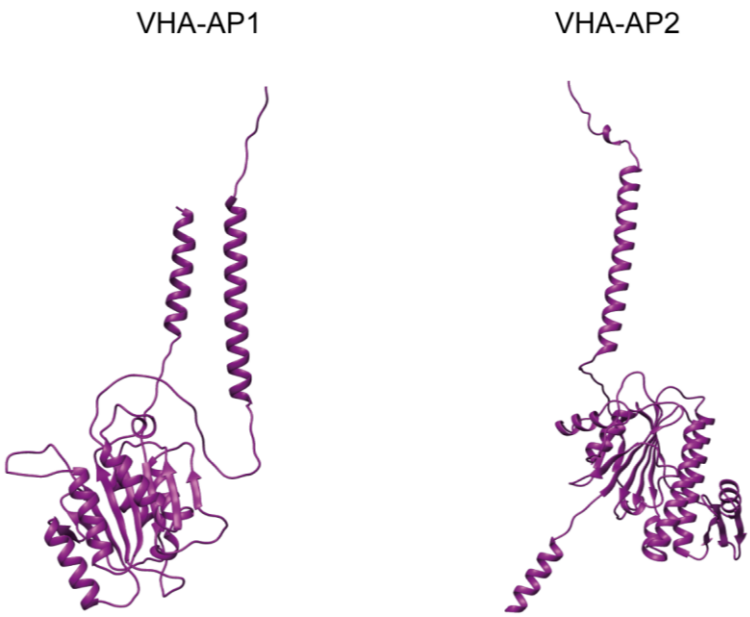

Figure 27. Structural models of VHA-AP1 and VHA-AP2. The 3D structures of VHA-AP1 and VHA-AP2 were created using AlphaFold (Jumper et al., 2021; Varadi et al., 2022) and visualized with UCSF Chimera (Goddard et al., 2018; Pettersen et al., 2004).

The Arabidopsis proteins VHA-AP1 and VHA-AP2, while only having 27% amino acid sequence identity (Röhrich Master Thesis, 2016), possess similar 3D structures (Figure 27). VHA-AP1 is also known as VHA-AP2L1 (Röhrich Master Thesis, 2016; Hinterberger Master Thesis, 2019). *VHA-AP1* and *VHA-AP2* were found co-expressed with genes encoding V-ATPase subunits (Fink Master Thesis, 2012 ; Röhrich Master Thesis, 2016). Both genes were targeted using CRISPR/Cas9 (Röhrich Master Thesis, 2016). Different homozygous *vha-ap2* mutants harboring independently generated mutant alleles that are likely null alleles showed no aberrant phenotype when grown under standard growth conditions (Rachel Röhrich, data not shown). In this work, the function of VHA-AP1 was investigated.

3.2 Results

3.2.1 VHA-AP1 is localized at the tonoplast in wildtype, while detected at the ER in *vha-a2 vha-a3*

The intracellular localization of VHA-AP1 was analyzed using VHA-AP1 tagged with mCherry expressed under the control of the *UBQ10* promoter (*UBQ10:VHA-AP1-mCherry*, Fabian Fink). In wildtype VHA-AP1 localized to the tonoplast and to punctate structures, which presumably are TGN/EE (Figure 28A). On the contrary, in *vha-a2 vha-a3,* which lacks V-ATPases at the tonoplast, while still present in punctae, VHA-AP1 was absent from the tonoplast and detected at the ER instead (Figure 28B and C). This suggests that VHA-AP1 travels in assembled V-ATPase complexes to its intracellular destinations.

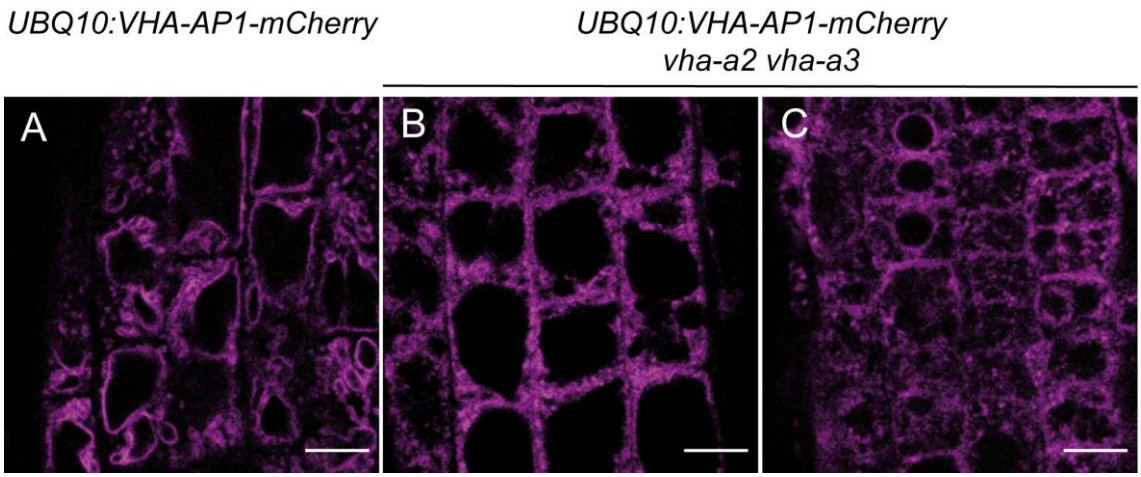

Figure 28. VHA-AP1-mCherry localizes to the tonoplast in wildtype but is retained in the ER in *vha-a2 vha-a3.* (A) VHA-AP1-mCherry localizes at the tonoplast and punctate structures, presumably TGN/EE, in wildtype. Root cells of the transition zone were imaged. **(B and C)** In *vha-a2 vha-a3,* which lacks V-ATPases at the tonoplast, VHA-AP1-mCherry is detected at the ER and punctate structures. Root cells of the transition zone were imaged in **(B)**. **(C)** shows root cells of the meristematic zone displaying prominent ring-shaped ER signal. CLSM analysis of 7-day-old seedlings. Scale bars = 10 µm.

3.2.2 VHA-AP1 is essential for male gametophyte development

To analyze if VHA-AP1 is required for V-ATPase function, CRISPR/Cas9 was used to generate *vha-ap1* mutant alleles. CRISPR constructs were cloned (*CRISPR VHA-AP1 I*, Röhrich Master Thesis, 2016; *CRISPR VHA-AP1 II, this work*) in which *Cas9* expression is driven by an egg cell-specific promoter (Wang et al., 2015). Wildtype plants were transformed with the CRISPR constructs targeting *VHA-AP1* at different target sites. Examples of the independent alleles that were obtained are *vha-ap1-1 and vha-ap1-2. vha-ap1-1* contains a 1 bp insertion, leading to a frameshift and an early stop codon. *vha-ap1-2* has a 4 bp deletion which also leads to a frameshift and a premature stop codon (Figure 29). According to their sequences, they are likely null alleles. Analysis of T1 generation plants showed that only heterozygous and no homozygous or bi-allelic mutants were present. In the T2, a *vha-ap1/+ (Cas9$^-$)* plant was selected and segregation of the mutant allele was monitored by genotyping of its progeny in the T3. Again, no homozygous plants were present (Figure 30A). Reciprocal crosses of *vha-ap1/+* and wildtype were performed next. Analysis of the F1 progeny of these crosses revealed that *vha-al1* is transmitted via the female gametophyte but not via the male gametophyte (Florian Hinterberger, Hinterberger Master Thesis, 2019 ; Figure 30B), suggesting that VHA-AP1 is required for V-ATPase function. Subsequently, I wanted to show that the lack of transmission is indeed due to a lack of VHA-AP1. Moreover, I intended to establish homozygous lines *vha-ap1* expressing VHA-AP1-mCherry. Therefore, *vha-ap1-1/+ (Cas9$^-$)* was crossed with *UBQ10:VHA-AP1-mCherry* carrying wildtype plants. In the F1 generation, a *vha-ap1-1/+* mutant expressing VHA-AP1-mCherry was identified via genotyping and CLSM analysis, respectively. I aimed to identify homozygous *vha-ap1-1* mutants carrying the transgene in the F2 generation. Therefore, I performed genotyping of plants that had been grown on hygromycin-containing plates to select for the *UBQ10:VHA-AP1-mCherry* containing T-DNA. However, no homozygous mutants were identified (Figure 30C), which indicates that *UBQ10:VHA-AP1-mCherry* does not rescue.

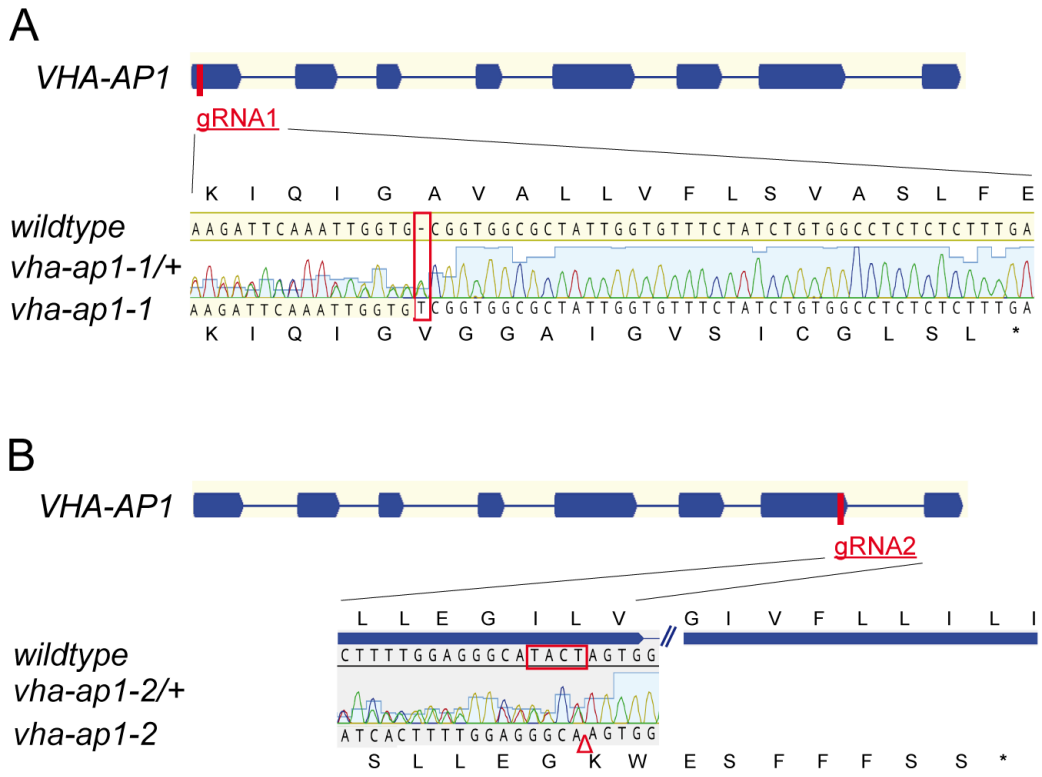

Figure 29. *vha-ap1* alleles that were generated using CRISPR/Cas9. Positions of the gRNA target sites in the coding sequence of *VHA-AP1* are shown. *vha-ap1-1* **(A)** and *vha-ap1-2* **(B)** are examples of alleles that were obtained in two independent CRISPR approaches. No homozygous mutants were identified. The chromatograms show the results of sequencing PCR amplicons of the targeted regions of heterozygous mutants. The reverse primers were used for sequencing. *vha-ap1-1* harbors a 1 bp insertion leading to a frameshift and an early stop codon (*). *vha-ap1-2* contains a 4 bp deletion which also causes a frameshift and an early stop codon. Δ marks the deletion site.

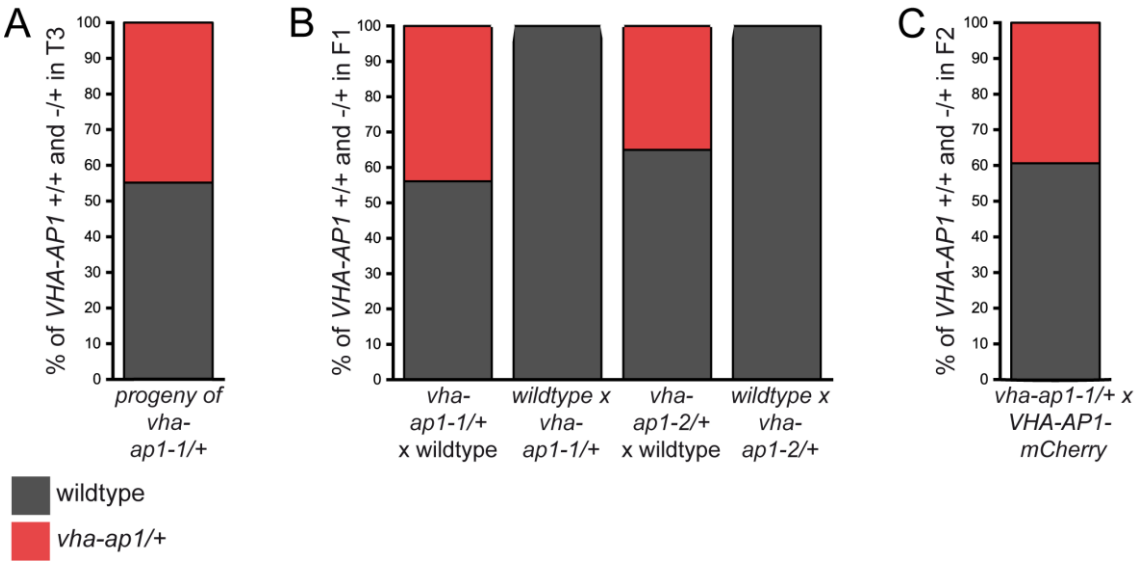

Figure 30. *vha-ap1* is not transmitted via the male gametophyte, and *UBQ10:VHA-AP1-mCherry* does not rescue. (A) In the progeny of a *vha-ap1/+* mutant no homozygous mutants were present. Only heterozygous mutants and wildtype plants were identified. n = 29. **(B)** Reciprocal crosses *vha-ap1/+* x wildtype revealed lack of transmission of the mutant allele via the male gametophyte. For *vha-ap1-1/+* x wildtype n = 41, for wildtype x *vha-ap1-1/+* n = 39, n=40 for *vha-ap1-2 x wildtype* and n = 17 for *wildtype x vha-ap1-2*. **(C)** Analysis of the progeny of the cross *vha-ap1/+* x *UBQ10:VHA-AP1-mCherry* in the F2 generation shows the lack of homozygous mutants, indicating that *UBQ10:VHA-AP1-mCherry* is not able to rescue. n = 33. The analysis shown in **(B)** was performed by Florian Hinterberger. Part **(B)** of this figure was made by Florian Hinterberger (Hinterberger Master Thesis, 2019) and was modified for this thesis.

3.2.3 Inducible knock-down of *VHA-AP1* leads to reduced cell expansion

As homozygous knock-out mutants seemed to be not viable, an inducible knock-down approach was performed to further analyze the function of VHA-AP1. Dexamethasone (Dex)-inducible artificial microRNA (amiR) constructs against *VHA-AP1* under the control of the pOp6/LhGR system (Craft et al., 2005) were cloned and wildtype plants were transformed. Induction of amiRs targeting *VHA-AP1* led to a reduction in cell expansion in the case of both amiR-*vha-ap1* 1 and *amiR-vha-ap1* 2 (Figure 31 and Hinterberger, Master Thesis, 2019). The cell expansion defect suggests once more that VHA-AP1 is required for V-ATPase function. *UBQ10:VHA-AP1-mCherry* is not targeted by amiR-*vha-ap1* 1 and *amiR-vha-ap1* 2, as they target sites in the 3' untranslated region of *VHA-AP1* which *UBQ10:VHA-AP1-mCherry* does not contain (Figure 31A). Hence, it

did not require introducing mutations to make *UBQ10:VHA-AP1-mCherry* resistant against the amiRs to analyze whether it rescues the cell expansion defect of the amiR-mediated knock-down. I crossed amiR-*vha-ap1* lines with plants with segregating *UBQ10:VHA-AP1-mCherry* and analyzed root length of F1 seedlings. No difference in root length was found between *UBQ10:VHA-AP1-mCherry* expressing plants and plants without *UBQ10:VHA-AP1-mCherry* upon amiR induction. This indicates that *UBQ10:VHA-AP1-mCherry* does not rescue, which is in accordance with the transmission results of the *vha-ap1/+* crossed with *UBQ10:VHA-AP1-mCherry.*

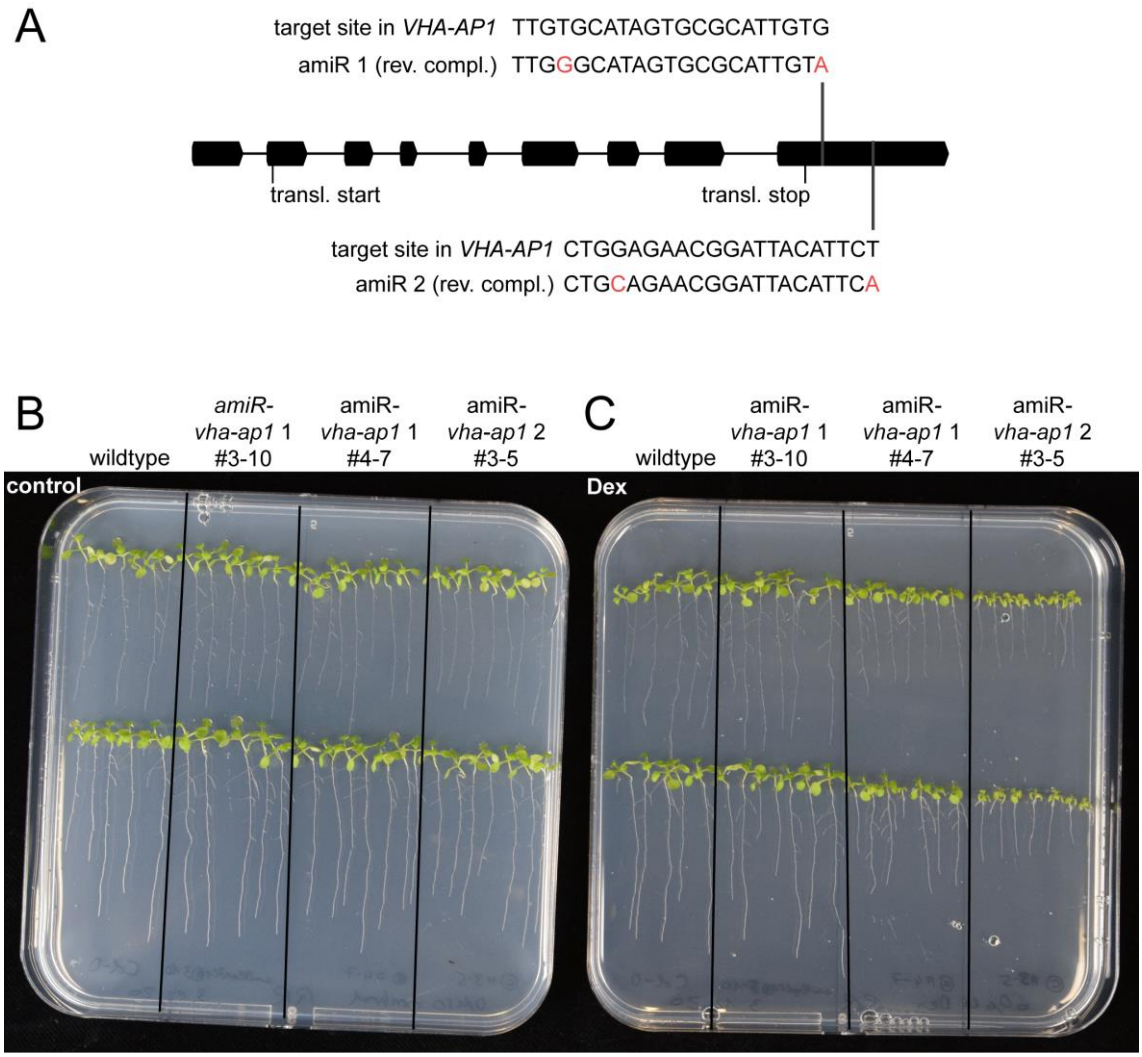

Figure 31. artificial microRNA-mediated inducible knock-down of *VHA-AP1* leads to reduced cell expansion. (A) The target sites of the dexamethasone (Dex)-inducible artificial microRNAs (amiR) targeting *VHA-AP1* are displayed. The bases shown in red in the reverse complement sequence of the amiRs are not complementary to the target site. **(B)** Seedlings grown on dimethyl sulfoxide-containing control plates. **(C)** Seedlings were grown on plates containing 60 µM Dex. 13-day-old plants are shown that were grown under long-day conditions (16 h of light and 22 °C).

3.2.4 VHA-AP1-GSL-phGFP shows a different localization than VHA-AP1-mCherry and VHA-AP1-GSL-mNeongreen

Considering that the mCherry tag could hamper the function of VHA-AP1, an untagged VHA-AP1 construct was made again using the *UBQ10* promoter. Moreover, a construct for expression of VHA-AP1 connected via a linker to a fluorescent protein was constructed, *UBQ10:VHA-AP1-GSL-phGFP*. *vha-ap1/+* and wildtype plants were transformed with the new constructs, as well as the TGN/EE marker line *VHA-a1:VHA-a1-RFP* (Fecht-Bartenbach et al., 2007) and the tonoplast marker line *VHA-a3:VHA-a3-RFP* (Brüx et al., 2008). CLSM analysis revealed a different localization for VHA-AP1-GSL-phGFP than for VHA-AP1-mCherry. While in wildtype VHA-AP1-mCherry had shown tonoplast localization and punctate signal, presumably due to TGN/EE localization, VHA-AP1-GSL-phGFP showed ER signal exclusively. It did neither co-localize with VHA-a1-RFP, nor with VHA-a3-RFP (Figure 32). The observed ER localization could either represent the true localization of endogenous VHA-AP1, or could result from retaining VHA-AP1-GSL-phGFP at the ER, for instance, due to not passing ER quality control, e.g., due to misfolding, possibly due to the GSL-phGFP tag.

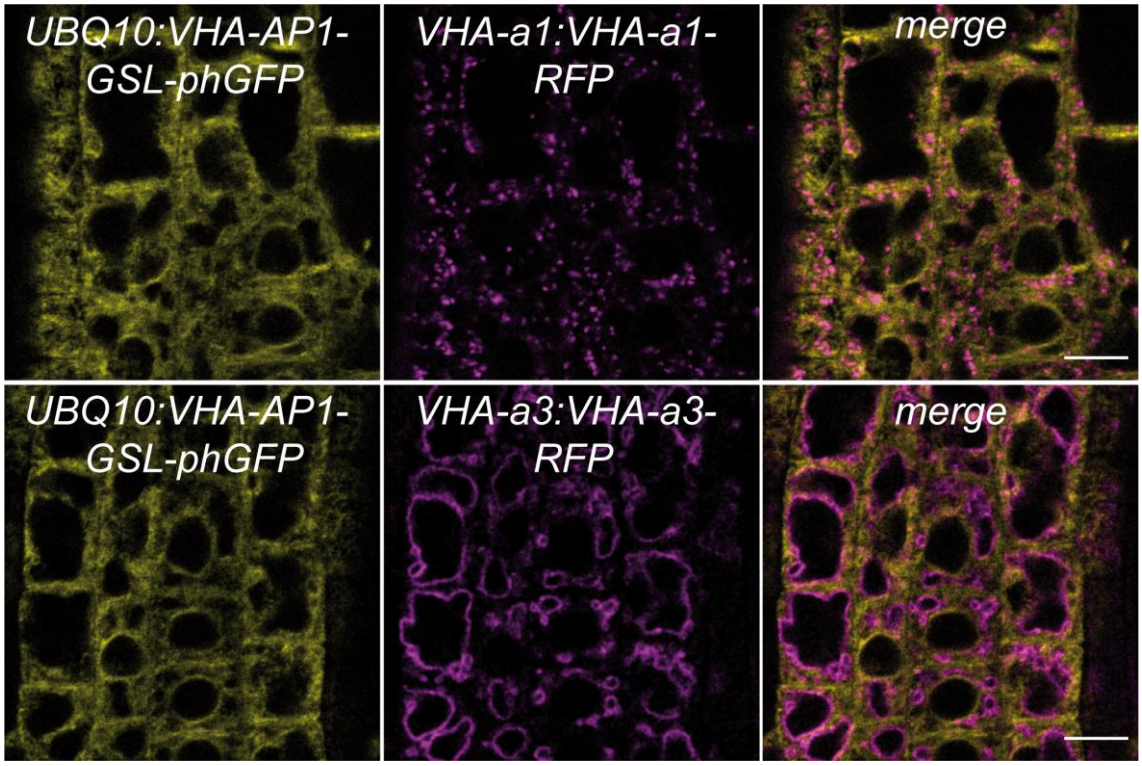

Figure 32. VHA-AP1-GSL-phGFP localizes to the ER. CLSM analysis of plants expressing *UBQ10:VHA-AP1-GSL-phGFP* in the TGN/EE marker background *VHA-a1:VHA-a1-RFP* and the tonoplast marker background *VHA-a3:VHA-a3-RFP, respectively.* Exclusively ER localization and no co-localization with VHA-a1-RFP or VHA-a3-RFP was found for VHA-AP1-GSL-phGFP. Root cells of the transition zone are shown. Scale bars = 10 µm.

As ER localization might stem from non-functionality resulting from the phGFP tag, a fourth VHA-AP1 construct was made, VHA-AP1-GSL-mNeongreen (Fabian Fink), again under the control of the *UBQ10* promoter. A *vha-a2 vha-a3* mutant generated via CRISPR/Cas9, *CR vha-a2 vha-a3-1* (Konopatzki Bachelor Thesis, 2021), as well as wildtype were transformed (Fabian Fink). The localization of VHA-AP1-GSL-mNeongreen was analyzed using CLSM and was found to be identical to the localization of VHA-AP1-mCherry (CLSM analysis Fabian Fink). In wildtype, it localized to the tonoplast and to punctate structures and in CR *vha-a2 vha-a3-1* it was detected at the ER and punctae (Figure 33).

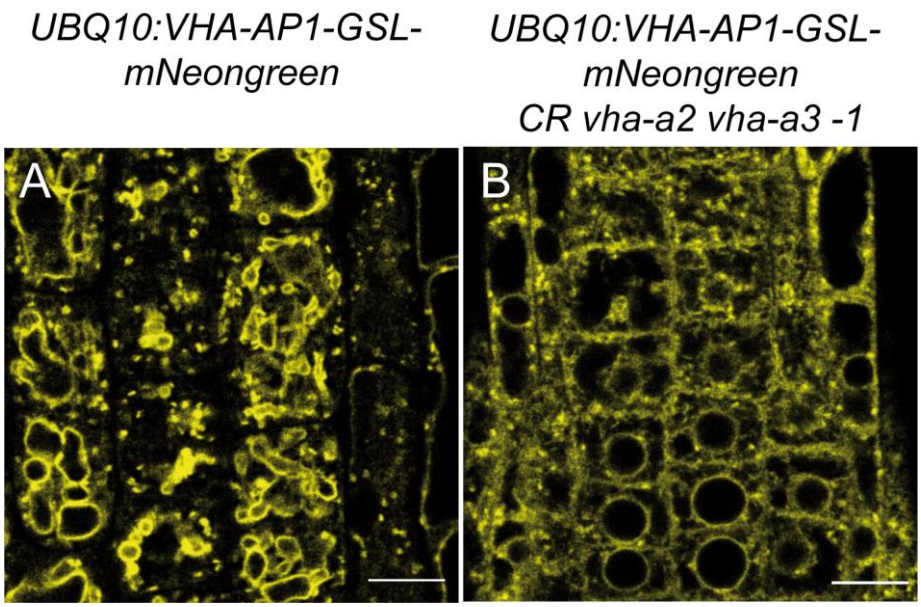

Figure 33. VHA-AP1-GSL-mNeongreen localizes to the tonoplast in wildtype and is retained in the ER in *CR vha-a2 vha-a3 -1* as VHA-AP1-mCherry.CLSM analysis of plants expressing *UBQ10:VHA-AP1-GSL-mNeongreen.* **(A)** In wildtype, VHA-AP1-GSL-mNeongreen is localized at the tonoplast and at punctate structures, which are presumably TGN/EE. **(B)** In contrast, in CR *vha-a2 vha-a3 -1* VHA-AP1-GSL-mNeongreen was detected at the ER and at punctate structures. Root cells of the transition zone are shown. Scale bars = 10 µm. This analysis was performed by Fabian Fink.

3.3 Discussion

3.3.1 Is VHA-AP1 required for V-ATPase function?

In yeast, V-ATPase subunit mutants have in common that they are able to grow on acidic media of pH 5, while they are unable to grow at pH 7.5 in 60 mM $CaCl_2$ (Sambade et al., 2005). In Arabidopsis, a characteristic of decreased V-ATPase activity at the TGN/EE is reduced cell expansion (Brüx et al., 2008; Luo et al., 2015). This work showed that inducible knock-down of *VHA-AP1* results in reduced cell expansion, suggesting that VHA-AP1 could be an essential component of V-ATPase complexes.

VHA-AP1-mCherry and VHA-AP1-GSL-mNeongreen were not detected at the tonoplast in *vha-a2 vha-a3* that lacks V-ATPases at the tonoplast. This suggests that VHA-AP1 exits the ER with V-ATPases. VHA-AP1-mCherry and VHA-AP1-GSL-mNeongreen were also found in punctate structures, presumably TGN/EE, the other destination of V-ATPase complexes in Arabidopsis. It remains to be investigated if the role of VHA-AP1 is restricted to a function at the ER or if it fulfills functions at the TGN/EE and the tonoplast. Functions outside the ER could be limited to representing a structural component of the V-ATPase complex or be beyond, such as acting in signaling through protein-protein interactions.

In contrast, VHA-AP1-GSL-phGFP was only detected at the ER, indicating that VHA-AP1 does not leave the ER. It needs to be determined which behavior reflects the behavior of the endogenous protein. As only the GSL-phGFP-tagged VHA-AP1 is unable to leave the ER, while the mCherry and the GSL-mNeongreen-tagged proteins both localize to the tonoplast and punctate structures, it is more likely that the latter represents the localization of the endogenous protein. The GSL-phGFP tag could hamper ER exit.

Targeted mutagenesis using CRISPR/Cas9 and analysis of *vha-ap1* alleles unveiled that *vha-ap1* is not transmitted via the male gametophyte. This further argues that VHA-AP1 is needed for V-ATPase function. V-ATPases are essential for pollen development (Dettmer et al., 2005; Chapter 2), and also *vha-a1* and *vha-A* are only transmitted via the female gametophyte to the next generation (Dettmer et al., 2005); this work). In contrast to *VHA-a1,* only heterozygous and no homozygous mutants were identified when targeting *VHA-AP1* using egg cell-controlled CRISPR/Cas9. This indicates that no other

protein functions redundantly with VHA-AP1 (or if another protein functions redundantly, it is not expressed at a stage at which it would be required).

To show that the cell expansion defect and the transmission defect via the male gametophyte indeed are due to missing VHA-AP1, the knock-down and knock-out lines should be rescued with a construct expressing VHA-AP1. The results of this work suggest that *UBQ10:VHA-AP1-mCherry* is not able to rescue. A reason for this could be that the *UBQ10* promoter does not provide for expression at a critical stage in development. Thus, a rescue approach in which VHA-AP1 is driven by its own promoter could be performed. However, *UBQ10:VHA-AP1-mCherry* did not rescue the inducible knock-down of VHA-AP1 which argues against absence of VHA-AP1 at a critical stage when driven by the *UBQ10* promoter. *UBQ10:VHA-AP1-mCherry* did not rescue the cell expansion defect, despite CLSM analyses showed the presence of VHA-AP1-mCherry in roots of seedling. Hence, it seems more likely, that mCherry that is fused with VHA-AP1 without a linker could represent a steric hindrance. The transmission of *vha-ap1* via the male gametophyte can be tried to be rescued by expressing a transgene encoding untagged VHA-AP1 in *vha-ap1*/+, potentially resulting in homozygous *vha-ap1* mutants.

Furthermore, it remains to be elucidated what the consequences of cleavage of VHA-AP1 (Hinterberger Master Thesis, 2019) are. Concerning ATP6AP2, Guida et al., 2018 reported that for the rescue of the yeast mutant lacking V_Oa1p with Drosophila ATP6AP2, the full length protein is required. In Drosophila, an uncleavable version of ATP6AP2 did not lead to obvious effects (Guida et al., 2018). However, before and after cleavage, VHA-AP2 and VHA-AP1 could fulfill different functions.

4 Conclusion

This study revealed the functional redundancy of tonoplast-destined V-ATPases and those dedicated to the TGN/EE in Arabidopsis. VHA-a1 seems not to have acquired novel functions during evolution aside from its specialization in localization at the TGN/EE. The TGN/EE localization of VHA-a1 is determined by the a1-TD in the N-terminal half of the protein (Lupanga et al., 2020) and the evolution of the a1-TD coincided with the evolution of non-motile sperm of seed plants. This work elucidated that VHA-a2/VHA-a2-containing V-ATPases are able to compensate for the lack of VHA-a1 during vegetative growth. It further uncovered that during pollen development, VHA-a3 is not able to rescue, but VHA-a3 containing the a1-TD can compensate for the lack of VHA-a1. Analysis of the *vha-a1* mutant contributed to the understanding of the process of primexine formation. *vha-a1* is defective in primexine formation. Pollen development of *vha-a1* could not be rescued by tapetum-specific expression of *VHA-a1* and no difference between the tapetum in *vha-a1* and wildtype was found. This argues for a largely gametophytic-controlled formation of the primexine and against a scenario in which primexine formation is mainly under the control of the sporophyte. Moreover, microscopy of fluorescently tagged VHA-a1, VHA-a3 and SRβ in microsporocytes, microspores and cells of the anther wall gave a detailed picture of the rapid remodeling of endomembranes in the anther.

Furthermore, the potential pH sensing function of the V-ATPase was analyzed and site-directed mutagenesis of histidine residues in the C-terminal half of VHA-a1 revealed potentially essential histidines and histidines that seem to be not essential for the function of VHA-a1. The results of this work suggest that VHA-a1 H738 is required for proton translocation. Additionally, VHA-a1 H434 and VHA-a1 H613 are potentially relevant for a function of VHA-a1, as they might not rescue pollen development in *vha-a1*. Moreover, site-directed mutagenesis of VHA-a1 H788 and VHA-a1 H793 to arginine led to the retention of the proteins at the ER in *Nicotiana benthamiana* and no detection in Arabidopsis. It remains to be determined if the V-ATPase has the capacity to sense pH via a conformational change triggered by differential protonation of histidine residues. In vegetative growth, VHA-a2/a3-containing V-ATPases compensate for the lack of VHA-a1. Thus, this study showed that the potential pH sensing function cannot be limited

to VHA-a1-containing V-ATPases. In future investigations, histidine residues that are conserved between the VHA-a1 and the VHA-a3 clade should be analyzed.

Finally, analysis of *VHA-AP1* showed that it is essential for the male gametophyte, and its inducible knock-down demonstrated that it is required for cell expansion, suggesting that it could be an essential component of V-ATPases.

5 Materials and methods

5.1 Plant material

Arabidopsis thaliana ecotype Columbia-0 was used in this work. Transgenic lines which were used in this study are listed in Table 1. CRISPR/Cas9-based *Cas9* ˉ lines are shown in Table 2 and Table 3.

Table 1: Transgenic lines used in this work

Name	**Reference**
VHA-a1:VHA-a1-GFP	Dettmer et al., 2006
VHA-a3:VHA-a3-RFP	Brüx et al., 2008
VHA-a1:VHA-a1-RFP	Fecht-Bartenbach et al., 2007
UBQ10:SRβ-mTurquoise	by Dr. Jana Askani
VHA-a3:VHA-a3-RFP x VHA-a1:VHA-a1-GFP F2	by Dr. Jana Askani, Askani Dissertation, 2022
UBQ10:SRβ-mTurquoise x (VHA-a3:VHA-a3-RFP x VHA-a1:VHA-a1-GFP) F1	this work
UBQ10:VHA-a1-GFP	this work, Lupanga et al., 2020
UBQ10:MpVHA-a-GSL-mVenus	by Dr. Upendo Lupanga, Lupanga et al., 2020
UBQ10:VHA-a3-mScarlet	by Dr. Upendo Lupanga, Lupanga et al., 2020
UBQ10:VHA-a3-GFP	by Dr. Melanie Krebs
UBQ10:VHA-a3-a1-TD-GFP	by Dr. Upendo Lupanga, Lupanga et al., 2020
VHA-a1:VHA-a1-RFP UBQ10:VHA-a1-GSL-mVenus	this work
VHA-a1:VHA-a1-RFP UBQ10:VHA-a1 H434R-GSL-mVenus	this work

VHA-a1:VHA-a1-RFP *UBQ10:VHA-a1H494R-GSL-mVenus*	this work
VHA-a1:VHA-a1-RFP *UBQ10:VHA-a1 H613R-GSL-mVenus*	this work
VHA-a1:VHA-a1-RFP *UBQ10:VHA-a1 H713R-GSL-mVenus*	this work
VHA-a1:VHA-a1-RFP *UBQ10:VHA-a1 H738R-GSL-mVenus*	this work
VHA-a1:VHA-a1-RFP *UBQ10:VHA-a1 H788R-GSL-mVenus*	this work
VHA-a1:VHA-a1-RFP *UBQ10:VHA-a1 H793R-GSL-mVenus*	this work
UBQ10:VHA-a1 H3A-GSL-mVenus	this work
vha-a2	SALK_142642, Krebs et al., 2010
vha-a3	SALK_29786, Brüx et al., 2008
vha-a2 vha-a3	Krebs et al., 2010
vha-a2 vha-a3 UBQ10:VHA-a1 ΔEEI-GSL-mVenus	this work
vha-a2 vha-a3 UBQ10:VHA-a1 ΔEEI H3A-GSL-mVenus	this work
vha-a2 vha-a3 UBQ10:VHA-a1 L159T-GSL-mVenus	this work
vha-a2 vha-a3 UBQ10:VHA-a1 L159T H3A-GSL-mVenus	this work
vha-a1 (Cas9$^+$) UBQ10:VHA-a3-GFP	this work
vha-a1 (Cas9$^+$) UBQ10:VHA-a3-mScarlet	this work
vha-a1 (Cas9$^+$) MSP1:VHA-a1	this work
vha-a1 (Cas9$^+$) MSP1:VHA-a1 *A9:VHA-a1-mScarlet*	by Fabian Fink
vha-a1 (Cas9$^+$) UBQ10:VHA-a1-GFP	this work, Lupanga et al., 2020
vha-a1 (Cas9$^+$)	this work, Lupanga et al., 2020
vha-a1/+ (Cas9$^+$)	this work, Lupanga et al., 2020
vha-a1 (Cas9$^+$) vha-a2/+ vha-a3/+	this work, Lupanga et al., 2020
vha-a1/+ (Cas9$^+$) vha-a2/+ vha-a3/+	this work, Lupanga et al., 2020

vha-a2/+ vha-a3/+	this work, Lupanga et al., 2020
vha-a1/+ (Cas9^{+}) vha-a2 vha-a3/+	this work, Lupanga et al., 2020
vha-a1/+ (Cas9^{+}) vha-a2/+ vha-a3	this work, Lupanga et al., 2020
vha-a1 (Cas9^{+}) vha-a2 vha-a3/+	this work, Lupanga et al., 2020
vha-a1 (Cas9^{+}) vha-a2/+	this work, Lupanga et al., 2020
vha-a1 (Cas9^{+}) vha-a3/+	this work¸ Lupanga et al., 2020
UBQ10:VHA-AP1-mCherry	by Fabian Fink, Hinterberger Master Thesis, 2019
vha-a2 vha-a3 UBQ10:VHA-AP1-mCherry	by Fabian Fink
UBQ10:VHA-AP1-GSL-mNeongreen	by Fabian Fink
CR vha-a2 vha-a3 -1 UBQ10:VHA-AP1-GSL-mNeongreen	by Fabian Fink
VHA-a1:VHA-a1-RFP UBQ10:VHA-AP1-GSL-phGFP	this work
VHA-a3:VHA-a3-RFP UBQ10:VHA-AP1-GSL-phGFP	this work
amiR-*vha-ap1* 1	this work, Hinterberger Master Thesis, 2019
amiR-*vha-ap1* 2	this work, Hinterberger Master Thesis, 2019

Table 2: *vha-a1 (Cas9 -)* lines that were generated and used in this work

Name
vha-a1-1 UBQ10:VHA-a1-GFP
vha-a1-2 UBQ10:VHA-a1-GFP
vha-a1-1 UBQ10:VHA-a1-GSL-mVenus
vha-a1-1 UBQ10:VHA-a1 H494R-GSL-mVenus
vha-a1-1 UBQ10:VHA-a1 H713R-GSL-mVenus
vha-a1-1 UBQ10:VHA-a1 H738R-GSL-mVenus
vha-a1-1 UBQ10:VHA-a3-a1-TD-GFP
vha-a1-1/+

vha-ap1-1/+
vha-ap1-2/+
vha-a1-1/+ x wildtype F1
wildtype x *vha-a1-1*/+ F1
vha-ap1-1/+ x wildtype F1
wildtype x *vha-ap1-1*/+ F1
vha-ap1-2/+ x wildtype F1
wildtype x *vha-ap1-2*/+ F1

Table 3: *CRISPR vha-a2 vha-a3 (Cas9 -)* line

Name	**Reference**
CR vha-a2 vha-a3 -1	Konopatzki Bachelor Thesis, 2021

5.2 Standard growth conditions

Plates were prepared using ½ Murashige and Skoog (MS) medium (Duchefa Biochemie), 0.5% sucrose and 0.55% phytoagar (Duchefa Biochemie) adjusted to pH 5.8 with KOH. Seeds were sterilized in 70% ethanol for 15 min and 99% ethanol for 5 min in 1.5 or 2 ml tubes on a rotating device. In the sterile hood, they were dried on filter paper and subsequently sown on plates. Plates were put at 4 °C into the dark for stratification for 2 days. Subsequently, plates were placed into growth chambers providing long-day conditions (16 h of light, 8 h of darkness) at 22 °C. After 9 to 11 days plants were transferred to soil if required and grown in growth rooms at long-day conditions, with the exception of *vha-a2 vha-a3* mutants, which were grown in growth chambers in constant light.

5.3 Plasmid and transgenic plants generation

Constructs were cloned using the GreenGate system, which allows the insertion of six entry modules into a destination vector in a defined order based on specific overhangs (Lampropoulos et al., 2013).

Entry modules that were generated in this work are described in 5.4 and 5.5. The components used for GreenGate reactions are listed in Table 4 and the thermocycler program used is shown in Table 5. After the GreenGate reaction, 5 µl of the reaction were used to transform *Escherichia coli (E. coli)* (5.9 Transformation of bacteria). Subsequently, plasmids were isolated from liquid cultures via miniprep and restriction endonuclease digestion was performed to test if the correct plasmid was obtained. For Agrobacterium-mediated transformation of Arabidopsis, the *Agrobacterium tumefaciens* (*A. tumefaciens)* strain ASE1 was used if the GreenGate construct possessed the destination vector pGGZ001 or pGGZ003 (Lampropoulos et al., 2013). If the GreenGate construct contained the destination vector pGGZ004 (Lupanga et al., 2020) the *Agrobacterium tumefaciens* strain GV3101 was used (5.9 Transformation of bacteria). pGGZ001 and pGGZ003 each confer resistance against spectinomycin, pGGZ004 mediates kanamycin resistance.

Primers used in this work were ordered from Eurofins Genomics and enzymes which were used were from Thermo Fisher Scientific. Restriction endonuclease digestion, isolation of plasmids from liquid cultures, polymerase chain reactions (PCRs), ligations, agarose gel electrophoresis and DNA purification from agarose gels were performed according to standard protocols. The Geneious 10.2.3 software (Biomatters inc., San Diego, California, USA) was used for *in silico* plasmid construction and alignment of sequences.

Table 4: GreenGate reaction components

Components	Volume
A module ~100 ng/µl	1.5 µl
B module ~100 ng/µl	1.5 µl
C module ~100 ng/µl	1.5 µl
D module ~100 ng/µl	1.5 µl
E module ~100 ng/µl	1.5 µl
F module ~100 ng/µl	1.5 µl
Destination vector ~100 ng/µl	1 µl
10 x Fast Digest buffer	1.5 µl
Eco31I Fast Digest	1.5 µl
T4 DNA Ligase 30 U/µl	1 µl
ATP 10 mM	1 µl

Table 5: Cycler program used for GreenGate reactions

Temperature	Time	Number of cycles
37 °C	3 min	] 50
16 °C	3 min	
50 °C	5 min	1
80 °C	5 min	1
16 °C	hold	

GreenGate constructs that were assembled in this work are specified in Table 6. GreenGate constructs that were assembled by others are shown in Table 7.

Table 6: GreenGate constructs assembled in this work

UBQ10:VHA-a1-GFP **°**						
A module	B module	C composite	D module	E module	F module	Destination vector
pGGA006 *****	pGGB003 *****	assembl.**°**	pGGD011 **ψ**	pGGE001 *****	pGGF007 *****	pGGZ001*****
UBQ10 promoter	*B-dummy*	*VHA-a1 intron 10*	*GFP A206K*	*RBCS* terminator	*pNOS:KanR:tNOS*	
UBQ10:VHA-a1-GSL-mVenus **ᶻ**						
A module	B module	C composite	D module	E module	F module	Destination vector
pGGA006 *****	pGGB003 *****	assembl.**°**	p2456 **°**	pGGE001 *****	pGGF005 *****	pGGZ001*****
UBQ10 promoter	*B-dummy*	*VHA-a1 intron 10*	*GSL-mVenus*	*RBCS* terminator	*pUBQ10:HygrR:tOCS*	
UBQ10: VHA-a1 L159T (H3A)-GSL-mVenus						
A module	B module	C composite	D module	E module	F module	Destination vector
pGGA006 *****	pGGB003 *****	L159T **°**, intron 10 **°** (H3A **ˣ**)	p2456 **°**	pGGE001 *****	pGGF005 *****	pGGZ001*****
UBQ10 promoter	*B-dummy*	*VHA-a1 159T intron 10 (H3A)*	*GSL-mVenus*	*RBCS* terminator	*pUBQ10:HygrR:tOCS*	
UBQ10: VHA-a1 ΔEEI (H3A)-GSL-mVenus						
A module	B module	C composite	D module	E module	F module	Destination vector
pGGA006 *****	pGGB003 *****	ΔEEI **°**, intron 10 **°** (H3A **ˣ**)	p2456 **°**	pGGE001 *****	pGGF005 *****	pGGZ001*****
UBQ10 promoter	*B-dummy*	*VHA-a1* ΔEEI *intron 10 (H3A)*	*GSL-mVenus*	*RBCS* terminator	*pUBQ10:HygrR:tOCS*	
MSP1:VHA-a1						
A module	B module	C composite	D module	E module	F module	Destination vector
p4187 **ˣ**	pGGB003 *****	assembl.**°**	pGGD002 *****	pGGE001 *****	pLB012 **§**	pGGZ004**°**
MSP1 promoter	*B-dummy*	*VHA-a1 intron 10*	*D-dummy*	*RBCS* terminator	*OLE1-mCherry*	

MSP3:VHA-a1						
A module	B module	C composite	D module	E module	F module	Destination vector
p4184 [x]	pGGB003 [*]	assembl.[°]	pGGD002 [*]	pGGE001 [*]	pLB012 [§]	pGGZ004[°]
MSP3 promoter	*B-dummy*	*VHA-a1 intron 10*	*D-dummy*	*RBCS* terminator	*OLE1-mCherry*	
UBQ10:VHA-AP1						
A module	B module	C module	D module	E module	F module	Destination vector
pGGA006 [*]	pGGB003 [*]	p2637 [ǂ]	pGGD002 [*]	pGGE001 [*]	pLB012 [§]	pGGZ004[°]
UBQ10 promoter	*B-dummy*	*VHA-AP1 (AT3G 13410) ORF*	*D-dummy*	*RBCS* terminator	*OLE1-mCherry*	
UBQ10:VHA-AP1-GSL-pHGFP						
A module	B module	C module	D module	E module	F module	Destination vector
pGGA006 [*]	pGGB003 [*]	p2637 [ǂ]	p3267 [¥]	pGGE001 [*]	pLB012 [§]	pGGZ004[°]
UBQ10 promoter	*B-dummy*	*VHA-AP1 (AT3G 13410) ORF*	*GSL-phGFP*	*RBCS* terminator	*OLE1-mCherry*	

[*] Lampropoulos et al., 2013
[°] Lupanga et al., 2020
[ǂ] by Fabian Fink
[¥] by Dr. Rainer Waadt
[§] A. Maizel lab
[Ψ] J. Lohmann lab
[x] this study
[z] The eight constructs of the VHA-a1 histidine mutants (VHA-a1 H434R, H494R, H613R, H713R, H738R, H788R, H793R and H3A were assembled accordingly. The only difference: C, harboring the mutations.

Table 7: GreenGate constructs assembled by others

***A9:VHA-a1-GSL-mScarlet* cloned by Fabian Fink**						
A module	B module	C module	D module	E module	F module	Destination vector
p4353 ǂ	pGGB003 *	assembl °	p1324°	pGGE001 *	pGGF007 *	pGGZ004 °
A9 promoter	*B-dummy*	*VHA-a1 intron 10*	*GSL-m Scarlet*	*RBCS* terminator	*pNOS:Kan R:tNOS*	
***UBQ10:SRβ-mTurquoise* cloned by Dr. Jana Askani**						
A module	B module	C module	D module	E module	F module	Destination vector
pGGA006 *	pGGB003 *	p1637 ᵞ	p2553 ¥	p1296 ^	pGGF001 *	pGGZ003 *
UBQ10 promoter	*B-dummy*	*SRβ (AT2G 18770) ORF*	*mTur-quoise*	*tHSP 18.2M*	BastaR	
***UBQ10:VHA-AP1-mCherry* cloned by Fabian Fink**						
A module	B module	C module	D module	E module	F module	Destination vector
pGGA006 *	pGGB003 *	p2637 ǂ	pGGD010 ψ	pGGE001 *	pGGF005 *	pGGZ001 *
UBQ10 promoter	*B-dummy*	*VHA-AP1 (AT3G13 410) ORF*	*mCherry*	*RBCS* terminator	*pUBQ10: HygrR:tOCS*	

* Lampropoulos et al., 2013
° Lupanga et al., 2020
^ Waadt et al., 2017
ψ J. Lohmann lab
ǂ by Fabian Fink
¥ by Dr. Rainer Waadt
ᵞ by Dr. Jana Askani

5.4 Cloning of pGGA modules containing the MSP1/MSP3 promoter

The MSP1 and MSP3 promoter sequences were amplified from wildtype gDNA according to Honys et al., 2006 using the primers listed in Table 8. The resulting PCR product (1047 bp in the case of the MSP1 promoter and 1035 bp for the MSP3 promoter) was subjected to agarose gel electrophoresis, purified, digested with *Eco31*I Fast Digest, again run on an agarose gel, purified and subsequently ligated into the backbone of *Eco31*I digested pGGA000 (Lampropoulos et al., 2013, ampicillin resistance). The plasmids were multiplied in *E. coli* and checked via test digest and sequencing.

Table 8: Primers used for cloning of pGGA-MSP1 and pGGA-MSP3

Cloning of	Primer name	Primer sequence
pGGA-MSP1 forward primer	KS-q4787	AAC AGG TCT CAA CCT CAG TTA GCA TGA AAA ATT GTA TG
reverse primer	KS-q4788	AAC AGG TCT CTT GTT CGT GCA ATG TGA AGA TTT TGT TG
pGGA-MSP3 forward primer	KS-q4789	AAC AGG TCT CAA CCT GCT GGT TGT GAT ATA ATA GG
reverse primer	KS-q4790	AAC AGG TCT CTT GTT TGC AAA CCC AAG TTT CAG CT

5.5 Site-directed mutagenesis of VHA-a1 histidine residues

VHA-a1 intron 10 as C-module was assembled from three parts: the coding sequence of the VHA-a1 N-terminal half, VHA-a1 intron 10 and the VHA-a1 C-terminal half coding sequence according to Lupanga et al., 2020. All parts were released from pJet1.2 prior to the GreenGate reactions by digestion with *Bgl*II, subjected to agarose gel electrophoresis, excised and purified. Site-directed mutagenesis of VHA-a1 C-terminal histidine residues was performed using pJet1.2 containing the VHA-a1 C-terminal half (p1251, Dr. Upendo Lupanga) as template and primers as indicated in Table 9 and according to Wang and Malcolm, 1999 . For the generation of VHA-a1 H3A (VHA-a1

H434A, H494A and H613A), three consecutive rounds of site-directed mutagenesis were performed. The plasmids were multiplied in *E.coli* and the presence of the desired mutations was monitored via sequencing after miniprep.

Table 9: Primers used for site-directed mutagenesis of VHA-a1 histidine residues

Mutation in *VHA-a1*	**Primer name**	**Primer sequence**
H434R forward	KS-q3759	TTT GGT GAT TGG GGT CGT GGT CTA TGC TTG CTG
reverse	KS-q3760	CAG CAA GCA TAG ACC ACG ACC CCA ATC ACC AAA
H713R forward	KS-q3761	GTA CAT CAA TTG ATT CGC TCC ATA GAA TTT GTT
reverse	KS-q3762	AAC AAA TTC TAT GGA GCG AAT CAA TTG ATG TAC
H738R forward	KS-q3763	GCT CTT AGT TTG GCT CGT TCG GAA TTG TCA ACA
reverse	KS-q3764	TGT TGA CAA TTC CGA ACG AGC CAA ACT AAG AGC
H788R forward	KS-q3765	CTA AGT GCA TTT CTC CGT GCT CTG CGT CTT CAC
reverse	KS-q3766	GTG AAG ACG CAG AGC ACG GAG AAA TGC ACT TAG
H793R forward	KS-q3767	CAT GCT CTG CGT CTT CGC TGG GTA GAA TTC ATG
reverse	KS-q3768	CAT GAA TTC TAC CCA GCG AAG ACG CAG AGC ATG
H494R forward	KS-q3769	TTC TCT GTT CCT TTC CGC ATC TTT GGT GGT TCA
reverse	KS-q3770	TGA ACC ACC AAA GAT GCG GAA AGG AAC AGA GAA
H613R forward	KS-q3771	CAA GCA GAC TTG TAT CGT GTA ATG ATC TAC ATG

reverse	KS-q3772	CAT GTA GAT CAT TAC ACG ATA CAA GTC TGC TTG
H434A forward	KS-q3818	TTT GGT GAT TGG GGT GCT GGT CTA TGC TTG CTG
reverse	KS-q3819	CAG CAA GCA TAG ACC AGC ACC CCA ATC ACC AAA
H494A forward	KS-q3828	TTC TCT GTT CCT TTC GCC ATC TTT GGT GGT TCA
reverse	KS-q3829	TGA ACC ACC AAA GAT GTG GAA AGG AAC AGA GAA
H613A forward	KS-q3830	CAA GCA GAC TTG TAT GCT GTA ATG ATC TAC ATG
reverse	KS-q3831	CAT GTA GAT CAT TAC ATG ATA CAA GTC TGC TTG

5.6 Cloning of CRISPR/Cas9 constructs

CRISPR target sites were selected using CHOPCHOP (https://chopchop.cbu.uib.no; Labun et al., 2016) and CCtop; (https://crispr.cos.uni-heidelberg.de, Stemmer et al., 2015). The selected gRNAs have at least 4 bp mismatch with every other region in the *Arabidopsis thaliana* genome as a precaution against off-target mutations. gRNA sequences were inserted into the plasmid pHEE401E between two *Bsa*I (*Eco*31I) cleavage sites according to the authors' description (Wang et al., 2015). For CRISPR constructs for the expression of one gRNA, forward and reverse oligonucleotides containing the gRNA sequence and the cloning overhangs were annealed (Table 10 and Table 11) 10 µl of 100 µM of forward and reverse oligonucleotide, each, were incubated in 5 µl 5x annealing buffer (5 M NaCl, 0.5 M ethylenediaminetetraacetic acid (EDTA), 1 M tris(hydoxymethyl)aminomethane (Tris)-HCl pH 7.5) at 95 °C for 5 min and let cool down at room temperature subsequently. The mix was diluted 1:100 in ddH_2O and a GreenGate reaction (Table 4 and Table 5) with 4 µl of this dilution and 2 µl 100 ng/µl pHEE401E was performed. For the CRISPR construct containing two gRNA sequences, the plasmid pHEE2E-TRI (Wang et al., 2015) was used as a template for a PCR with primers containing the gRNA sequences (Table 11). The purified PCR product was

ligated into previously *Eco*31I digested and purified pHEE401E. pHEE401 carries a kanamycin resistance for bacterial selection and hygromycin resistance as plant selection marker.

Table 10: CRISPR/Cas9 target sites

Gene	Construct	gRNA	CRISPR/Cas9 target site
VHA-a1	*CRISPR VHA-a1 I*	gRNA 1	TCTCATGTCAGTTGTCGAC
VHA-a1	*CRISPR VHA-a1 I*	gRNA 2	AGCTCGCCGAGATAAGTGA
VHA-a1	*CRISPR VHA-a1 II*	gRNA 3	ATCACCTGCTCAAGTAAAG
VHA-a1	*CRISPR VHA-a1 III*	gRNA 4	AATTGCTATCCTGTCCCCG
VHA-AP1	*CRISPR VHA-AP1 I*	gRNA 1	AAGATTCAAATTGGTGCGG
VHA-AP1	*CRISPR VHA-AP1 II*	gRNA 2	CTTTTGGAGGGCATACTAG

Table 11: Primers used for cloning CRISPR constructs

Construct	Purpose	Primer name	Sequence
CRISPR VHA a1 I	PCR	KS-q4259	ATA TAT GGT CTC GAT TGA GCT CGC CGA GAT AAG TGA GTT TTA GAG CTA GAA ATA GC
CRISPR VHA a1 I	PCR	KS-q4260	ATT ATT GGT CTC TAA ACG TCG ACA ACT GAC ATG AGA CAA TCT CTT AGT CGA CTC TAC
CRISPR VHA-a1 II	annealing	KS-q4345	ATT GAT CAC CTG CTC AAG TAA AG
CRISPR VHA-a1 II	annealing	KS-q4346	AAA CCT TTA CTT GAG CAG GTG AT
CRISPR VHA-a1 III	annealing	KS-q4347	ATT GAA TTG CTA TCC TGT CCC CG
CRISPR VHA-a1 III	annealing	KS-q4348	AAA CCG GGG ACA GGA TAG CAA TT
CRISPR VHA-AP1 I	annealing	KS-q3582	ATT GGA AGA TTC AAA TTG GTG CGG
CRISPR VHA-AP1 I	annealing	KS-q3583	AAA CCC GCA CCA ATT TGA ATC TTC
CRISPR VHA-AP1 II	annealing	KS-q3954	ATT GCT TTT GGA GGG CAT ACT AG
CRISPR VHA-AP1 II	annealing	KS-q3955	AAA CCT AGT ATG CCC TCC AAA AG

5.7 Cloning of artificial microRNAs

Target sites for amiRs were selected using the Web MicroRNA Designer (WMD3, http://wmd3.weigelworld.org/cgi-bin/webapp.cgi, Schwab et al., 2006), and are shown in Table 12. According to the online tool's description, the amiR sequence containing precursor was generated in three PCRs using pRS300 as a template and primers A, B and the target-specific primers I to IV (Table 13). The purified PCR products a, b, c served as a template for a fourth PCR with primers A and B (http://wmd3.weigelworld.org/cgi-bin/webapp.cgi). The final PCR product was purified and ligated into pGGI000 (Lampropoulos et al., 2013) and the resulting plasmid was multiplied in *E. coli* and sequenced. Next, the GreenGate intermediate vector pGGN was cloned that was assembled with the intermediate vector pGGM-UBQ10:GR-LhG4 (Lupanga et al., 2020) into the destination vector pGGZ003 (Lampropoulos et al., 2013) in a GreenGate reaction (Table 4 and Table 5). The pGGN module was created in a GreenGate reaction composed of the HA adapter (Lampropoulos et al., 2013), *pOp6* (pGGAA016; Schürholz et al., 2018), pGGI-*amiRap1* (this work), *RBCS* terminator (pGGE001; Lampropoulos et al., 2013), *pNOS:HygR* (p1317; Waadt et al., 2017) and pGGN000 (Lampropoulos et al., 2013). The intermediate vectors pGGN and pGGM possess kanamycin resistance for bacterial selection, and the final vector pGGZ003 has spectinomycin resistance.

Table 12: Artificial microRNAs target sites

Target site *amiR-vha-ap1* 1	TTGTGCATAGTGCGCATTGTG
Target site *amiR-vha-ap1* 2	CTGGAGAACGGATTACATTCT

Table 13: Primers used for cloning artificial microRNAs

Construct	**Purpose**	**Primer name**	**Sequence**
amiR-vha-ap1 1	Primer I	KS-q4016	GAT ACA ATG CGC ACT ATG CCC AAT CTC TCT TTT GTA TTC C
	Primer II	KS-q4017	GAT TGG GCA TAG TGC GCA TTG TAT CAA AGA GAA TCA ATG A
	Primer III	KS-q4018	GAT TAG GCA TAG TGC CCA TTG TTT CAC AGG TCG TGA TAT G
	Primer IV	KS-q4019	GAA ACA ATG GGC ACT ATG CCT AAT CTA CAT ATA TAT TCC T

amiR-vha-ap1 2	Primer I	KS-q4024	GAT GAA TGT AAT CCG TTC TGC AGT CTC TCT TTT GTA TTC C
	Primer II	KS-q4025	GAC TGC AGA ACG GAT TAC ATT CAT CAA AGA GAA TCA ATG A
	Primer III	KS-q4026	GAC TAC AGA ACG GAT AAC ATT CTT CAC AGG TCG TGA TAT G
	Primer IV	KS-q4027	GAA GAA TGT TAT CCG TTC TGT AGT CTA CAT ATA TAT TCC T

5.8 Bacteria growth conditions

Bacteria were grown in LB medium composed of 1% (v/w) Bacto™ Tryptone (Becton Dickinson), 0.5% (w/v) yeast extract (Carl Roth), (w/v) 1% NaCl, 0.1% glucose in H_2O of pH 7 adjusted with NaOH, supplemented with the appropriate antibiotics for selection. To get solid plates, 1% (w/v) Bacto™ Agar (Becton Dickinson) was added. The final concentrations of antibiotics which were used are listed in Table 15.

5.9 Transformation of bacteria

E. coli of the strain NEB 5α F'I^q (New England Biolabs) that were chemically competent were transformed with the respective plasmids. Approximately 2 µg DNA was added to bacteria after gently unfreezing them. After 30 min on ice, heat-shock was performed at 42 °C for 45 sec, followed by 5 min on ice. 1 ml LB was added and incubated for 1h at 37 °C while shaking. Bacteria were distributed on plates containing antibiotics for selection and grown at 37 °C for about 15 h.

A. tumefaciens of the strains GV3101 and ASE1 were used. Chemically competent cells supplemented with approximately 2 µg DNA were incubated for 10 min on ice after unfreezing them. Then, they were kept for 5 min in liquid nitrogen, followed by 5 min at 37 °C. 800 µl LB was added and 3 h incubation at 28 °C followed, after which bacteria were distributed on plates containing antibiotics for selection (Table 14). They were grown for about 40 h at 42 °C.

Table 14: Antibiotics used for selection of Agrobacteria

A. tumefaciens	**Antibiotics**	**Selection for**
GV3101	rifampicin	chromosome
	gentamycin	Ti plasmid

ASE1	chloramphenicol	chromosome
	kanamycin	Ti plasmid
	tetracycline	pSOUP

Table 15: Concentrations of antibiotics/herbicides used in this study

Antibiotics	**Final concentration (µg/ml)**	**Solvent**	**Manufacturer**
ampicillin	150	H_2O	Carl Roth
spectinomycin	100	H_2O	Duchefa Biochemie
rifampicin	5	DMSO	Carl Roth
gentamycin	15	H_2O	Carl Roth
chloramphenicol	25	ethanol	Carl Roth
kanamycin	50	H_2O	Carl Roth
tetracycline	10	ethanol	Carl Roth
hygromycin	25	H_2O	Merck
Basta (glufosinate ammonium)	10	H_2O	Merck

5.10 Transformation of *Arabidopsis thaliana*

Agrobacterium-mediated transformation of *Arabidopsis thaliana* was performed using the floral dip method (Clough and Bent, 1998). 5 ml LB medium supplemented with the appropriate antibiotics was inoculated with *A. tumefaciens* carrying the desired construct and incubated for about 15 h at 28 °C whilst shaking. 400 µl of this culture were used to inoculate 200 ml LB medium with the respective antibiotics in a 1 l flask. After incubation for about 15 h at 28 °C whilst shaking, the cultures were centrifuged at 5000 rpm for 15 min at 4 °C. The bacterial pellet was resuspended in 200 ml solution composed of 5% (w/v) sucrose, 0.05% (v/v) Silwet L-77 (Lehle Seeds) and a few crystals $MgSO_4$. The inflorescences of approximately 6-week-old plants were dipped into the infiltration solution. Plants were placed into trays and covered with plastic bags for about 15 h and grown as before after unwrapping.

5.11 Transient expression in *Nicotiana benthamiana*

Nicotiana benthamiana leaves were infiltrated with *A. tumefaciens*-containing solution for transient expression. Plants that were grown at 25 °C, long-day conditions (16 h of light, 8 h of darkness) were used at the age of about 4 weeks. 5 h before infiltration plants were sprinkled with water in a tray which was then covered with a transparent cover. Agrobacteria carrying the desired constructs were grown in 10 ml LB containing the respective antibiotics in a 100 ml flask at 28 °C for about 15 h. After centrifugation at 4500 rpm at 4 °C for 15 min, the pellet was resuspended in 2 ml infiltration solution (10 mM 2-(4-morpholino)-ethanesulphonic acid (MES) adjusted to pH 5,6 with KOH, 10 mM $MgCl_2$ and 150 µM acetosyringone (Merck)). OD_{600} was adjusted to 0.7 with infiltration solution. Agrobacteria carrying the P19 silencing suppressor that had been processed in the same way were mixed with agrobacteria containing the construct of interest in a ratio of 1:1. Incubation at room temperature for 2 h 45 min followed. The lower sides of *Nicotiana benthamiana* leaves were infiltrated with a 1 ml syringe. 3 days after infiltration, small pieces of the leaves were excised and subjected to CLSM analysis (Leica TCS SP5II microscope).

5.12 Crossing *Arabidopsis thaliana*

For crossing *Arabidopsis thaliana,* flower buds at stage 12 (Smyth et al., 1990) were emasculated using a Zeiss Stemi 2000-CS dissecting microscope at a magnification of 50x. Flowers at stage 13 (Smyth et al., 1990) were used as pollen donors. A flower was picked and its anthers were brought in contact with the stigma of the emasculated flower at the dissecting microscope.

5.13 Extraction of genomic DNA

Extraction of genomic DNA (gDNA) was performed according to Edwards et al., 1991 . Leaf tip tissue was harvested and macerated in a 1.5 ml tube at room temperature for 10 sec with a sterile plastic pestle. 400 µl extraction buffer (250 mM NaCl, 25 mM ethylenediaminetetraacetic acid (EDTA), 200 mM tris(hydoxymethyl)aminomethane (Tris) adjusted to pH 8 with HCl, 0.5% sodium dodecyl sulfate (SDS)) was added, followed by vortexing of the sample for 5 sec. Centrifugation at 13 000 rpm for 5 min in a tabletop centrifuge followed. Fresh 1.5 ml tubes were filled with 300 µl isopropanol and

300 µl of the supernatant was added. After 2 min at room temperature, centrifugation at 13 000 rpm for 5 min was performed. The supernatant was discarded by inverting the tube and the pellet was washed with 700 µl 70% ethanol. Centrifugation at 13 000 rpm for 5 min was performed, after which the supernatant was thoroughly removed by pipetting and the pellet was vacuum dried. The pellet was dissolved in 50 µl ddH_2O. The gDNA was stored at -20 °C.

5.14 Genotyping of mutant alleles

For the genotyping of mutant alleles, gDNA was extracted and PCRs amplifying the relevant regions were performed (Table 16). PCR products were submitted for sequencing (Eurofins Genomics) or genotyping was performed using agarose gel electrophoresis (in the case of *vha-a1-1*). The 260 bp deletion in *vha-a1-1* causes a visible band shift compared to the wildtype allele (Figure 4). In the case of *vha-ap1-1* sequencing or restriction digest using Fast digest *Ssi*I (Thermo Scientific) followed by agarose gel electrophoresis was used. The 1 bp insertion in *vha-ap1-1* abolishes a recognition site of *Ssi*I, leading to two instead of three fragments as for the wildtype allele upon digestion with *Ssi*I.

5.15 Sequencing of PCR products and plasmid DNA

DNA for sequencing was submitted to Eurofins Genomics. Unpurified PCR products of 300 to 1000 bp were submitted at a concentration of about 10 ng/µl as recommended by the company. Plasmid DNA was sent at a concentration of 50 to 100 ng/µl. The sample volume was 15 µl plus 2 µl (10 µM) primer (in case primers were sent; otherwise, primers were selected from the company's list).

Table 16: Primers used for genotyping PCRs

Genotyping PCR	Forward primer	Reverse primer	PCR product length (bp)
CRISPR site 1 and 2 *(VHA-a1 specific)*	CCACCAGACTT ATACCGGACG	GCAACACCAATT GAAATCCGC	635
CRISPR site 2 *(VHA-a1-GFP specific)*	CTGAGTTTTTCT GATTAACAAACA	CGTGGTGAACAT CTTAGACC	329
CRISPR site 2	GACGGGAACAAA	GCAACACCAATTG	546

(VHA-a1 specific)	AACTGAACTC	AAATCCGC	
CRISPR site 3 *(VHA-a1)*	CCTTGTCTCAAGT AATACTCATG	GATGTTGAAGGAT CCATGATTTC	358
CRISPR site 4 *(VHA-a1)*	GAAATCATGGATC CTTCAACATC	TTAAGCTATAGCC AACAGAATTAAG	553
CRISPR site 1 *(VHA-AP1)*	TGAATTTGCTGA TTGTTTCGTT	TATCACAAGTCC CAGGCTTTTT	286
CRISPR site 2 *(VHA-AP1)*	GAAATTGCTACT GGCTGTGATG	CAGCAAAGTCCA CTGATCAAGATG	295
Cas9 specific	AACCCCATTAAT GCGTCAGGCG	GTCAATGTACCCA GCGTAGCCG	498
VHA-a2 specific*	CTCTCTCCATGA TCGTCTCTCTCG	GCGGTAGCACTTC TATGGGCTG	898
vha-a2 specific*	GCGTGGACCGCT TGCTGCAACT	GCGGTAGCACTTC TATGGGCTG	678
VHA-a3 specific*	GAACGAACGATG GCGGAAAG	TGAATGTACCTGT GCTGCGT	565
vha-a3 specific*	GAACGAACGATG GCGGAAAG	GCGTGGACCGCT TGCTGCAACT	264

* designed by Dr. Melanie Krebs

5.16 Hypocotyl length measurement of etiolated seedlings

For hypocotyl length measurements of etiolated seedlings, seeds were sown on agar plates made with ddH_2O without nutrients containing 2.5 mM 2-(4-morpholino)-ethanesulphonic acid (MES), pH 5.8 adjusted with KOH, 0.8% phytoagar and 125 nM Concanamycin A (Santa Cruz Biotechnology) dissolved in DMSO. The plates were placed for 2 days into the dark at 4 °C for stratification. A light stimulus for 4 h at 22 °C followed. Subsequently, plates were wrapped in aluminum foil and seedlings were grown for 4 days in the dark at 22 °C. Seedlings grown on horizontally oriented plates were laid on overhead transparency sheets in drops of water which were then placed on a scanner for image acquisition. Seedlings grown on vertically oriented plates were photographed with a digital single-lens reflex camera. Quantification of hypocotyl length was done with Fiji (Fiji is just image J) (Schindelin et al., 2012).

5.17 Quantification of rosette areas

For quantification of rosette areas, plants were grown for 3.5 weeks under long-day conditions (16 h of light and 22 °C) and were photographed with a digital single-lens reflex camera. Quantification of rosette area was performed with the ImageJ plug-in Rosette Tracker (De Vylder et al., 2012).

5.18 Prediction of pK_a values

Calculation of pK_a values was done using PROPKA3.0 (Olsson et al., 2011) with a specification of pH 5.6. The calculations were based on the 3D model of the VHA-a1 C-terminal half obtained via homology modeling by Dr. Upendo Lupanga (Lupanga Dissertation, 2017).

5.19 Confocal laser scanning microscopy

CLSM analyses were performed either with a Leica TCS SP5II microscope or a Leica STELLARIS 8 microscope. For analyses at the Leica TCS SP5II a Leica HCX PL APO lambda blue 63x/1.20 water immersion objective and the Leica Application Suite Advanced Fluorescence software were used. Analyses at the Leica STELLARIS 8 microscope were performed with a HC PL APO CS2 63x/1.20 water immersion objective and the Leica Application Suite X software. Excitation and emission wavelengths used are shown in Table 17.

Table 17: Fluorescence microscopy excitation and emission wavelengths

Settings used at the TCS SP5II microscope:		
Fluorophore/dye	**Excitation (nm)**	**Emission (nm)**
DAPI (imaged alone)	405	440 - 572
DAPI (imaged together with aniline blue)	405	410 - 437
aniline blue (imaged together with DAPI)	405	585 - 600
mVenus	514	520 - 550
GFP, phGFP	488	498 - 545
mNeongreen	488	525 - 590
RFP, mCherry	561	578 - 650
mScarlet	561	580 - 620
FM4-64	561	650 - 770
Settings used at the STELLARIS 8 microscope:		
Fluorophore/dye	**Excitation (nm)**	**Emission (nm)**
mTurquoise (together with GFP and RFP)	440	478 - 485
GFP (together with mTurquoise and RFP)	489	500 - 520
RFP (together with mTurquoise and GFP)	585	595 - 615
GFP (together with RFP)	488	495 - 520
RFP (together with GFP)	590	603 - 623
DAPI	405	425 - 490

5.20 CLSM analysis of Arabidopsis anthers

For CLSM analysis, anthers were fixed and cleared using ClearSee solution adapted from Kurihara et al., 2015. Flower buds were dissected using a Zeiss Stemi 2000-CS stereomicroscope at a magnification of 50x. Anthers at the desired developmental stages (Sanders et al., 1999) were kept attached to the pedicel and all other flower parts were removed. Anthers were fixed in 4% (w/v) paraformaldehyde in phosphate-buffered saline (PBS) for about 1h at room temperature in a volume of 1 mL in 24-well plates. Afterwards they were washed twice in PBS for 1 min and cleared in ClearSee solution (10% (w/v) xylitol, 25% (w/v) urea, 15% (w/v) sodium deoxycholate) for 6 to 9 days at room temperature in the dark. After 3 days the ClearSee solution was replaced by new ClearSee solution. For 4′,6-diamidino-2-phenylindole (DAPI, Carl Roth) staining of anthers, post-clearing, anthers were incubated in DAPI (10 µg/ml) in ClearSee solution for about 20 h in the dark. Before imaging, anthers were washed for 30 min in ClearSee solution. For imaging, anthers were mounted in 50 µl ClearSee solution on a microscope slide and covered with a cover slip sized 22 x 22 mm. CLSM analyses were performed with a Leica TCS SP5II microscope and a Leica STELLARIS 8 microscope.

Staining of anthers with aniline blue and DAPI was performed based on Tsuchimatsu et al., 2020 . Flower buds were dissected using a Zeiss Stemi 2000-CS stereomicroscope at a magnification of 50x. Anthers were kept attached to the pedicel while removing all other flower parts. They were fixed in 3:1 (vol:vol) ethanol:acetic acid for 16 h at room temperature. Subsequently, anthers were rehydrated in 99%, 70% and 50% ethanol for 30 min each and incubated in 1N NaOH for 3 h at room temperature in the dark. Incubation in DAPI (10 µg/ml) in 100 mM K_2HPO_4 for 1 h followed. After that, anthers were mounted in DAPI (10 µg/ml) and aniline blue (0.1%) (Merck) in 100 mM K_2HPO_4 on microscope slides and incubated for about 3h at room temperature in the dark. CLSM was performed with a Leica TCS SP5II microscope and a Leica STELLARIS 8 microscope.

5.21 Alexander staining of Arabidopsis anthers

According to Alexander et al., 1969 staining of *Arabidopsis thaliana* anthers was performed. Flower buds at stage 12 (Smyth et al., 1990) were dissected using a Zeiss Stemi 2000-CS stereomicroscope at a magnification of 50x. Stamens were mounted onto

microscope slides by slightly pressing the filaments against the glass to bring and keep the anthers in the desired orientation. Staining solution (Table 18) was added and incubation for about 20 h at room temperature followed. Brightfield images were acquired using a Zeiss Axio Imager M1 microscope.

Table 18: Staining solution used for Alexander staining of anthers

1 ml	95% ethanol
200 µl	Malachite Green (1% solution in 95% ethanol) (Thermo Fisher Scientific)
4 ml	ddH_2O
2,5 ml	glycerol
500 µl	Fuchsin, acid (1% solution in ddH_2O) (Thermo Fisher Scientific)
50 µl	Orange G (1% solution in ddH_2O) (Thermo Fisher Scientific)
400 µl	glacial acetic acid
0,5 g	chloral hydrate
5 µl	phenol
up to 10 ml with ddH_2O	

5.22 CLSM analysis of exine morphology

The autofluorescence properties of the exine were used for the analysis of exine morphology. Pollen were dipped into liquid ½ MS, pH 5.8 adjusted with KOH, on a microscope slide and covered with a cover slip. CLSM analysis was performed at a Leica TCS SP5II microscope equipped with a Leica HCX PL APO lambda blue 63.0x/1.20 water immersion objective. For excitation, a laser line of 488 nm was used and emission was recorded between 505 and 550 nm.

5.23 FM4-64 staining

For FM4-64 staining, seedlings were incubated for 7 min at room temperature in liquid ½ MS media, pH 5.8 adjusted with KOH, containing 1 µM FM4-64 (Thermo Fisher

Scientific) in a volume of 1 ml in 24-well plates. Seedlings were washed for 30 sec in liquid ½ MS media (pH 5.8 adjusted with KOH), mounted in liquid ½ MS on microscope slides and imaged with a Leica TCS SP5II microscope.

5.24 Transmission electron microscopy

Flower buds were dissected using a stereomicroscope and high-pressure freezing of anthers was performed by Dr. Stefan Hillmer as described in Scheuring et al., 2011 . Freeze substitution using a Leica EM AFS2 freeze substitution device followed as detailed in Hillmer et al., 2012 . The samples were further processed by Dr. Stefan Hillmer and Steffi Gold by embedding in resin, cutting ultrathin sections with a Leica Ultracut S microtome and performing microscopy analysis using a JEM1400 transmission electron microscope. Micrographs were taken using a TVIPS TemCam F416 digital camera.

5.25 Image processing using Fiji

Image processing post-acquisition was performed using Fiji (Fiji is just image J; Schindelin et al., 2012). Generally, brightness and contrast were adjusted and background subtraction and Gaussian blur were used.

5.26 Data analysis using OriginPro

Quantitative data analysis and plotting were conducted with the OriginPro 2020b software (OriginLab Corporation, Northampton, Massachusetts, USA).

5.27 Generation and visualization of 3D models

Structural models of proteins were generated with the AlphaFold Monomer v2.0 pipeline (Jamper et al., 2021; Varadi et al., 2021) developed by DeepMind and EMBL-EBI and analyzed with the tool University of California, San Francisco (UCSF) Chimera 1.11rc (Goddard et al., 2018; Pettersen et al., 2004).

5.28 Creation of figures in Adobe Illustrator

Images were assembled and figures were created in Abobe Illustrator CS4 (Adobe inc., San Jose, California, USA).

5.29 Specification of genes

The accession numbers of genes relevant to this work are shown in Table 19.

Table 19: Accession numbers of genes

Gene	Accession number
VHA-a1	AT2G28520
VHA-a2	AT2G21410
VHA-a3	AT4G39080
VHA-AP1	AT3G13410
VHA-AP2	AT3G24160
SRβ	AT2G18770
UBQ10	AT4G05320
COPT3 (MSP1)	AT5G59040
WRKY34 (MSP3)	AT4G26440
A9	AT5G07230
MpVHA-a	MP3G15140

6 Supplementary material

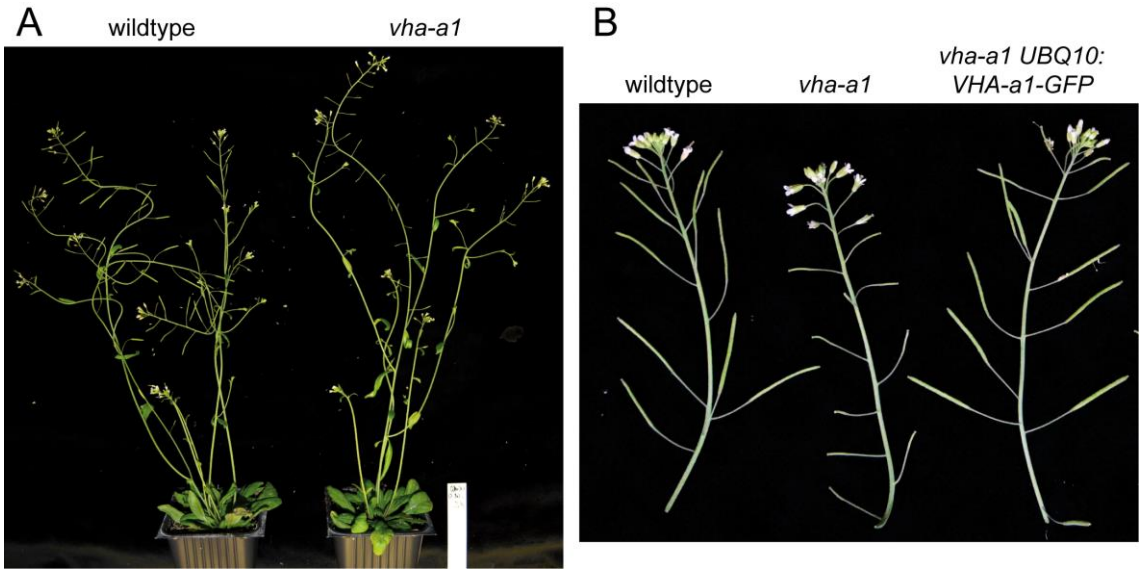

Supplementary Figure 1. Plant and silique phenotype of *vha-a1.* (A) Wildtype and *vha-a1* mutant plants. 6-week-old plants are shown, which were grown under long-day conditions (16 h of light and 22 °C). **(B)** Siliques of wildtype, *vha-a1* and *vha-a1* expressing *UBQ10:VHA-a1-GFP*.

VHA-a1	+ +	- -	- -	- -
VHA-a2	+ +	+ +	+ -	+ +
VHA-a3	+ +	+ +	+ +	+ -

Supplementary Figure 2. Rosette sizes of *vha-a1 vha-a2/+* and *vha-a1 vha-a3/+* are reduced. *vha-a1 (Cas9^{+})* was crossed with the *vha-a2* and the *vha-a3* single mutant and the F1 progeny was analyzed. *vha-a1 vha-a2/+* and *vha-a1 vha-a3/+* had reduced rosette sizes. Plants were grown for 5 weeks under long-day conditions (16 h of light and 22 °C). This figure was created by Dr. Upendo Lupanga and myself, is published in Lupanga et al., 2020, and has been modified for this thesis.

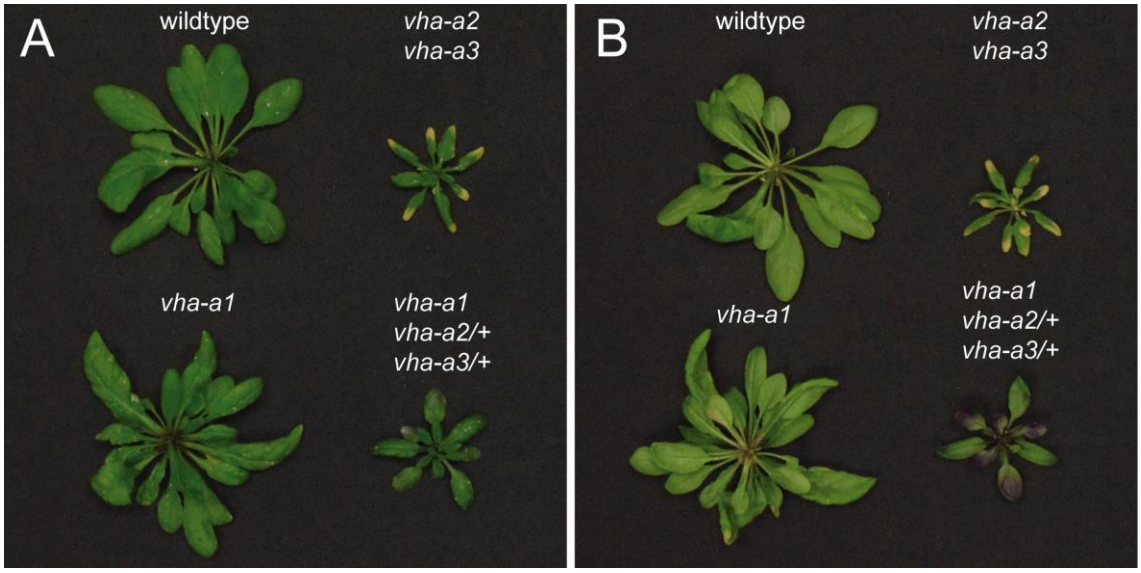

Supplementary Figure 3. *vha-a1 vha-a2/+ vha-a3/+* is small and stressed. Upper leaf side (A) and lower leaf side (B) of wildtype and *vha-a1, vha-a2 vha-a3 and vha-a1 vha-a2/+ vha-a3/+* mutants. While *vha-a2 vha-a3* has yellow leaf tips, several leaves of *vha-a1 vha-a2/+ vha-a3/+* show purple color, especially at the lower leaf side. Plants were grown for 4.5 weeks under long-day conditions (16 h of light and 22 °C).

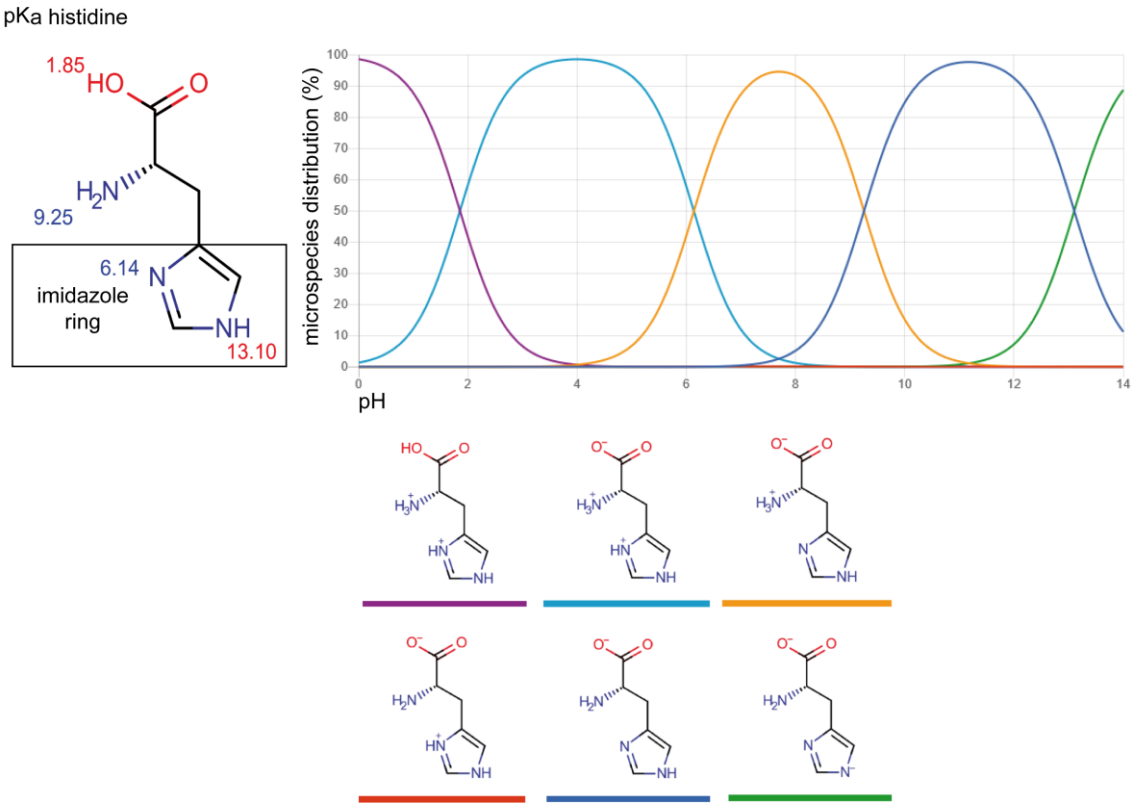

Supplementary Figure 4. Protonation states of histidine residues. Histidine microspecies at different pH conditions. The histidine imidazole ring can be singly protonated and neutral or doubly protonated and positively charged. The figure was made using Chemicalize (https://chemicalize.com) from ChemAxon (http://www.chemaxon.com).

Supplementary Table 1: Predicted pK_a values of VHA-a1 C-terminal half histidines with PROPKA3.0 (Olsson et al., 2011):

VHA-a1 histidine residue	Predicted pK_a
H434	3.31
H494	6.57
H613	6.25
H665	7.06
H696	6.18
H697	6.45
H709	7.24
H713	4.07
H738	5.34
H788	5.61
H793	3.59

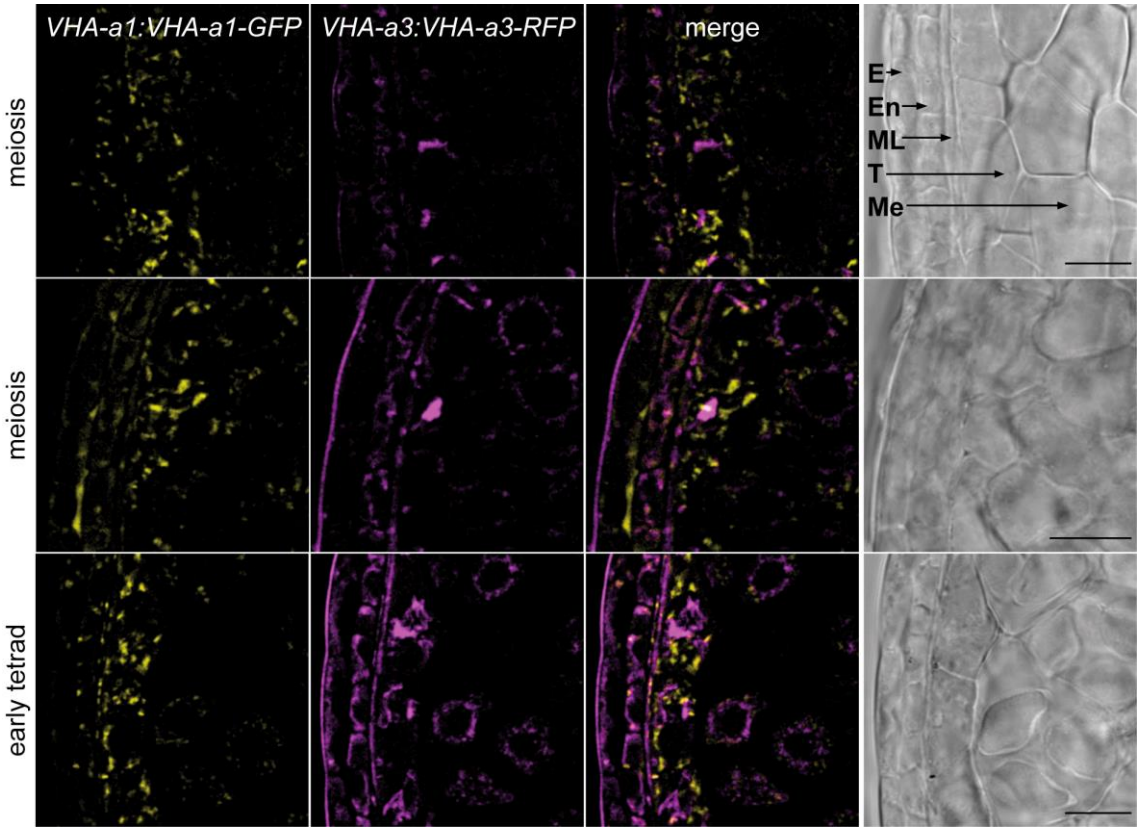

Supplementary Figure 5. VHA-a1-GFP and VHA-a3-RFP in early stages of pollen development. Anthers were harvested from plants expressing *VHA-a1-GFP* and *VHA-a3-RFP* under the control of their own promoters. CLSM analysis was performed using cleared anthers. E, epidermis; En, endothecium; ML, middle layer; T, tapetum; Me, meiocyte; scale bars = 10 µm.

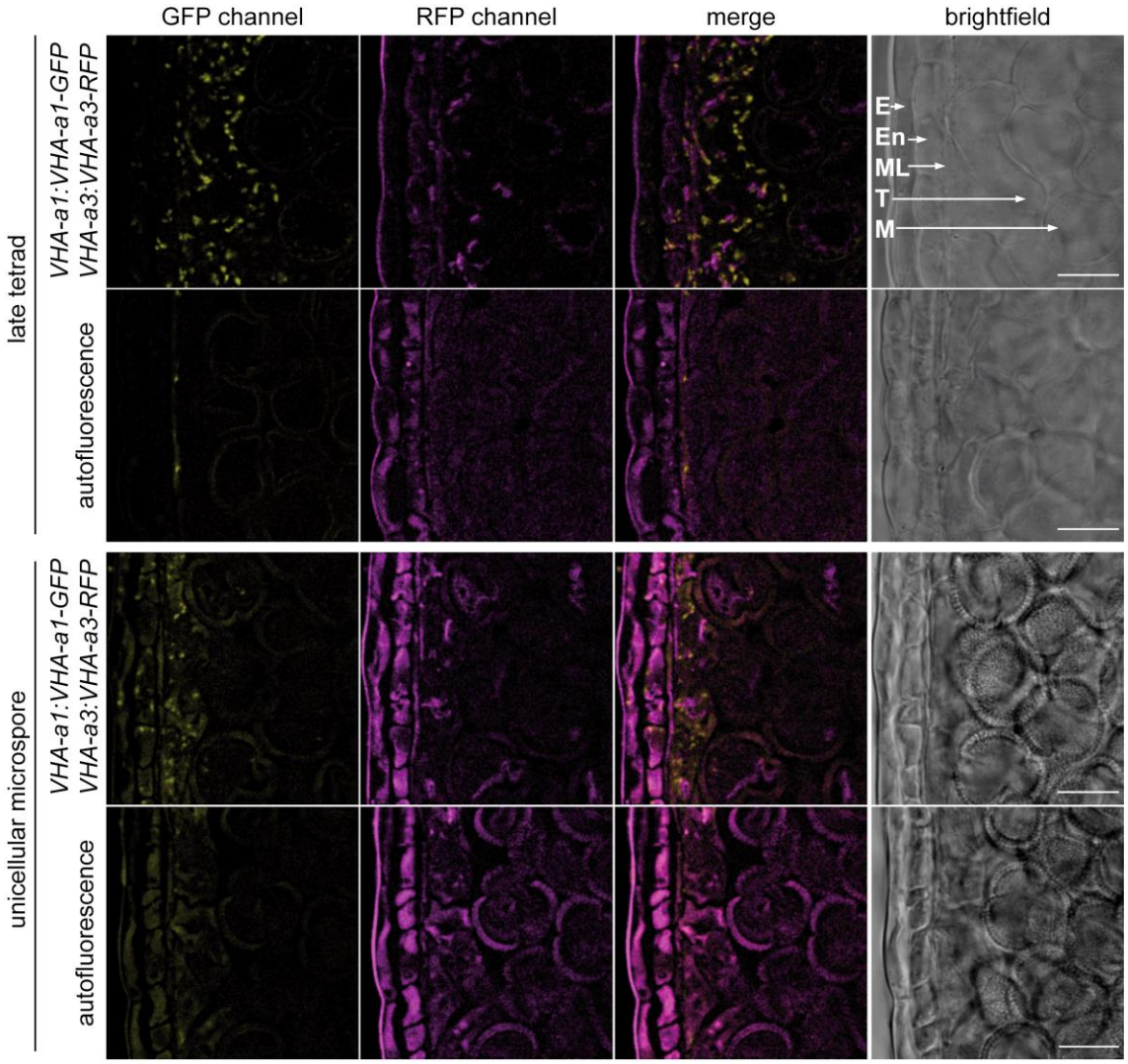

Supplementary Figure 6. Autofluorescence control for imaging VHA-a1-GFP and VHA-a3-RFP in anthers – late tetrad and unicellular microspore stage. Anthers from plants expressing *VHA-a1:VHA-a1-GFP* and *VHA-a1:VHA-a3-RFP* were treated and imaged with the same conditions as non-transgenic wildtype plants. In this way, VHA-a1-GFP and VHA-a3-RFP signal can be distinguished from autofluorescence. CLSM analysis was performed using cleared anthers. E, epidermis; En, endothecium; ML, middle layer; T, tapetum; M, microspore; scale bars = 10 µm.

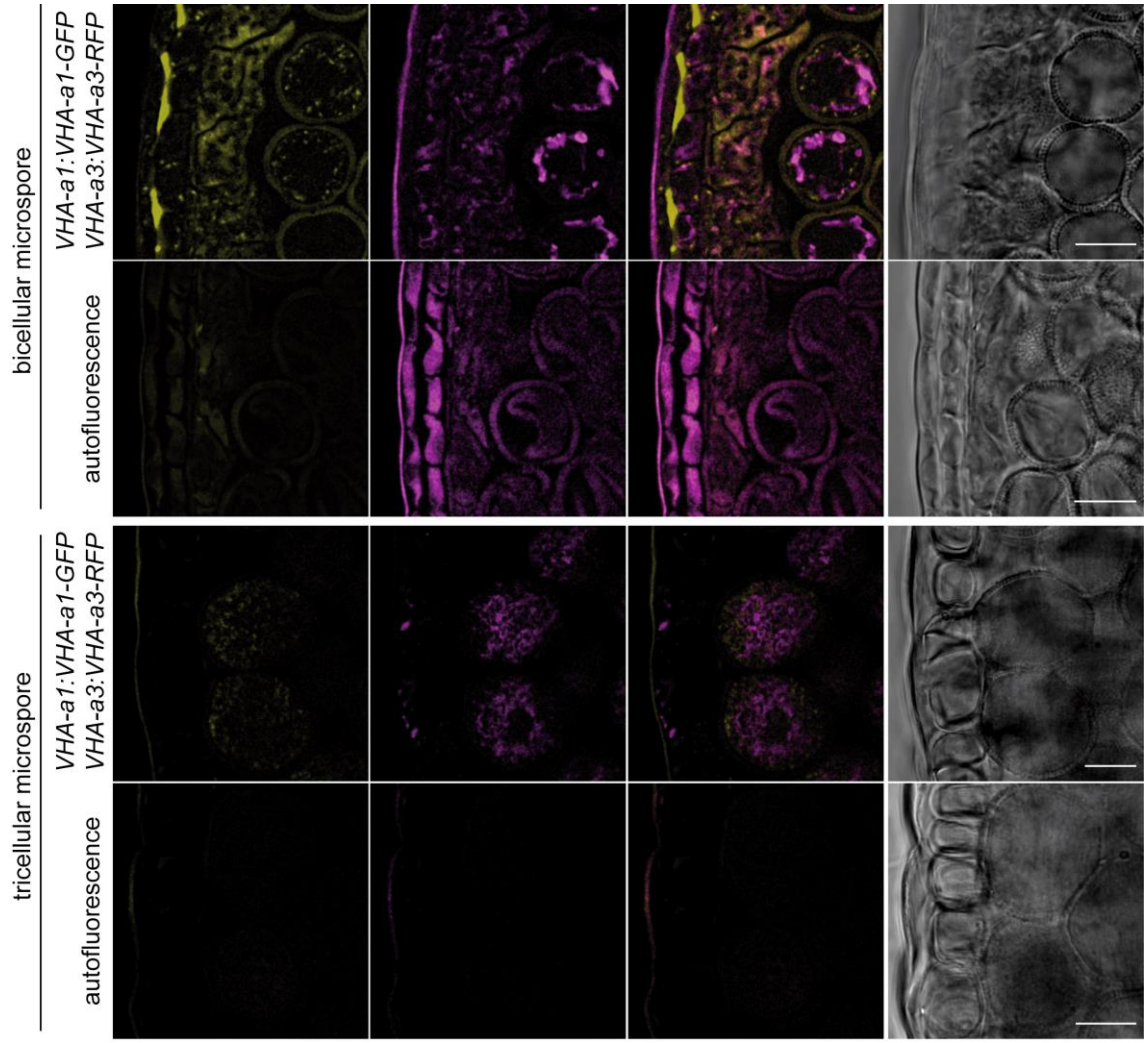

Supplementary Figure 7. Autofluorescence control for imaging VHA-a1-GFP and VHA-a3-RFP in anthers – bicellular and tricellular microspore stage. Anthers from plants expressing *VHA-a1:VHA-a1-GFP* and *VHA-a1:VHA-a3-RFP* were treated and imaged with the same conditions as non-transgenic wildtype plants. In this way, VHA-a1-GFP and VHA-a3-RFP signal can be distinguished from autofluorescence. CLSM analysis was performed using cleared anthers. Scale bars = 10 µm.

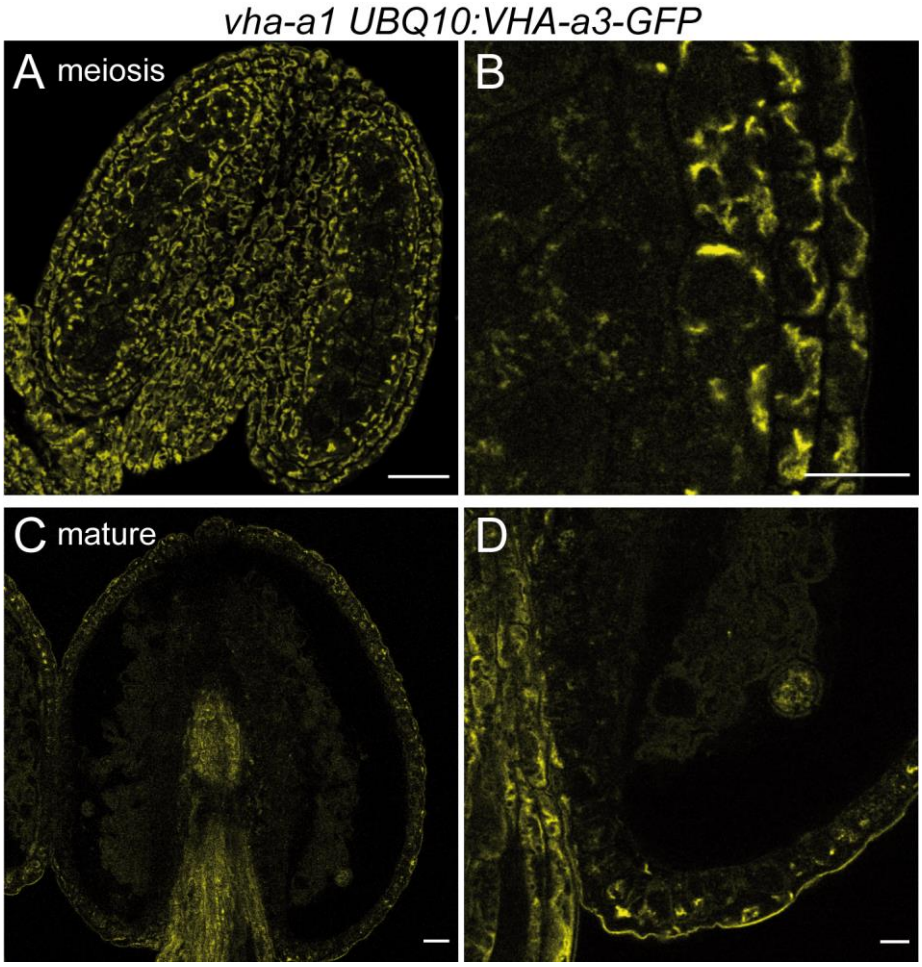

Supplementary Figure 8. *UBQ10:VHA-a3-GFP* in *vha-a1.* **(A)** Anther at meiosis of *vha-a1* expressing *UBQ10:VHA-a3-GFP*. **(B)** Close-up of the anther shown in A. **(C)** Mature anther of *vha-a1* expressing *UBQ10:VHA-a3-GFP.* **(D)** Close-up of the anther shown in C. CLSM images of cleared anthers were taken. Scale bars in A and C = 25 µm, and scale bars in B and D = 10 µm.

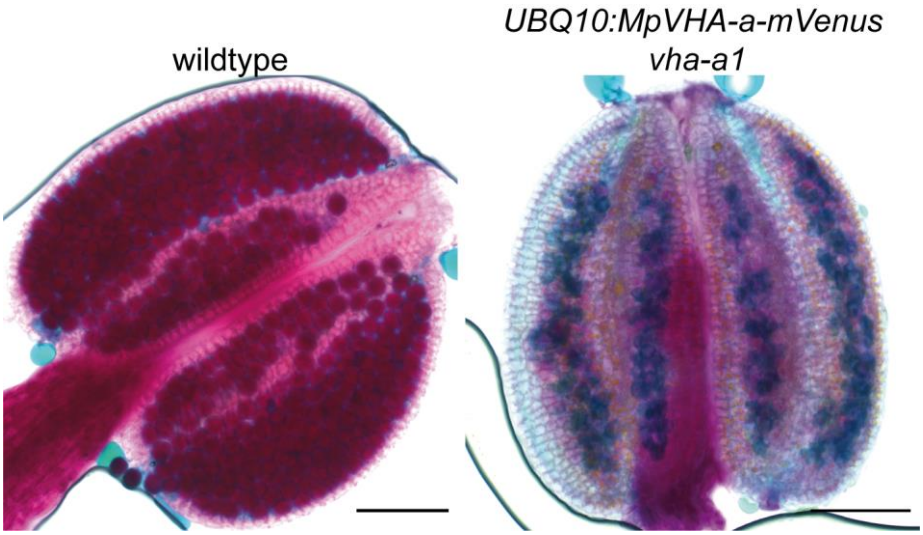

Supplementary Figure 9. *UBQ10:MpVHA-a-mVenus* does not rescue pollen development of *vha-a1.* Alexander staining of anthers shows aborted microspores in *vha-a1 UBQ10:MpVHA-a-mVenus*. Scale bars = 100 µm. The results of this figure are published in Lupanga et al., 2020. Different images were used for this thesis. All images were acquired by myself.

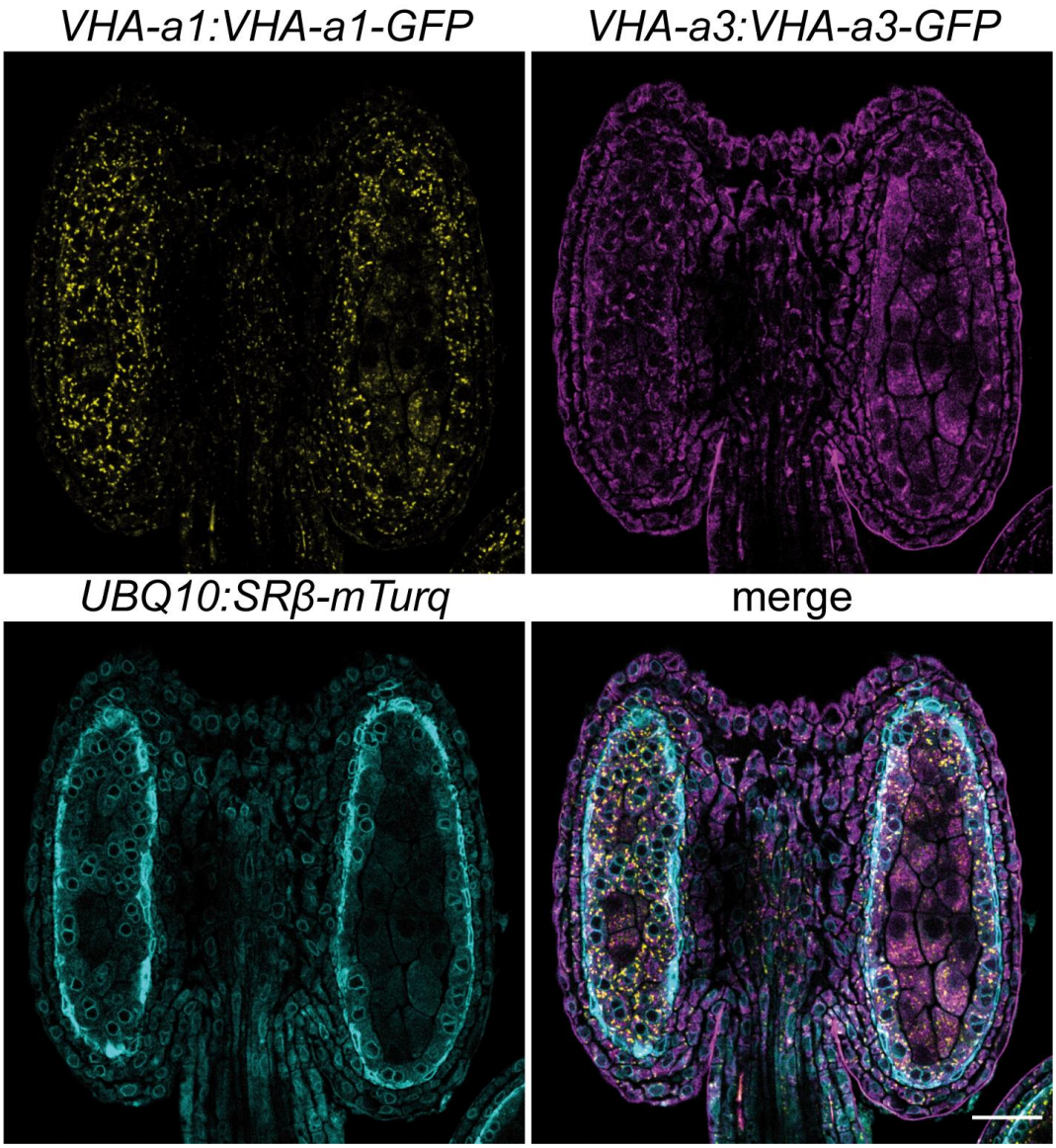

Supplementary Figure 10. Anther at the stage of meiosis expressing VHA-a1-GFP, VHA-a3-RFP and SRβ-mTurquoise. An anther from an F1 plant expressing *VHA-a1:VHA-a1-GFP*, *VHA-a3:VHA-a3-RFP* and *UBQ10:SRβ-mTurquoise* is shown. VHA-a1-GFP signal was found in the meiocytes as well as in the sporophytic cells of the anther wall. CLSM images of cleared anthers were taken. Scale bar = 25 µm.

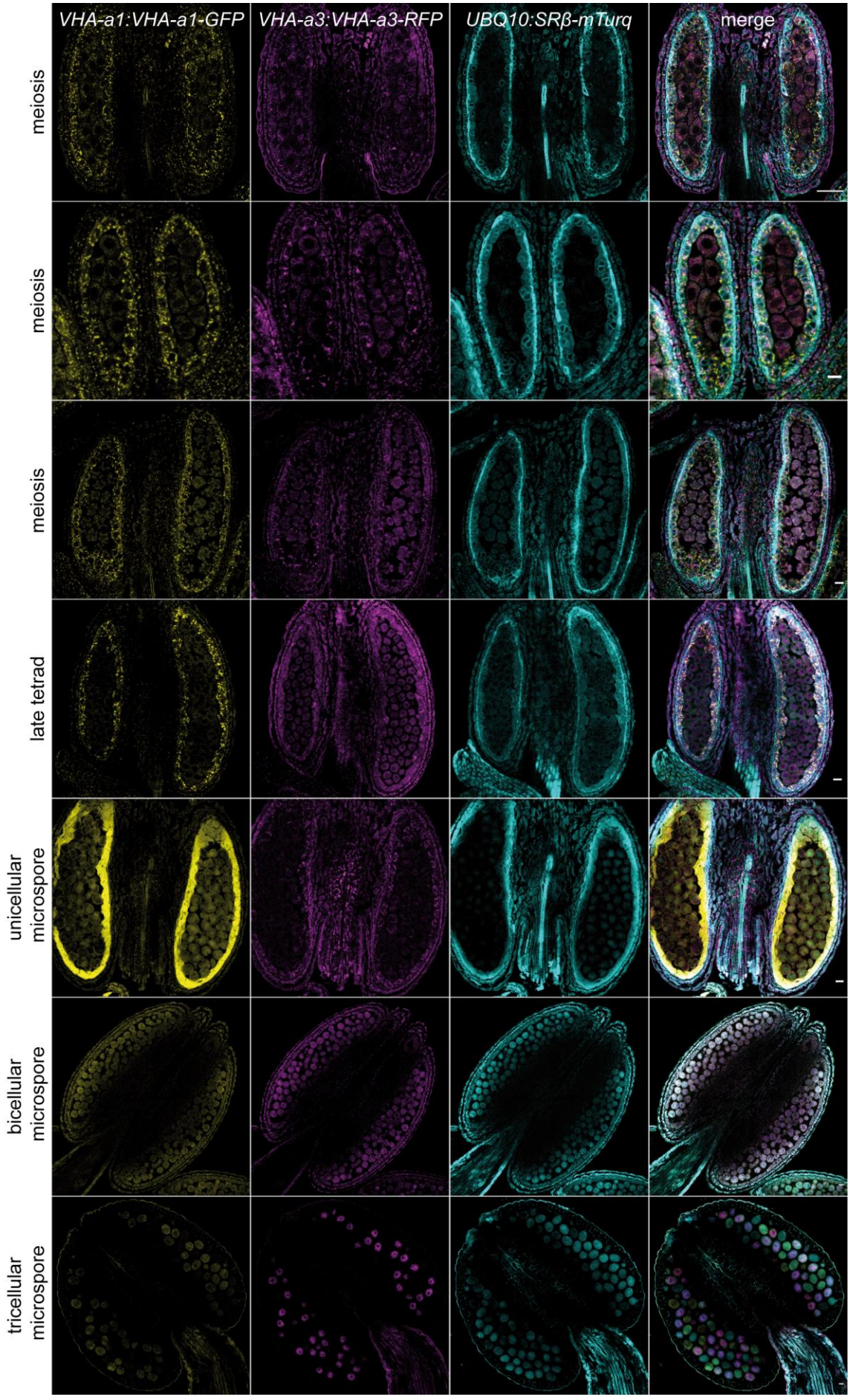
VHA-a1:VHA-a1-GFP
VHA-a3:VHA-a3-RFP
UBQ10:SRβ-mTurq
merge
meiosis
meiosis
meiosis
late tetrad
unicellular microspore
bicellular microspore
tricellular microspore

Supplementary Figure 11. Anthers expressing VHA-a1-GFP, VHA-a3-RFP and SRβ-mTurquoise. Anthers were harvested from F1 plants with segregating *VHA-a1:VHA-a1-GFP*, *VHA-a3:VHA-a3-RFP* and *UBQ10:SRβ-mTurquoise.* CLSM images of cleared anthers of the developmental stages from meiosis to the tricellular microspore stage were taken. Scale bars = 10 µm.

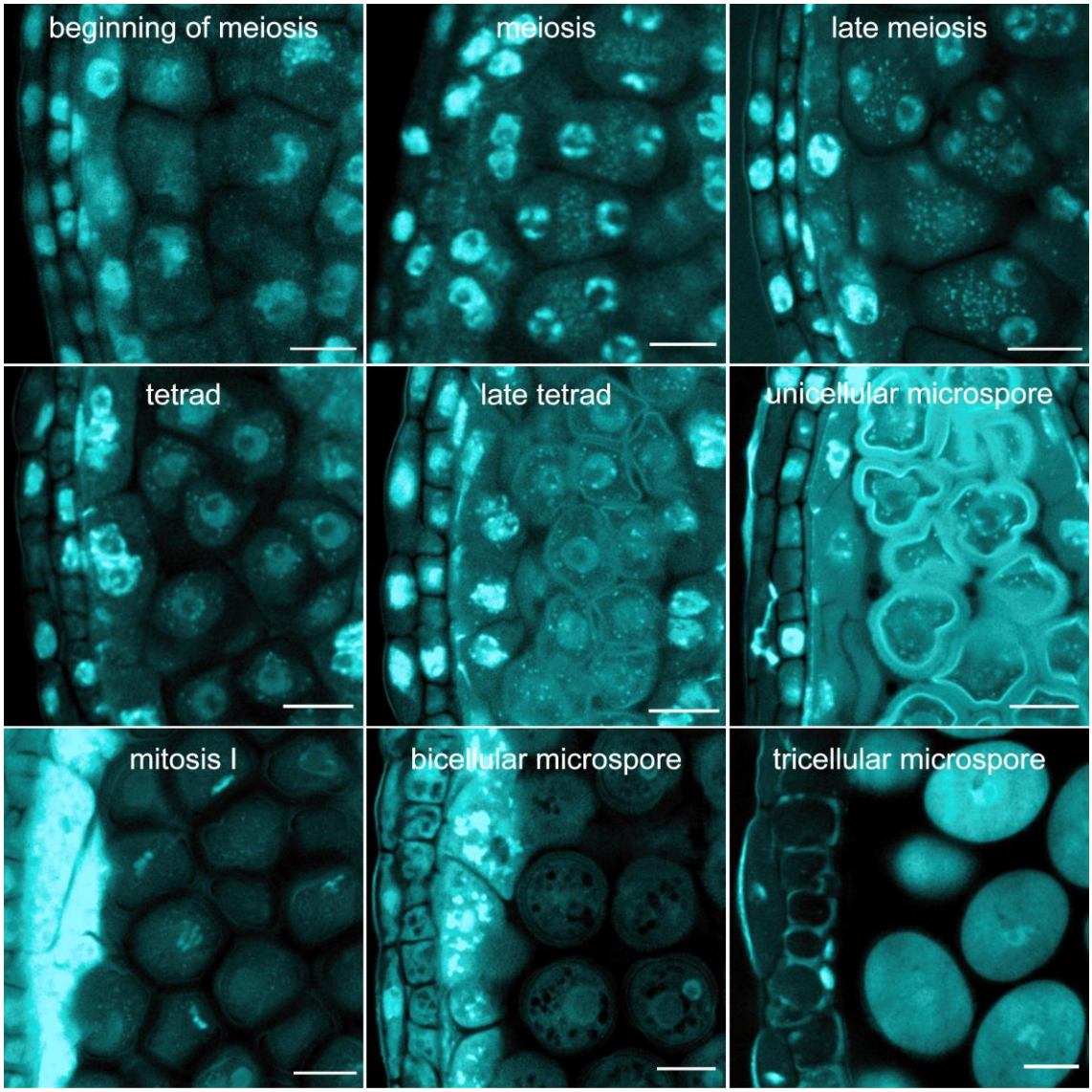

Supplementary Figure 12. Pollen development in wildtype. Pollen development in wildtype from meiosis to the tricellular microspore stage. DAPI staining enabled to distinguish the different stages during meiosis and to find microspores that were undergoing mitosis. Anthers were cleared prior to staining with DAPI. CLSM images are shown. Scale bars = 10 µm.

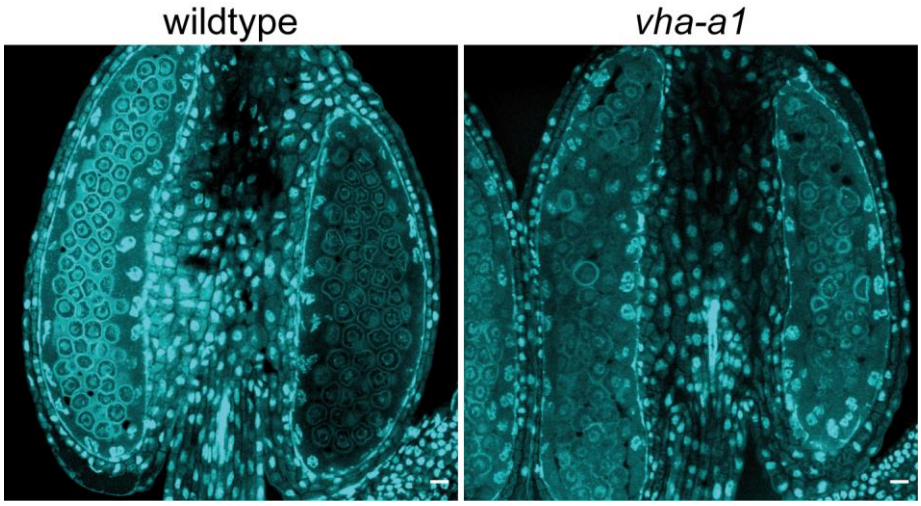

Supplementary Figure 13. Pollen wall formation is defective in *vha-a1*. Wildtype and *vha-a1* anthers at the late tetrad stage. In wildtype microspores are evenly surrounded by developing pollen walls. In *vha-a1* many microspores show abnormal surroundings. Degenerated microspores are visible in *vha-a1*. CLSM images of cleared anthers that were stained with DAPI are shown. Scale bars = 10 µm.

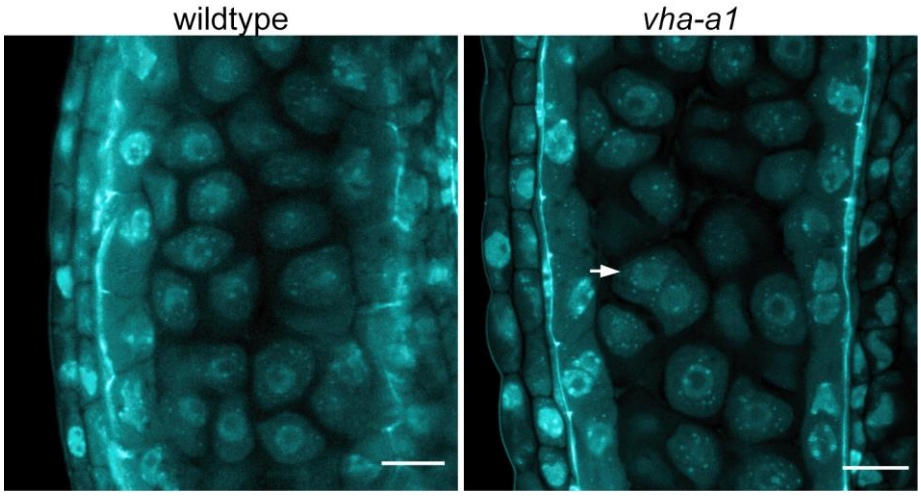

Supplementary Figure 14. Multinucleated cells were observed in *vha-a1* at a low frequency. Wildtype and *vha-a1* anthers at the early tetrad stage. A binucleated cell is visible in *vha-a1* (white arrow). Anthers that were cleared and stained with DAPI were analyzed using CLSM. Scale bars = 10 µm.

7 References

Abbas YM, Wu D, Bueler SA, Robinson C V., Rubinstein JL. 2020. Structure of V-ATPase from the mammalian brain. *Science* **367**:1240–1246. doi:10.1126/science.aaz2924

Aboulela M, Nakagawa T, Oshima A, Nishimura K, Tanaka Y. 2018. The Arabidopsis COPII components, AtSEC23A and AtSEC23D, are essential for pollen wall development and exine patterning. *J Exp Bot* **69**:1615–1633. doi:10.1093/jxb/ery015

Abuammar H, Bhattacharjee A, Simon-Vecsei Z, Blastyák A, Csordás G, Páli T, Juhász G. 2021. Ion Channels and Pumps in Autophagy: A Reciprocal Relationship. *Cells* **10**:3537. doi:10.3390/cells10123537

Alexander MP. 1969. Differential staining of aborted and nonaborted pollen. *Biotech Histochem* **44**:117–122. doi:10.3109/10520296909063335

Anzalone A V., Randolph PB, Davis JR, Sousa AA, Koblan LW, Levy JM, Chen PJ, Wilson C, Newby GA, Raguram A, Liu DR. 2019. Search-and-replace genome editing without double-strand breaks or donor DNA. *Nature* **576**:149–157. doi:10.1038/s41586-019-1711-4

Ariizumi T, Toriyama K. 2011. Genetic regulation of sporopollenin synthesis and pollen exine development. *Annu Rev Plant Biol* **62**:437–460. doi:10.1146/annurev-arplant-042809-112312

Ariizumi T, Toriyama K. 2007. Pollen exine pattern formation is dependent on three major developmental processes in Arabidopsis thaliana. *Int J Plant Dev Biol* **1**:106–115.

Askani J. 2022. Dissertation, The role of membrane tethering complexes in vacuolar trafficking and vacuole biogenesis. Ruprecht-Karls-University Heidelberg. doi:10.11588/heidok.00032152

Åstrand J, Knight C, Robson J, Talle B, Wilson ZA. 2021. Evolution and diversity of the angiosperm anther: trends in function and development. *Plant Reprod* **34**:307–319. doi:10.1007/s00497-021-00416-1

Bassil E, Ohto M aki, Esumi T, Tajima H, Zhu Z, Cagnac O, Belmonte M, Peleg Z, Yamaguchi T, Blumwald E. 2011. The Arabidopsis intracellular Na+/H+ antiporters NHX5 and NHX6 are endosome associated and necessary for plant growth and development. *Plant Cell* **23**:224–239. doi:10.1105/tpc.110.079426

Benlekbir S, Bueler S a, Rubinstein JL. 2012. Structure of the vacuolar-type ATPase from Saccharomyces cerevisiae at 11-Å resolution. *Nat Struct Mol Biol* **19**:1356–1362. doi:10.1038/nsmb.2422

Berger F, Hamamura Y, Ingouff M, Higashiyama T. 2008. Double fertilization - caught in the act. *Trends Plant Sci* **13**:437–443. doi:10.1016/j.tplants.2008.05.011

Blackmore S, Wortley AH, Skvarla JJ, Rowley JR. 2007. Pollen wall development in flowering plants: Tansley review. *New Phytol* **174**:483–498. doi:10.1111/j.1469-8137.2007.02060.x

Bolte S, Talbot C, Boutte Y, Catrice O, Read ND, Satiat-Jeunemaitre B. 2004. FM-dyes as experimental probes for dissecting vesicle trafficking in living plant cells. *J Microsc* **214**:159–173. doi:10.1111/j.0022-2720.2004.01348.x

Brandizzi F. 2018. Transport from the endoplasmic reticulum to the Golgi in plants: Where are we now? *Semin Cell Dev Biol* **80**:94–105. doi:10.1016/j.semcdb.2017.06.024

Brüx A, Liu T-Y, Krebs M, Stierhof Y-D, Lohmann JU, Miersch O, Wasternack C, Schumacher K. 2008. Reduced V-ATPase activity in the trans-Golgi network causes oxylipin-dependent hypocotyl growth Inhibition in Arabidopsis. *Plant Cell* **20**:1088–1100. doi:10.1105/tpc.108.058362

Buechling T, Bartscherer K, Ohkawara B, Chaudhary V, Spirohn K, Niehrs C, Boutros M. 2010. Wnt/Frizzled Signaling Requires dPRR, the Drosophila Homolog of the Prorenin Receptor. *Curr Biol* **20**:1263–1268. doi:10.1016/j.cub.2010.05.028

Cairo A, Vargova A, Shukla N, Capitao C, Mikulkova P, Valuchova S, Pecinkova J, Bulankova P, Riha K. 2022. Meiotic exit in Arabidopsis is driven by P-body-mediated inhibition of translation. *Science* **377**:629–634. doi:10.1126/science.abo0904

Çetinbaş-Genç A, Conti V, Cai G. 2022. Let's shape again: the concerted molecular action that builds the pollen tube. *Plant Reprod* **35**:77–103. doi:10.1007/s00497-022-00437-4

Chechenova MB, Maes S, Oas ST, Nelson C, Kiani KG, Bryantsev AL, Cripps RM. 2017. Functional redundancy and nonredundancy between two Troponin C isoforms in Drosophila adult muscles. *Mol Biol Cell* **28**:760–770. doi:10.1091/mbc.E16-07-0498

Chen LQ, Hou BH, Lalonde S, Takanaga H, Hartung ML, Qu XQ, Guo WJ, Kim JG, Underwood W, Chaudhuri B, Chermak D, Antony G, White FF, Somerville SC, Mudgett MB, Frommer WB. 2010. Sugar transporters for intercellular exchange and nutrition of pathogens. *Nature* **468**:527–532. doi:10.1038/nature09606

Chen Y, Tao K, Ji W, Kumar VB, Rencus-lazar S, Gazit E. 2022. Histidine as a key modulator of molecular supramolecular materials inspired by biological systems. *Mater Today* 1–22. doi:10.1016/j.mattod.2022.08.011

Clough SJ, Bent AF. 1998. Floral dip: a simplified method forAgrobacterium-mediated transformation ofArabidopsis thaliana. *Plant J* **16**:735–743. doi:10.1046/j.1365-313x.1998.00343.x

Cong L, Ran FA, Cox D, Lin S, Barretto R, Habib N, Hsu PD, Wu X, Jiang W, Marraffini L a, Zhang F. 2013. Multiplex Genome Engineering Using CRISPR/Cas Systems. *Science* **339**:819–823. doi:10.1126/science.1231143

Conger R, Chen Y, Fornaciari S, Faso C, Held MA, Renna L, Brandizzi F. 2011. Evidence for the involvement of the Arabidopsis SEC24A in male transmission. *J Exp Bot* **62**:4917–4926. doi:10.1093/jxb/err174

Cousin C, Bracquart D, Contrepas A, Corvol P, Muller L, Nguyen G. 2009. Soluble Form of the (Pro)Renin Receptor Generated by Intracellular Cleavage by Furin Is Secreted in Plasma. *Hypertension* **53**:1077–1082. doi:10.1161/HYPERTENSIONAHA.108.127258

Craft J, Samalova M, Baroux C, Townley H, Martinez A, Jepson I, Tsiantis M, Moore I. 2005. New pOp/LhG4 vectors for stringent glucocorticoid-dependent transgene expression in Arabidopsis. *Plant J* **41**:899–918. doi:10.1111/j.1365-313X.2005.02342.x

Cruciat C, Ohkawara B, Acebron SP, Karaulanov E, Reinhard C, Ingelfinger D, Boutros M, Niehrs C. 2010. Requirement of Prorenin Receptor and Vacuolar H + -ATPase–Mediated Acidification for Wnt Signaling. *Science* **327**:459–463. doi:10.1126/science.1179802

Cui Y, Xu J, Cheng M, Liao X, Peng S. 2018. Review of CRISPR/Cas9 sgRNA Design Tools. *Interdiscip Sci Comput Life Sci* **10**:455–465. doi:10.1007/s12539-018-0298-z

Dahhan DA, Bednarek SY. 2022. Advances in structural, spatial, and temporal mechanics of plant endocytosis. *FEBS Lett* **596**:2269–2287. doi:10.1002/1873-3468.14420

daSilva LLP, Snapp EL, Denecke J, Lippincott-Schwartz J, Hawes C, Brandizzi F. 2004. Endoplasmic reticulum export sites and Golgi bodies behave as single mobile secretory units in plant cells. *Plant Cell* **16**:1753–1771. doi:10.1105/tpc.022673

Daxinger L, Hunter B, Sheikh M, Jauvion V, Gasciolli V, Vaucheret H, Matzke M, Furner I. 2008. Unexpected silencing effects from T-DNA tags in Arabidopsis. *Trends Plant Sci* **13**:4–6. doi:10.1016/j.tplants.2007.10.007

De Vylder J, Vandenbussche F, Hu Y, Philips W, Van Der Straeten D. 2012. Rosette Tracker: An Open Source Image Analysis Tool for Automatic Quantification of Genotype Effects. *Plant Physiol* **160**:1149–1159. doi:10.1104/pp.112.202762

Decaestecker W, Buono RA, Pfeiffer ML, Vangheluwe N, Jourquin J, Karimi M, van Isterdael G, Beeckman T, Nowack MK, Jacobs TB. 2019. CRISPR-Tsko: A technique for efficient mutagenesis in specific cell types, tissues, or organs in Arabidopsis[open]. *Plant Cell* **31**:2868–2887. doi:10.1105/tpc.19.00454

Deschamps A, Colinet AS, Zimmermannova O, Sychrova H, Morsomme P. 2020. A new pH sensor localized in the Golgi apparatus of Saccharomyces cerevisiae reveals unexpected roles of Vph1p and Stv1p isoforms. *Sci Rep* **10**:1–11. doi:10.1038/s41598-020-58795-w

Dettmer J, Hong-Hermesdorf A, Stierhof Y-D, Schumacher K. 2006. Vacuolar H+-ATPase Activity Is Required for Endocytic and Secretory Trafficking in Arabidopsis. *Plant Cell* **18**:715–730. doi:10.1105/tpc.105.037978

Dettmer J, Liu TY, Schumacher K. 2010. European Journal of Cell Biology Functional analysis of Arabidopsis V-ATPase subunit VHA-E isoforms. *Eur J Cell Biol* **89**:152–156. doi:10.1016/j.ejcb.2009.11.008

Dettmer J, Schubert D, Calvo-Weimar O, Stierhof Y-D, Schmidt R, Schumacher K. 2005.

Essential role of the V-ATPase in male gametophyte development. *Plant J* **41**:117–124. doi:10.1111/j.1365-313X.2004.02282.x

Dragwidge JM, Scholl S, Schumacher K, Gendall AR. 2019. NHX-type Na+(K+)/H+antiporters are required for TGN/EE trafficking and endosomal ion homeostasis in Arabidopsis thaliana. *J Cell Sci* **132**:2–11. doi:10.1242/jcs.226472

Eaton AF, Merkulova M, Brown D. 2021. The H + -ATPase (V-ATPase): from proton pump to signaling complex in health and disease. *Am J Physiol Physiol* **320**:C392–C414. doi:10.1152/ajpcell.00442.2020

Edwards K, Johnstone C, Thompson C. 1991. A simple and rapid method for the preparation of plant genomic DNA for PCR analysis. *Nucleic Acids Res* **19**:1349–1349. doi:10.1093/nar/19.6.1349

El-Brolosy MA, Stainier DYR. 2017. Genetic compensation: A phenomenon in search of mechanisms. *PLoS Genet* **13**:1–17. doi:10.1371/journal.pgen.1006780

El-Kasmi F, Pacher T, Strompen G, Stierhof YD, Müller LM, Koncz C, Mayer U, Jürgens G. 2011. Arabidopsis SNARE protein SEC22 is essential for gametophyte development and maintenance of Golgi-stack integrity. *Plant J* **66**:268–279. doi:10.1111/j.1365-313X.2011.04487.x

Fecht-Bartenbach J Von Der, Bogner M, Krebs M, Stierhof YD, Schumacher K, Ludewig U. 2007. Function of the anion transporter AtCLC-d in the trans-Golgi network. *Plant J* **50**:466–474. doi:10.1111/j.1365-313X.2007.03061.x

Feng QN, Zhang Y, Li S. 2017. Tonoplast targeting of VHA-a3 relies on a Rab5-mediated but Rab7-independent vacuolar trafficking route. *J Integr Plant Biol* **59**:230–233. doi:10.1111/jipb.12526

Feng X, Dickinson HG. 2010. Tapetal cell fate, lineage and proliferation in the Arabidopsis anther. *Development* **137**:2409–2416. doi:10.1242/dev.049320

Fink F. 2012. Master Thesis, The V-ATPase in Arabidopsis thaliana: A closer look to targeting, new interaction partners and its role for ER acidification. Ruprecht-Karls-University Heidelberg.

Finnigan GC, Cronan GE, Park HJ, Srinivasan S, Quiocho F a., Stevens TH. 2012. Sorting of the Yeast Vacuolar-type, Proton-translocating ATPase Enzyme Complex (V-ATPase). *J Biol Chem* **287**:19487–19500. doi:10.1074/jbc.M112.343814

Finnigan GC, Hanson-Smith V, Houser BD, Park HJ, Stevens TH. 2011. The reconstructed ancestral subunit a functions as both V-ATPase isoforms Vph1p and Stv1p in Saccharomyces cerevisiae. *Mol Biol Cell* **22**:3176–3191. doi:10.1091/mbc.E11-03-0244

Gendre D, Oh J, Boutté Y, Best JG, Samuels L, Nilsson R, Uemura T, Marchant A, Bennett MJ, Grebe M, Bhalerao RP. 2011. Conserved Arabidopsis ECHIDNA protein mediates trans-Golgi-network trafficking and cell elongation. *Proc Natl Acad Sci U S A* **108**:8048–8053. doi:10.1073/pnas.1018371108

Goddard TD, Huang CC, Meng EC, Pettersen EF, Couch GS, Morris JH, Ferrin TE. 2018. UCSF ChimeraX: Meeting modern challenges in visualization and analysis. *Protein*

Sci **27**:14–25. doi:10.1002/pro.3235

Grabe M, Wang H, Oster G. 2000. The mechanochemistry of V-ATPase proton pumps. *Biophys J* **78**:2798–2813. doi:10.1016/S0006-3495(00)76823-8

Grefen C, Donald N, Hashimoto K, Kudla J, Schumacher K, Blatt MR. 2010. A ubiquitin-10 promoter-based vector set for fluorescent protein tagging facilitates temporal stability and native protein distribution in transient and stable expression studies. *Plant J* **64**:355–365. doi:10.1111/j.1365-313X.2010.04322.x

Gregorini M, Wang J, Xie XS, Milligan RA, Engel A. 2007. Three-dimensional reconstruction of bovine brain V-ATPase by cryo-electron microscopy and single particle analysis. *J Struct Biol* **158**:445–454. doi:10.1016/j.jsb.2007.01.002

Grienenberger E, Quilichini TD. 2021. The Toughest Material in the Plant Kingdom: An Update on Sporopollenin. *Front Plant Sci* **12**:1–9. doi:10.3389/fpls.2021.703864

Guan YF, Huang XY, Zhu J, Gao JF, Zhang HX, Yang ZN. 2008. Ruptured pollen grain1, a member of the MtN3/ saliva gene family, is crucial for exine pattern formation and cell integrity of microspores in Arabidopsis. *Plant Physiol* **147**:852–863. doi:10.1104/pp.108.118026

Guida MC, Hermle T, Graham LA, Hauser V, Ryan M, Stevens TH, Simons M. 2018. ATP6AP2 functions as a V-ATPase assembly factor in the endoplasmic reticulum. *Mol Biol Cell* **29**:2156–2164. doi:10.1091/mbc.E18-04-0234

Hackenberg D, Twell D. 2019. The evolution and patterning of male gametophyte development, 1st ed, Current Topics in Developmental Biology. Elsevier Inc. doi:10.1016/bs.ctdb.2018.10.008

Hafidh S, Honys D. 2021. Reproduction Multitasking: The Male Gametophyte. *Annu Rev Plant Biol* **72**:581–614. doi:10.1146/annurev-arplant-080620-021907

Hermle T, Guida MC, Beck S, Helmstädter S, Simons M. 2013. Drosophila ATP6AP2/VhaPRR functions both as a novel planar cell polarity core protein and a regulator of endosomal trafficking. *EMBO J* **32**:245–259. doi:10.1038/emboj.2012.323

Hille F, Richter H, Wong SP, Bratovič M, Ressel S, Charpentier E. 2018. The Biology of CRISPR-Cas: Backward and Forward. *Cell* **172**:1239–1259. doi:10.1016/j.cell.2017.11.032

Hillmer S, Viotti C, Robinson DG. 2012. An improved procedure for low-temperature embedding of high-pressure frozen and freeze-substituted plant tissues resulting in excellent structural preservation and contrast. *J Microsc* **247**:43–47. doi:10.1111/j.1365-2818.2011.03595.x

Hinterberger F. 2019. Master Thesis, Regulator of the V-ATPase? Characterization of the V-ATPase associated protein VHA-AP2L1 in Arabidopsis thaliana. Ruprecht-Karls-University Heidelberg.

Holthuis JCM, Jansen EJR, Schoonderwoert VTG, Burbach JPH, Martens GJM. 1999. Biosynthesis of the vacuolar H+-ATPase accessory subunit Ac45 in Xenopus pituitary. *Eur J Biochem* **262**:484–491. doi:10.1046/j.1432-1327.1999.00396.x

Honys D, Oh SA, Reňák D, Donders M, Šolcová B, Johnson JA, Boudová R, Twell D. 2006. Identification of microspore-active promoters that allow targeted manipulation of gene expression at early stages of microgametogenesis in Arabidopsis. *BMC Plant Biol* **6**:1–9. doi:10.1186/1471-2229-6-31

Horvath P, Barrangou R. 2010. CRISPR/Cas, the immune system of Bacteria and Archaea. *Science* **327**:167–170. doi:10.1126/science.1179555

Hosokawa H, Dip PV, Merkulova M, Bakulina A, Zhuang Z, Khatri A, Jian X, Keating SM, Bueler SA, Rubinstein JL, Randazzo PA, Ausiello DA, Grüber G, Marshansky V. 2013. The n termini of a-subunit isoforms are involved in Signaling between Vacuolar H+-ATPase (V-ATPase) and Cytohesin-2. *J Biol Chem* **288**:5896–5913. doi:10.1074/jbc.M112.409169

Howell SH. 2013. Endoplasmic reticulum stress responses in plants. *Annu Rev Plant Biol* **64**:477–499. doi:10.1146/annurev-arplant-050312-120053

Hsu PD, Scott DA, Weinstein JA, Ran FA, Konermann S, Agarwala V, Li Y, Fine EJ, Wu X, Shalem O, Cradick TJ, Marraffini LA, Bao G, Zhang F. 2013. DNA targeting specificity of RNA-guided Cas9 nucleases. *Nat Biotechnol* **31**:827–832. doi:10.1038/nbt.2647

Hurtado-Lorenzo A, Skinner M, El Annan J, Futai M, Sun-Wada G-H, Bourgoin S, Casanova J, Wildeman A, Bechoua S, Ausiello D a, Brown D, Marshansky V. 2006. V-ATPase interacts with ARNO and Arf6 in early endosomes and regulates the protein degradative pathway. *Nat Cell Biol* **8**:124–136. doi:10.1038/ncb1348

Huss M, Ingenhorst G, König S, Gaßel M, Dröse S, Zeeck A, Altendorf K, Wieczorek H. 2002. Concanamycin A, the specific inhibitor of V-ATPases, binds to the VO subunit c. *J Biol Chem* **277**:40544–40548. doi:10.1074/jbc.M207345200

Jansen EJR, Holthuis JCM, McGrouther C, Burbach JPH, Martens GJM. 1998. Intracellular trafficking of the vacuolar H+-ATPase accessory subunit Ac45. *J Cell Sci* **111**:2999–3006. doi:10.1242/jcs.111.20.2999

Jansen EJR, Timal S, Ryan M, Ashikov A, van Scherpenzeel M, Graham LA, Mandel H, Hoischen A, Iancu TC, Raymond K, Steenbergen G, Gilissen C, Huijben K, van Bakel NHM, Maeda Y, Rodenburg RJ, Adamowicz M, Crushell E, Koenen H, Adams D, Vodopiutz J, Greber-Platzer S, Müller T, Dueckers G, Morava E, Sykut-Cegielska J, Martens GJM, Wevers RA, Niehues T, Huynen MA, Veltman JA, Stevens TH, Lefeber DJ. 2016. ATP6AP1 deficiency causes an immunodeficiency with hepatopathy, cognitive impairment and abnormal protein glycosylation. *Nat Commun* **7**:11600. doi:10.1038/ncomms11600

Jia PF, Xue Y, Li HJ, Yang WC. 2018. Golgi-localized LOT regulates trans-Golgi network biogenesis and pollen tube growth. *Proc Natl Acad Sci U S A* **115**:12307–12312. doi:10.1073/pnas.1809206115

Jinek M, Chylinski K, Fonfara I, Hauer M, Doudna JA, Charpentier E. 2012. A programmable dual-RNA-guided DNA endonuclease in adaptive bacterial immunity. *Science* **337**:816–821. doi:10.1126/science.1225829

Jumper J, Evans R, Pritzel A, Green T, Figurnov M, Ronneberger O, Tunyasuvunakool K, Bates R, Žídek A, Potapenko A, Bridgland A, Meyer C, Kohl SAA, Ballard AJ,

Cowie A, Romera-Paredes B, Nikolov S, Jain R, Adler J, Back T, Petersen S, Reiman D, Clancy E, Zielinski M, Steinegger M, Pacholska M, Berghammer T, Bodenstein S, Silver D, Vinyals O, Senior AW, Kavukcuoglu K, Kohli P, Hassabis D. 2021. Highly accurate protein structure prediction with AlphaFold. *Nature* **596**:583–589. doi:10.1038/s41586-021-03819-2

Kanafi MM, Tavallaei M. 2022. Overview of advances in CRISPR/deadCas9 technology and its applications in human diseases. *Gene* **830**:146518. doi:10.1016/j.gene.2022.146518

Kawasaki-Nishi S, Nishi T, Forgac M. 2001. Yeast V-ATPase Complexes Containing Different Isoforms of the 100-kDa a-subunit Differ in Coupling Efficiency and in Vivo Dissociation. *J Biol Chem* **276**:17941–17948. doi:10.1074/jbc.M010790200

Kawasaki-Nishi S, Nishi T, Forgac M. 2001. Arg-735 of the 100-kDa subunit a of the yeast V-ATPase is essential for proton translocation. *Proc Natl Acad Sci U S A* **98**:12397–402. doi:10.1073/pnas.221291798

Kinouchi K, Ichihara A, Sano M, Sun-Wada G-H, Wada Y, Kurauchi-Mito A, Bokuda K, Narita T, Oshima Y, Sakoda M, Tamai Y, Sato H, Fukuda K, Itoh H. 2010. The (Pro)renin Receptor/ATP6AP2 is Essential for Vacuolar H + -ATPase Assembly in Murine Cardiomyocytes. *Circ Res* **107**:30–34. doi:10.1161/CIRCRESAHA.110.224667

Konopatzki K. 2021. Bachelor Thesis, Lessons from a CRISPR vha-a2 vha-a3 screen - How targeting and screening procedures can be improved by a modular CRISPR/Cas9 system. Ruprecht-Karls-University Heidelberg.

Koonin E V., Makarova KS. 2019. Origins and evolution of CRISPR-Cas systems. *Philos Trans R Soc B Biol Sci* **374**:20180087. doi:10.1098/rstb.2018.0087

Krebs M, Beyhl D, Gorlich E, Al-Rasheid K a. S, Marten I, Stierhof Y-D, Hedrich R, Schumacher K. 2010. Arabidopsis V-ATPase activity at the tonoplast is required for efficient nutrient storage but not for sodium accumulation. *Proc Natl Acad Sci* **107**:3251–3256. doi:10.1073/pnas.0913035107

Kurihara D, Mizuta Y, Sato Y, Higashiyama T. 2015. ClearSee: a rapid optical clearing reagent for whole-plant fluorescence imaging. *Development* **142**:4168–4179. doi:10.1242/dev.127613

Labun K, Montague TG, Gagnon JA, Thyme SB, Valen E. 2016. CHOPCHOP v2: a web tool for the next generation of CRISPR genome engineering. *Nucleic Acids Res* **44**:W272–W276. doi:10.1093/nar/gkw398

LaMontagne ED, Heese A. 2017. Trans-Golgi network/early endosome: a central sorting station for cargo proteins in plant immunity. *Curr Opin Plant Biol* **40**:114–121. doi:10.1016/j.pbi.2017.08.012

Lampropoulos A, Sutikovic Z, Wenzl C, Maegele I, Lohmann JU, Forner J. 2013. GreenGate - A Novel, Versatile, and Efficient Cloning System for Plant Transgenesis. *PLoS One* **8**:e83043. doi:10.1371/journal.pone.0083043

Lander ES. 2016. The Heroes of CRISPR. *Cell* **164**:18–28. doi:10.1016/j.cell.2015.12.041

Lei X, Liu B. 2020. Tapetum-Dependent Male Meiosis Progression in Plants: Increasing Evidence Emerges. *Front Plant Sci* **10**:1–10. doi:10.3389/fpls.2019.01667

Lei Y, Klionsky DJ. 2022. The coordination of V-ATPase and ATG16L1 is part of a common mechanism of non-canonical autophagy ABSTRACT. *Autophagy* **0**:1–3. doi:10.1080/15548627.2022.2100678

Li WL, Liu Y, Douglas CJ. 2017. Role of glycosyltransferases in pollen wall primexine formation and exine patterning. *Plant Physiol* **173**:167–182. doi:10.1104/pp.16.00471

Liang X, Li SW, Gong LM, Li S, Zhang Y. 2020. COPII components sar1b and sar1c play distinct yet interchangeable roles in pollen development. *Plant Physiol* **183**:974–985. doi:10.1104/pp.20.00159

Lin CW, Tsai FJ, Wan L, Lai CC, Lin KH, Hsieh TH, Shiu SY, Li JY. 2005. Binding interaction of SARS coronavirus 3CLpro protease with vacuolar-H+ ATPase G1 subunit. *FEBS Lett* **579**:6089–6094. doi:10.1016/j.febslet.2005.09.075

Liu L, Wang T. 2021. Male gametophyte development in flowering plants: A story of quarantine and sacrifice. *J Plant Physiol* **258**–**259**:153365. doi:10.1016/j.jplph.2021.153365

Ludwig J, Kerscher S, Brandt U, Pfeiffer K, Getlawi F, Apps DK, Schägger H. 1998. Identification and characterization of a novel 9.2-kDa membrane sector- associated protein of vacuolar proton-ATPase from chromaffin granules. *J Biol Chem* **273**:10939–10947. doi:10.1074/jbc.273.18.10939

Luo Y, Scholl S, Doering A, Zhang Y, Irani NG, Di S, Neumetzler L, Krishnamoorthy P, Houtte I Van, Mylle E. 2015. V-ATPase-activity in the TGN / EE is required for exocytosis and recycling in Arabidopsis. *Nat Plants* **1**:1–24. doi:10.1038/nplants.2015.94.V-ATPase-activity

Lupanga U. 2017. Dissertation, A tale of two routes: The role of subunit a in targeting and regulation of the V-ATPase in Arabidopsis thaliana. Ruprecht-Karls-University Heidelberg. doi:10.11588/heidok.00022941

Lupanga U, Roehrich R, Askani J, Hilmer S, Kiefer C, Krebs M, Kanazawa T, Ueda T, Schumacher K. 2020. The Arabidopsis V-ATPase is localized to the TGN / EE via a seed plant-specific motif. *Elife* 1–40. doi:10.7554/eLife.60568

Mair CM, Meyer T, Schneider K, Huang Q, Veit M, Herrmann A. 2014. A Histidine Residue of the Influenza Virus Hemagglutinin Controls the pH Dependence of the Conformational Change Mediating Membrane Fusion. *J Virol* **88**:13189–13200. doi:10.1128/jvi.01704-14

Marshansky V. 2007. The V-ATPase a2-subunit as a putative endosomal pH-sensor. *Biochem Soc Trans* **35**:1092–1099. doi:10.1042/BST0351092

Martinière A, Bassil E, Jublanc E, Alcon C, Reguera M, Sentenac H, Blumwald E, Paris N. 2013. In vivo intracellular pH measurements in tobacco and arabidopsis reveal an unexpected pH gradient in the endomembrane system. *Plant Cell* **25**:4028–4043. doi:10.1105/tpc.113.116897

Mazhab-Jafari MT, Rohou A, Schmidt C, Bueler SA, Benlekbir S, Robinson C V., Rubinstein JL. 2016. Atomic model for the membrane-embedded VO motor of a eukaryotic V-ATPase. *Nature* **539**:1–5. doi:10.1038/nature19828

McKay WD, McFarlane EH, Qu Y, Situmorang A, Gilliham M, Wege S. 2022. Plant Trans-Golgi Network/Early Endosome pH regulation requires Cation Chloride Cotransporter (CCC1). *Elife* **11**:1–28. doi:10.7554/eLife.70701

Miller EA, Beilharz TH, Malkus PN, Lee MCS, Hamamoto S, Orci L, Schekman R. 2003. Multiple cargo binding sites on the COPII subunit Sec24p ensure capture of diverse membrane proteins into transport vesicles. *Cell* **114**:497–509. doi:10.1016/S0092-8674(03)00609-3

Mlotshwa S, Pruss GJ, Gao Z, Mgutshini NL, Li J, Chen X, Bowman LH, Vance V. 2010. Transcriptional silencing induced by Arabidopsis T-DNA mutants is associated with 35S promoter siRNAs and requires genes involved in siRNA-mediated chromatin silencing. *Plant J* **64**:699–704. doi:10.1111/j.1365-313X.2010.04358.x

Muench SP, Huss M, Song CF, Phillips C, Wieczorek H, Trinick J, Harrison MA. 2009. Cryo-electron Microscopy of the Vacuolar ATPase Motor Reveals its Mechanical and Regulatory Complexity. *J Mol Biol* **386**:989–999. doi:10.1016/j.jmb.2009.01.014

Nelms B, Walbot V. 2022. Gametophyte genome activation occurs at pollen mitosis I in maize. *Science* **375**:424–429. doi:10.1126/science.abl7392

Neubert C. 2012. Dissertation, Assembly and quality control of the V- ATPase in Arabidopsis. Ruprecht-Karls-University Heidelberg. doi:10.11588/heidok.00013463

Neubert C, Graham L a., Black-Maier EW, Coonrod EM, Liu TY, Stierhof YD, Seidel T, Stevens TH, Schumacher K. 2008. Arabidopsis has two functional orthologs of the yeast V-ATPase assembly factor Vma21p. *Traffic* **9**:1618–1628. doi:10.1111/j.1600-0854.2008.00799.x

Nishi T, Forgac M. 2002. The vacuolar (H+)-ATPases - Nature's most versatile proton pumps. *Nat Rev Mol Cell Biol* **3**:94–103. doi:10.1038/nrm729

Olsson MHM, SØndergaard CR, Rostkowski M, Jensen JH. 2011. PROPKA3: Consistent treatment of internal and surface residues in empirical p K a predictions. *J Chem Theory Comput* **7**:525–537. doi:10.1021/ct100578z

Oot RA, Kane PM, Berry EA, Wilkens S. 2016. Crystal structure of yeast V_1-ATPase in the autoinhibited state. *EMBO J* **35**:1694 LP-1706.

Paul W, Hodge R, Smartt S, Draper J, Scott R. 1992. The isolation and characterisation of the tapetum-specific Arabidopsis thaliana A9 gene. *Plant Mol Biol* **19**:611–622. doi:10.1007/BF00026787

Pettersen EF, Goddard TD, Huang CC, Couch GS, Greenblatt DM, Meng EC, Ferrin TE. 2004. UCSF Chimera - A visualization system for exploratory research and analysis. *J Comput Chem* **25**:1605–1612. doi:10.1002/jcc.20084

Piffanelli P, Ross JHE, Murphy DJ. 1998. Biogenesis and function of the lipidic structures of pollen grains. *Sex Plant Reprod* **11**:65–80. doi:10.1007/s004970050122

Poëa-Guyon S, Ammar MR, Erard M, Amar M, Moreau AW, Fossier P, Gleize V, Vitale N, Morel N. 2013. The V-ATPase membrane domain is a sensor of granular ph that controls the exocytotic machinery. *J Cell Biol* **203**:283–298. doi:10.1083/jcb.201303104

Preuss D, Rhee SY, Davis RW. 1994. Tetrad Analysis Possible in Arabidopsis with Mutation of the QUARTET (QRT) Genes. *Science* **264**:1458–1460. doi:10.1126/science.8197459

Quilichini TD, Douglas CJ, Lacey Samuels A. 2014. New views of tapetum ultrastructure and pollen exine development in Arabidopsis thaliana. *Ann Bot* **114**:1189–1201. doi:10.1093/aob/mcu042

Ran FA, Hsu PD, Wright J, Agarwala V, Scott DA, Zhang F. 2013. Genome engineering using the CRISPR-Cas9 system. *Nat Protoc* **8**:2281–2308. doi:10.1038/nprot.2013.143

Rienmüller F, Dreyer I, Schönknecht G, Schulz A, Schumacher K, Nagy R, Martinoia E, Marten I, Hedrich R. 2012. Luminal and cytosolic pH feedback on proton pump activity and ATP affinity of V-type ATPase from Arabidopsis. *J Biol Chem* **287**:8986–8993. doi:10.1074/jbc.M111.310367

Roh SH, Stam NJ, Hryc CF, Couoh-Cardel S, Pintilie G, Chiu W, Wilkens S. 2018. The 3.5-Å CryoEM Structure of Nanodisc-Reconstituted Yeast Vacuolar ATPase Vo Proton Channel. *Mol Cell* **69**:993–1004.e3. doi:10.1016/j.molcel.2018.02.006

Röhrich R. 2016. Master Thesis, Analysis of the V-ATPase associated protein VHA-AP2 and in vivo measurements of cytosolic pH in Arabidopsis thaliana. Ruprecht-Karls-University Heidelberg.

Rosquete MR, Davis DJ, Drakakaki G. 2018. The plant trans-golgi network: Not just a matter of distinction. *Plant Physiol* **176**:187–198. doi:10.1104/pp.17.01239

Rujano MA, Cannata Serio M, Panasyuk G, Péanne R, Reunert J, Rymen D, Hauser V, Park JH, Freisinger P, Souche E, Guida MC, Maier EM, Wada Y, Jäger S, Krogan NJ, Kretz O, Nobre S, Garcia P, Quelhas D, Bird TD, Raskind WH, Schwake M, Duvet S, Foulquier F, Matthijs G, Marquardt T, Simons M. 2017. Mutations in the X-linked *ATP6AP2* cause a glycosylation disorder with autophagic defects. *J Exp Med* **214**:3707–3729. doi:10.1084/jem.20170453

Ryan M, Graham LA, Stevens TH. 2008. Voa1p Functions in V-ATPase Assembly in the Yeast Endoplasmic Reticulum. *Mol Biol Cell* **19**:5131–5142. doi:10.1091/mbc.e08-06-0629

Sambade M, Alba M, Smardon AM, West RW, Kane PM. 2005. A Genomic Screen for Yeast Vacuolar Membrane ATPase Mutants. *Genetics* **170**:1539–1551. doi:10.1534/genetics.105.042812

Sanderfoot AA, Kovaleva V, Bassham DC, Raikhel N V. 2001. Interactions between syntaxins identify at least five SNARE complexes within the golgi/prevacuolar system of the arabidopsis cell. *Mol Biol Cell* **12**:3733–3743. doi:10.1091/mbc.12.12.3733

Sanders PM, Bui AQ, Weterings K, McIntire KN, Hsu YC, Lee PY, Truong MT, Beals TP,

Goldberg RB. 1999. Anther developmental defects in Arabidopsis thaliana male-sterile mutants. *Sex Plant Reprod* **11**:297–322. doi:10.1007/s004970050158

Sauquet H, Von Balthazar M, Magallón S, Doyle JA, Endress PK, Bailes EJ, Barroso De Morais E, Bull-Hereñu K, Carrive L, Chartier M, Chomicki G, Coiro M, Cornette R, El Ottra JHL, Epicoco C, Foster CSP, Jabbour F, Haevermans A, Haevermans T, Hernández R, Little SA, Löfstrand S, Luna JA, Massoni J, Nadot S, Pamperl S, Prieu C, Reyes E, Dos Santos P, Schoonderwoerd KM, Sontag S, Soulebeau A, Staedler Y, Tschan GF, Wing-Sze Leung A, Schönenberger J. 2017. The ancestral flower of angiosperms and its early diversification. *Nat Commun* **8**. doi:10.1038/ncomms16047

Scheuring D, Viotti C, Krüger F, Künzl F, Sturm S, Bubeck J, Hillmer S, Frigerio L, Robinson DG, Pimpl P, Schumacher K, Ku F. 2011. Multivesicular Bodies Mature from the Trans-Golgi Network/Early Endosome in Arabidopsis. *Plant Cell* **23**:1–20. doi:10.1105/tpc.111.086918

Schindelin J, Arganda-Carreras I, Frise E, Kaynig V, Longair M, Pietzsch T, Preibisch S, Rueden C, Saalfeld S, Schmid B, Tinevez JY, White DJ, Hartenstein V, Eliceiri K, Tomancak P, Cardona A. 2012. Fiji: An open-source platform for biological-image analysis. *Nat Methods* **9**:676–682. doi:10.1038/nmeth.2019

Scholl S, Hillmer S, Krebs M, Schumacher K. 2021. ClCd and ClCf act redundantly at the trans-Golgi network/early endosome and prevent acidification of the Golgi stack. *J Cell Sci* **134**. doi:10.1242/jcs.258807

Schumacher K. 2014. pH in the plant endomembrane system-an import and export business. *Curr Opin Plant Biol* **22**:71–76. doi:10.1016/j.pbi.2014.09.005

Schumacher K, Vafeados D, McCarthy M, Sze H, Wilkins T, Chory J. 1999. The Arabidopsis det3 mutant reveals a central role for the vacuolar H+- ATPase in plant growth and development. *Genes Dev* **13**:3259–3270. doi:10.1101/gad.13.24.3259

Schürholz A-KK, López-Salmerón V, Li Z, Forner J, Wenzl C, Gaillochet C, Augustin S, Barro AV, Fuchs M, Gebert M, Lohmann JU, Greb T, Wolf S. 2018. A comprehensive toolkit for inducible, cell type-specific gene expression in Arabidopsis. *Plant Physiol* **178**:40–53. doi:10.1104/pp.18.00463

Schwab R, Ossowski S, Riester M, Warthmann N, Weigel D. 2006. Highly Specific Gene Silencing by Artificial MicroRNAs in Arabidopsis. *Plant Cell* **18**:1121–1133. doi:10.1105/tpc.105.039834

Shi J, Cui M, Yang L, Kim YJ, Zhang D. 2015. Genetic and Biochemical Mechanisms of Pollen Wall Development. *Trends Plant Sci* **20**:741–753. doi:10.1016/j.tplants.2015.07.010

Smits AH, Ziebell F, Joberty G, Zinn N, Mueller WF, Clauder-Münster S, Eberhard D, Fälth Savitski M, Grandi P, Jakob P, Michon AM, Sun H, Tessmer K, Bürckstümmer T, Bantscheff M, Steinmetz LM, Drewes G, Huber W. 2019. Biological plasticity rescues target activity in CRISPR knock outs. *Nat Methods* **16**:1087–1093. doi:10.1038/s41592-019-0614-5

Smyth DR, Bowman JL, Meyerowitz EM. 1990. Early flower development in Arabidopsis. *Plant Cell* **2**:755–767. doi:10.1105/tpc.2.8.755

Stemmer M, Thumberger T, Del Sol Keyer M, Wittbrodt J, Mateo JL. 2015. CCTop: An intuitive, flexible and reliable CRISPR/Cas9 target prediction tool. *PLoS One* **10**:1–11. doi:10.1371/journal.pone.0124633

Strompen G, Dettmer J, Stierhof YD, Schumacher K, Jürgens G, Mayer U. 2005. Arabidopsis vacuolar H+-ATPase subunit E isoform 1 is required for Golgi organization and vacuole function in embryogenesis. *Plant J* **41**:125–132. doi:10.1111/j.1365-313X.2004.02283.x

Sun MX, Huang XY, Yang J, Guan YF, Yang ZN. 2013. Arabidopsis RPG1 is important for primexine deposition and functions redundantly with RPG2 for plant fertility at the late reproductive stage. *Plant Reprod* **26**:83–91. doi:10.1007/s00497-012-0208-1

Supek F, Supekova L, Mandiyan S, Pan YCE, Nelson H, Nelson N. 1994. A novel accessory subunit for vacuolar H+-ATPase from chromaffin granules. *J Biol Chem* **269**:24102–24106.

Sze H, Schumacher K, Müller ML, Padmanaban S, Taiz L. 2002. A simple nomenclature for a complex proton pump: VHA genes encode the vacuolar H+-ATPase. *Trends Plant Sci* **7**:157–161. doi:10.1016/S1360-1385(02)02240-9

Takemoto K, Ebine K, Askani JC, Krüger F, Gonzalez ZA, Ito E, Goh T, Schumacher K, Nakano A, Ueda T. 2018. Distinct sets of tethering complexes, SNARE complexes, and Rab GTPases mediate membrane fusion at the vacuole in Arabidopsis. *Proc Natl Acad Sci* **115**:201717839. doi:10.1073/pnas.1717839115

Takeuchi M, Ueda T, Sato K, Abe H, Nagata T, Nakano A. 2000. A dominant negative mutant of Sar1 GTPase inhibits protein transport from the endoplasmic reticulum to the Golgi apparatus in tobacco and Arabidopsis cultured cells. *Plant J* **23**:517–525. doi:10.1046/j.1365-313X.2000.00823.x

Tan YZ, Keon KA, Abdelaziz R, Imming P, Schulze W, Schumacher K, Rubinstein JL. 2022. Structure of V-ATPase from citrus fruit. *Structure* **30**:1403–1410.e4. doi:10.1016/j.str.2022.07.006

Tanaka Y, Nishimura K, Kawamukai M, Oshima A, Nakagawa T. 2013. Redundant function of two Arabidopsis COPII components, AtSec24B and AtSec24C, is essential for male and female gametogenesis. *Planta* **238**:561–575. doi:10.1007/s00425-013-1913-1

Toei M, Toei S, Forgac M. 2011. Definition of membrane topology and identification of residues important for transport in subunit a of the vacuolar ATPase. *J Biol Chem* **286**:35176–35186. doi:10.1074/jbc.M111.273409

Tsuchimatsu T, Kakui H, Yamazaki M, Marona C, Tsutsui H, Hedhly A, Meng D, Sato Y, Städler T, Grossniklaus U, Kanaoka MM, Lenhard M, Nordborg M, Shimizu KK. 2020. Adaptive reduction of male gamete number in the selfing plant Arabidopsis thaliana. *Nat Commun* **11**:2885. doi:10.1038/s41467-020-16679-7

Twell D. 2010. Male gametophyte development. *Plant Dev Biol* **1**:225–244. doi:10.1007/978-3-642-02301-9_12

Uemura T, Suda Y, Ueda T, Nakano A. 2014. Dynamic behavior of the trans-golgi

network in root tissues of arabidopsis revealed by super-resolution live imaging. *Plant Cell Physiol* **55**:694–703. doi:10.1093/pcp/pcu010

Varadi M, Anyango S, Deshpande M, Nair S, Natassia C, Yordanova G, Yuan D, Stroe O, Wood G, Laydon A, Zídek A, Green T, Tunyasuvunakool K, Petersen S, Jumper J, Clancy E, Green R, Vora A, Lutfi M, Figurnov M, Cowie A, Hobbs N, Kohli P, Kleywegt G, Birney E, Hassabis D, Velankar S. 2022. AlphaFold Protein Structure Database: Massively expanding the structural coverage of protein-sequence space with high-accuracy models. *Nucleic Acids Res* **50**:D439–D444. doi:10.1093/nar/gkab1061

Vasanthakumar T, Bueler SA, Wu D, Beilsten-Edmands V, Robinson C V., Rubinstein JL. 2019. Structural comparison of the vacuolar and Golgi V-ATPases from saccharomyces cerevisiae. *Proc Natl Acad Sci U S A* **116**:7272–7277. doi:10.1073/pnas.1814818116

Vasanthakumar T, Keon KA, Bueler SA, Jaskolka MC, Rubinstein JL. 2022. Coordinated conformational changes in the V1 complex during V-ATPase reversible dissociation. *Nat Struct Mol Biol* **29**:430–439. doi:10.1038/s41594-022-00757-z

Vasanthakumar T, Rubinstein JL. 2020. Structure and Roles of V-type ATPases. *Trends Biochem Sci* **45**:295–307. doi:10.1016/j.tibs.2019.12.007

Vercoulen Y, Kondo Y, Iwig JS, Janssen AB, White KA, Amini M, Barber DL, Kuriyan J, Roose JP. 2017. A histidine pH sensor regulates activation of the Ras-specific guanine nucleotide exchange factor RasGRP1. *Elife* **6**:1–26. doi:10.7554/eLife.29002

Viotti C, Bubeck J, Stierhof Y-D, Krebs M, Langhans M, van den Berg W, van Dongen W, Richter S, Geldner N, Takano J, Ju¨rgens G, de Vries SC, Robinson DG, Schumacher K. 2010. Endocytic and secretory traffic in Arabidopsis merge in the trans-Golgi network/early endosome, an independent and highly dynamic organelle. *Plant Cell* **22**:1344–1357. doi:10.1105/tpc.109.072637

Viotti C, Krüger F, Krebs M, Neubert C, Fink F, Lupanga U, Scheuring D, Boutté Y, Frescatada-Rosa M, Wolfenstetter S, Sauer N, Hillmer S, Grebe M, Schumacher K, Greb M, Schumacher K. 2013. The endoplasmic reticulum is the main membrane source for biogenesis of the lytic vacuole in Arabidopsis. *Plant Cell* **25**:3434–49. doi:10.1105/tpc.113.114827

Waadt R, Krebs M, Kudla J, Schumacher K. 2017. Multiparameter imaging of calcium and abscisic acid and high-resolution quantitative calcium measurements using R-GECO1-mTurquoise in Arabidopsis. *New Phytol* **216**:303–320. doi:10.1111/nph.14706

Wang J, Pielak RM, McClintock MA, Chou JJ. 2009. Solution structure and functional analysis of the influenza B proton channel. *Nat Struct Mol Biol* **16**:1267–1271. doi:10.1038/nsmb.1707

Wang L, Wu D, Robinson C V, Wu H, Fu T. 2020. Structures of a Complete Human V-ATPase Reveal Mechanisms of Its Assembly. *Mol Cell* **80**:501–511.e3. doi:10.1016/j.molcel.2020.09.029

Wang R, Long T, Hassan A, Wang J, Sun Y, Xie X-S, Li X. 2020. Cryo-EM structures of

intact V-ATPase from bovine brain. *Nat Commun* **11**:3921. doi:10.1038/s41467-020-17762-9

Wang R, Owen HA, Dobritsa AA. 2021. Dynamic changes in primexine during the tetrad stage of pollen development. *Plant Physiol* **187**:2393–2404. doi:10.1093/plphys/kiab426

Wang W, Malcolm BA. 1999. Two-Stage PCR Protocol Allowing Introduction of Multiple Mutations, Deletions and Insertions Using QuikChange TM Site-Directed Mutagenesis. *Biotechniques* **26**:680–682. doi:10.2144/99264st03

Wang ZP, Xing HL, Dong L, Zhang HY, Han CY, Wang XC, Chen QJ. 2015. Egg cell-specific promoter-controlled CRISPR/Cas9 efficiently generates homozygous mutants for multiple target genes in Arabidopsis in a single generation. *Genome Biol* **16**:1–12. doi:10.1186/s13059-015-0715-0

Wu W, Celma CC, Kerviel A, Roy P. 2019. Mapping the pH Sensors Critical for Host Cell Entry by a Complex Nonenveloped Virus. *J Virol* **93**:1–14. doi:10.1128/jvi.01897-18

Xing H-L, Dong L, Wang Z-P, Zhang H-Y, Han C-Y, Liu B, Wang X-C, Chen Q-J. 2014. A CRISPR/Cas9 toolkit for multiplex genome editing in plants. *BMC Plant Biol* **14**:327. doi:10.1186/s12870-014-0327-y

Xu M, Yan X, Wang Y, Liu C, Yang Q, Tian D, Bednarek SY, Pan J, Wang C. 2022. ADAPTOR PROTEIN-1 complex-mediated post-Golgi trafficking is critical for pollen wall development in Arabidopsis. *New Phytol* **235**:472–487. doi:10.1111/nph.18170

Xu Y, Cheng S, Zeng H, Zhou P, Ma Y, Li L, Liu X, Shao F, Ding J. 2022. ARF GTPases activate Salmonella effector SopF to ADP-ribosylate host V-ATPase and inhibit endomembrane damage-induced autophagy. *Nat Struct Mol Biol* **29**:67–77. doi:10.1038/s41594-021-00710-6

Xu Y, Zhou P, Cheng S, Lu Q, Nowak K, Hopp AK, Li L, Shi X, Zhou Z, Gao W, Li D, He H, Liu X, Ding J, Hottiger MO, Shao F. 2019. A Bacterial Effector Reveals the V-ATPase-ATG16L1 Axis that Initiates Xenophagy. *Cell* **178**:552–566.e20. doi:10.1016/j.cell.2019.06.007

Xue JS, Yao C, Xu QL, Sui CX, Jia XL, Hu WJ, Lv YL, Feng YF, Peng YJ, Shen SY, Yang NY, Lou YX, Yang ZN. 2021. Development of the Middle Layer in the Anther of Arabidopsis. *Front Plant Sci* **12**:1–9. doi:10.3389/fpls.2021.634114

Zhang C, Ren MY, Han WJ, Zhang YF, Huang MJ, Wu SY, Huang J, Wang Y, Zhang Z, Yang ZN. 2022. Slow development allows redundant genes to restore the fertility of rpg1, a TGMS line in Arabidopsis. *Plant J* **109**:1375–1385. doi:10.1111/tpj.15635

Zhang Q, Xing HL, Wang ZP, Zhang HY, Yang F, Wang XC, Chen QJ. 2018. Potential high-frequency off-target mutagenesis induced by CRISPR/Cas9 in Arabidopsis and its prevention. *Plant Mol Biol* **96**:445–456. doi:10.1007/s11103-018-0709-x

Zhang Y, Zhang H, Zheng Q. 2019. A unique activation-promotion mechanism of the influenza B M2 proton channel uncovered by multiscale simulations. *Phys Chem Chem Phys* **21**:2984–2991. doi:10.1039/c9cp00130a

Zhao B, Shi H, Wang W, Liu X, Gao H, Wang X, Zhang Y, Yang M, Li R, Guo Y. 2016.

Secretory COPII protein SEC31B is required for pollen wall development. *Plant Physiol* **172**:1625–1642. doi:10.1104/pp.16.00967

Zhao J, Benlekbir S, Rubinstein JL. 2015. Electron cryomicroscopy observation of rotational states in a eukaryotic V-ATPase. *Nature* **521**:241–245. doi:10.1038/nature14365

Acknowledgements

This work, as it is today, developed in a process of many small steps and required going in many different directions and finding new paths that could be taken. I would like to sincerely thank Prof. Dr. Karin Schumacher for always being there to discuss results and build hypotheses and for the many ideas that led to the success of this study. I am very grateful for the inspiring discussions, lab meetings and the support during my years at COS.

Furthermore, this work is based on the support of many people. I am very grateful to Dr. Melanie Krebs for a lot of help and advice and great working time together, for example, in the joint sessions at the microscope.

Thanks a lot to Prof. Dr. Alexis Maizel and Prof. Dr. Sebastian Schuck for advice and support throughout my PhD time as my thesis advisory committee. Also, thanks to Prof. Dr. Thomas Greb for being part of my PhD defense examination committee.

For countless nice working time together, making tough days less tough and many unforgettable moments, many thanks to Fabian Fink.

I am very grateful to Dr. Upendo Lupanga, for steady help and advice and very fun times.

With great gratitude, I would like to thank Dr. Michael Stitz, for much help, advice and great times throughout my PhD, who is easily capable of cheering up people.

Many thanks to Dr. Jazmin Reyes-Hernández, who is always there with help and up for great times in and outside the lab.

I would like to greatly thank Dr. Béatrice Berthet for plenty of fun time during our joint time in the lab and later outside the lab and for lots of encouragement.

Thanks a lot to Ines Steins, Beate Schöfer and Barbara Jesenofsky for a lot of nice time together and many times nice words at the right moment and great support.

For always being there with help and advice at the beginning of my PhD, I would like to thank Dr. Stefan Scholl a lot.

Many thanks to Dr. John Walden, Dr. Tobias Ziegler, Martin Schubert and Dr. Apolonio Huerta for making the times of our Master studies a blast and for being great friends.

I am very grateful to Dr. Eleonore Holzwart, Dr. Jana Askani, Dr. Zaida Andrés González, Dr. Rainer Waadt, Dr. Jonathan Dragwidge, Dr. Vanessa Fuchs, Dr. Zhaoxue Ma, Dr. Falco Krüger, Dr. Amaya Vilches-Barro, Dr. Zhenni Li, Dr. Ann-Kathrin Schürholz, Dr. Borja Garnelo Gómez, Dr. Andrea Scarpa, Dr. Paola Ruiz-Duarte, Lotte Bald, Dr. Belén Rombolá Caldentey, Dr. Tomás Tessi, Marcel Piepers, Dr. Alyona Minina, Dr. Paula Ragel, Dr. Nana Keinath, Catharina Larasati, Kristin Konopatzki and Marlene Handl for help, support and making COS far more than a workplace as all people above.

Thanks very much to Fabian Fink, Dr. Melanie Krebs, Dr. Upendo Lupanga, Elias Naber and Dr. Michael Stitz for proofreading parts of this thesis.

Moreover, I am grateful to the Schmeil Foundation for supporting me with the “Schmeil PhD Degree Extension Award”. Also, I am grateful to HBIGS for the valuable offer of courses and activities and the support during my PhD.

The final part is dedicated to my parents, Birgit Schmid-Röhrich and Werner Röhrich, who already, before I could make conscious decisions, let me experience kindness and support. Many thanks that although time brought not just happiness, on their kindness and support, I can always count.

I would like to greatly thank my siblings, Almut, Solveig and Carl Röhrich, for being encouraging and providing great help in many situations.

Thanks very much to my grandparents, Doris and Josef Schmid and Lidwina Röhrich, for great support and the ability to lift my spirits in a single phone call.

To my aunt Ute Schmid to whom I am very grateful for her support and whom I miss deeply.

To Elias Naber who is proficient in making situations gorgeous and has infinite great ideas. Great thanks for being encouraging and the dedication to make everyday life functioning and beautiful.